STRUCTURE-SWITCHING SELEX FOR SELECTION OF APTAMERS OF DAMAGED NUCLEOSIDES AND NUCLEOBASES 8-OXOGUANINE AND SPIROIMINODIHYDANTOIN

by

Pranjali Ghude

A dissertation submitted to the faculty of
The University of Utah
in partial fulfillment of the requirements for the degree of

Doctor of Philosophy

Department of Chemistry

The University of Utah

August 2015

The University of Utah Graduate School

STATEMENT OF DISSERTATION APPROVAL

The dissertation of **Pranjali Ghude**

has been approved by the following supervisory committee members:

Cynthia J. Burrows	, Chair	**05/20/2014** Date Approved
Jennifer Heemstra	, Member	**05/20/2014** Date Approved
Janis Louie	, Member	**05/20/2014** Date Approved
Charles B. Grissom	, Member	**05/20/2014** Date Approved
Amy Barrios	, Member	**05/20/2014** Date Approved

and by **Cynthia J. Burrows** , Chair/Dean of

the Department/College/School of **Chemistry**

and by David B. Kieda, Dean of The Graduate School.

ABSTRACT

SELEX technology has been a powerful tool to evolve aptamers that can bind tightly and specifically to a target. Aptamers are nucleic acids with the propensity to assume three-dimensional structures facilitating specific binding interactions with high affinity to the target. Principally, aptamers are selected from a large pool of random sequences by an iterative *in vitro* method. The main advantages of this technology are that aptamers can be produced in a large scale by a controlled combinatorial chemistry method, easily derivatized regioselectively for detection using dyes, and they are stable for long periods at room temperature when dry. Therefore, single-stranded DNA aptamers are robust binding agents with good shelf-life and easy production and do not require a biological host. One of the most difficult challenges of this technology is that there is no standardized SELEX protocol applicable for all types of target, which in this dissertation includes damaged bases and nucleosides.

The first work presented here focuses on identification of products that formed from the reaction of Ni(II)-mediated sulfate radical oxidation of the guanine base. It was observed that a Ni(II)-macrocyclic square-planar complex, NiCR, in the presence of $KHSO_5$ can generate a specific hydantoin lesion called 2-iminohydantoin (2-Ih) in both nucleoside and single-stranded DNA, along with the other well-known guanine oxidation products. The initial goal was to optimize the 2-Ih formation followed by isolation of this

lesion. Fine tuning the oxidation conditions with respect to the concentration of $KHSO_5$ added in certain time intervals made it possible to generate 2-Ih exclusively.

Secondly, SELEX technology was used to select aptamers for the oxidized damaged bases and nucleosides as an approach toward detection of these targets. The structure-switching or capture SELEX technique was used as a successful method to generate DNA aptamers for these targets that are difficult to immobilize or derivatize and purify in the large quantities needed to perform typical SELEX procedures. The targets include the most common oxidation products that are generated as a part of the most important cellular repair pathways, base excision and nuclear excision repair. These products are the damaged nucleobases and 2'-deoxynucleosides of 8-oxo-7,8-dihydroguanine (8-oxo-G) and spiroiminodihydantoin (Sp). This is the first time that aptamers are reported for the damaged diastereomeric lesions, dSp.

Lastly, sensors have been developed by truncating these aptamers as a part of post-SELEX modification and the binding affinities for these sensors toward the damaged lesions were determined. The future direction aims toward testing these aptamers by using split aptamer technology and testing these in cellular samples.

TABLE OF CONTENTS

LIST OF FIGURES

LIST OF TABLES

LIST OF SCHEMES

LIST OF ABBREVIATIONS

DNA: deoxyribonucleic acid

ROS: reactive oxygen species

RNS: reactive nitrogen species

mtDNA: mitochondrial DNA

ntDNA: nuclear DNA

ETS: electron transport system

dG: 2'-deoxyguanosine

8-oxo-dG: 8-oxo-7,8-dihydro2'-deoxyguanosine

dSp: spiroiminodihydantoin-2'-deoxyribonucleoside

dGh: 5-guanidinohydantoin-2'-deoxyribonucleoside

2-Ih: 2-iminohydantoin

WC: Watson Crick

bp: base pair

SELEX: systematic enrichment of ligand by exponential enrichment

BER: base-excision repair

NER: nucleotide-excision repair

PCR: polymerase chain reaction

PBS: primer binding sequence

Bio: biotin

FP: forward primer

RP: reverse primer

ECD: electronic circular dichroism

dsDNA: double-strand DNA

ODN: oligodeoxynucleotide

8-oxo-G: 8-oxo-7,8-dihydroguanine

ssDNA: single-stranded DNA

T_m: melting temperature

UDG: uracil-DNA glycosylase

OGG: oxoguanine glycosylase

APE: apurinic endonuclease

PNK: polynucleotide kinase

MS-SELEX: Milan Stojanovic SELEX

YL-SELEX: Yingfu Li SELEX

ACKNOWLEDGMENTS

I would like to thank my advisor, Prof. Cynthia J. Burrows, for her support and professional guidance in my research career. She encouraged me to pursue new projects in the laboratory and also in trying to set up new instrumentation and techniques in the lab. I would like to thank her for always being supportive and helping me get in touch with professional experts in the field every time I had a setback in my research.

I am thankful to all the present and past members of the Burrows group. All of them have been helpful and supportive in my career as a graduate student. I am extremely thankful to Prof. Aaron M. Fleming, who has guided me from the first day of my graduate school. I would like to thank Prof. Aaron M. Fleming, Dr. Na An, Dr. Jan Riedl, Anna H. Wolna, Yun Ding, and Judy Zhu for useful input in editing my thesis.

I am thankful to my dissertation committee members, Prof. Dale C. Poulter, Prof. Janis Louie, Prof. Amy M. Barrios, Prof. Charles B. Grissom, and Prof. Jennifer M. Heemstra. Prof. Heemstra and her research group members Dr. Ashwani Sharma, Trevor Feagin, David Olsen, and Nicholas G. Spiropulos have always been there to attend my group meetings, make suggestions, and provide useful input in my project. I am extremely thankful to Prof. Matthew Sigman who has helped me in my initial transfer to the graduate school. I appreciate all the help offered by Prof. Kenneth J. Woycechowsky for letting me use the nanodrop instrumentation throughout my project.

I have had the opportunity to get useful suggestions and guidance from experts in my research field outside of the department. I am grateful to Prof. Dipankar Sen and his post-doctoral fellow Dr. Jason Thomas at The Simon Fraser University for their guidance. I am extremely appreciative of all the help in my research from Prof. Milan Stojanovic and his post-doctoral fellow Dr. Kasi Yang at Columbia University. Kasi has been patient with thousands of my emails and I am extremely appreciative of her help in my research.

My research would not have been possible without the support of my family and friends. My parents, Mr. Vinod and Mrs. Vaishalee Ghude, have worked hard and sacrificed for me to be here and have always been there for me every day encouraging me in my tough times. My brother, Prasad Ghude has been a great support in my life. My husband, Kaveri B. Urkalan, has sacrificed being alone for too long so I could finish my degree. I have a very encouraging sister-in-law, Shilpi Bhatia, and I am blessed with a cute niece, Sanvi Ghude, who cheers me in tough times. Bhatia and Urkalan family have always encouraged me to reach my goal.

Finally, I would like to thank all my friends who have helped me reach here. My friends in India, Ohio state, and SLC, with all of whom I had a great time in my life.

CHAPTER 1

INTRODUCTION

Mitochondrial (mt) and nuclear (nt) DNA oxidation

An imbalance between the generation of reactive oxygen species (ROS) and the activity of repair enzymes or detoxification processes can result in the deregulation of homeostasis generating oxidative stress in a cell (Figure 1.1). ROS are the byproducts of cellular metabolic cycles that consist of different types of oxygen ions and peroxides.[1-3] Besides ROS, reactive nitrogen species (RNS) also play an important role in the process of energy production, lipid peroxidation, oxygenation, nitration, and deamination of DNA.[4, 5] There are ramifications to excessive production of either of these reactive species in a cell leading to various pathological conditions. These free radicals can result in destruction of tissue leading to tumor progression. It also influences signal transduction cascade in a cell by activating transcription factors that have cellular response to stress, or initiate damage to DNA, lipids, and proteins that can increase the risk of mutations.[6, 7] Exposure to exogenous sources such as ionizing radiation, therapeutic drug, occupational, or habitual exposure to oxidizing agents results in the generation of free radicals and disturbs the normal cellular metabolism. The effect of these free radicals in both mt and nt DNA include depurination, DNA strand breaks, and oxidation of DNA bases.[8]

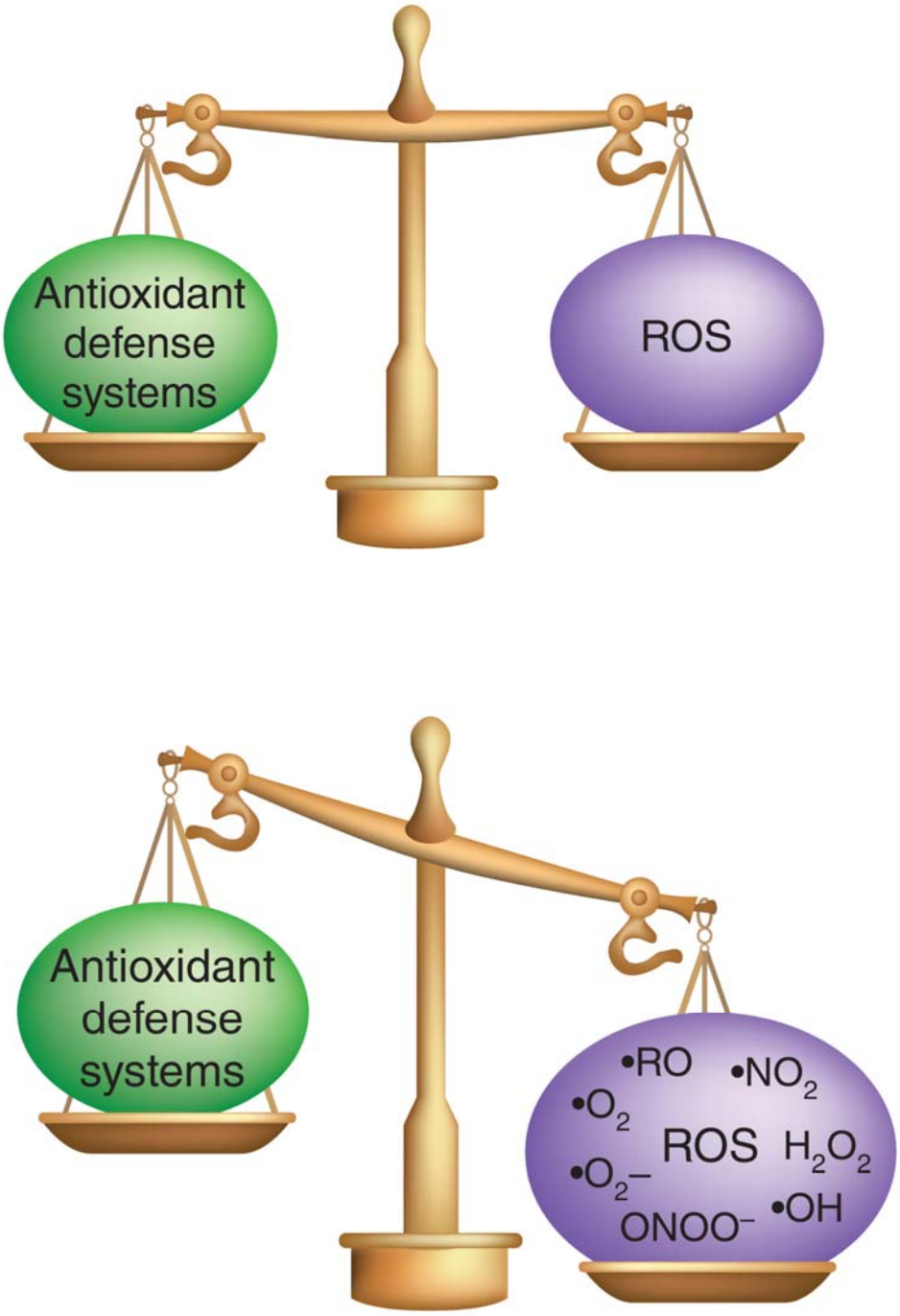

Figure 1.1. A balance between the levels of free radicals and antioxidants is important for normal functioning of a cell. Oxidative stress in a cell due to an imbalance in the production of these results in an imbalance in homeostasis and a diseased state. This figure has been adapted from Tomaselli, G. F.; Barth, A. S. *Nat. Med.* **2010**, 16, 648-649.

The mtDNA is circular and encodes two ribosomal RNAs, 22 transfer RNAs, and 13 proteins that are subunits of the oxidative phosphorylation system. Mitochondrial respiration is an endogenous source of ROS that comprises hydroxyl radical ($^{\bullet}OH$), superoxide ($O_2^{\bullet-}$), and hydrogen peroxide (H_2O_2).[9] During high metabolic demand, it is noted that ~1% of electrons leak from the electron transport system (ETS) converting molecular oxygen (O_2) to $O_2^{\bullet-}$, and a significant amount of superoxide is also liberated by the ETS.[10] An accurate functioning of the mitochondria is important to avoid imbalance in generation of ROS. Mitochondria function as an alarm system that accumulates biomarkers of stress indicating diseased state. The proximity of mtDNA to oxidative phosphorylation system accounts for higher mutational frequency in mtDNA as compared to ntDNA.[11] Deletions to the mtDNA result in Kearns-Sayer syndrome (KSS) and myopathies,[12, 13] while point mutations in mtDNA have been found in Leber's hereditary optic neuropathy (LHON).[14] More than 200 pathogenic mtDNA mutations have been identified.[15] These mutations have also been correlated to aging and neurodegenerative diseases.[16-19] Although mitochondrial disorders do not follow Mendelian inheritance like other genetic disorders, they are significant as they are exclusively inherited maternally.

Oxidation of ntDNA from both endogenous and exogenous sources results in disruption of normal cellular metabolism.[20-22] Oxidation of the four canonical DNA bases with various ROS affect cellular proliferation, damage to repair enzymes, and polymerases and result in enzymatic infidelity during replication. Also, binding of the end products of lipid peroxidation to DNA results in mutagenesis.[23] Chronic inflammation, exposure to radiation, and cigarette smoke are all known to cause DNA oxidation by free radicals. The physiologically relevant hydroxyl radical can react either with C-4, C-5, and C-8 positions

of purines or C-4 and C-5 of pyrimidines. DNA oxidation by highly reactive radicals yields various pyrimidine and purine adducts; some of these are thymine glycol (Tg), 5-hydoxycytosine (5-hC), 2,6-diamino-4-hydroxy-5-formamidopyrimidine (Fapy-G or Fapy-A), 8-hydroxy adenine, and numerous other oxidation products.[24]

Oxidation of 2'-deoxyguanosine

The most vulnerable purine to oxidation is 2'-deoxyguanosine (dG) because of its low redox potential with $E°$ of 1.29 V vs. NHE at pH 7 (Figure 1.2).[25] In Chapter 2, we discuss the oxidation of dG using the nickel-mediated square planar complex, NiCR and $KHSO_5$ resulting in exclusive formation of a relatively new oxidation product 2-iminohydantoin (2-Ih) that is a lesion.[26] dG reacts by one-electron oxidation to form a guanine radical cation ($dG^{\bullet+}$) that can form a plethora of oxidation products including 8-oxo-7,8-dihydro-2'-deoxyguanosine (8-oxo-dG).[27, 28] 8-oxo-dG is formed by hydration followed by one-electron oxidation of the guanine radical cation. The chemistry of dOG has been of great significance as it is the most common oxidative lesion studied. It is an important biomarker to monitor oxidative stress in a cell that reaches levels of 0.1- 4.0 per 10^6 dGs in the ntDNA.[29, 30] If left unrepaired, it can result in dG to T transversion mutations.[31] Increased levels of dOG have been reported in the early stages of patients with Alzheimer's disease in both mt and ntDNA.[32]

8-Oxo-dG is further susceptible to oxidation because of its lower redox potential of 0.7 V vs. NHE at pH 7 .[33] 8-Oxo-dG can undergo further two-electron oxidation to form the lesions spiroiminodihydantoin-2'-deoxyribonucleoside (dSp) and 5-guanidinohydantoin-2'- deoxyribonucleoside (dGh).[34-36] The formation of these products

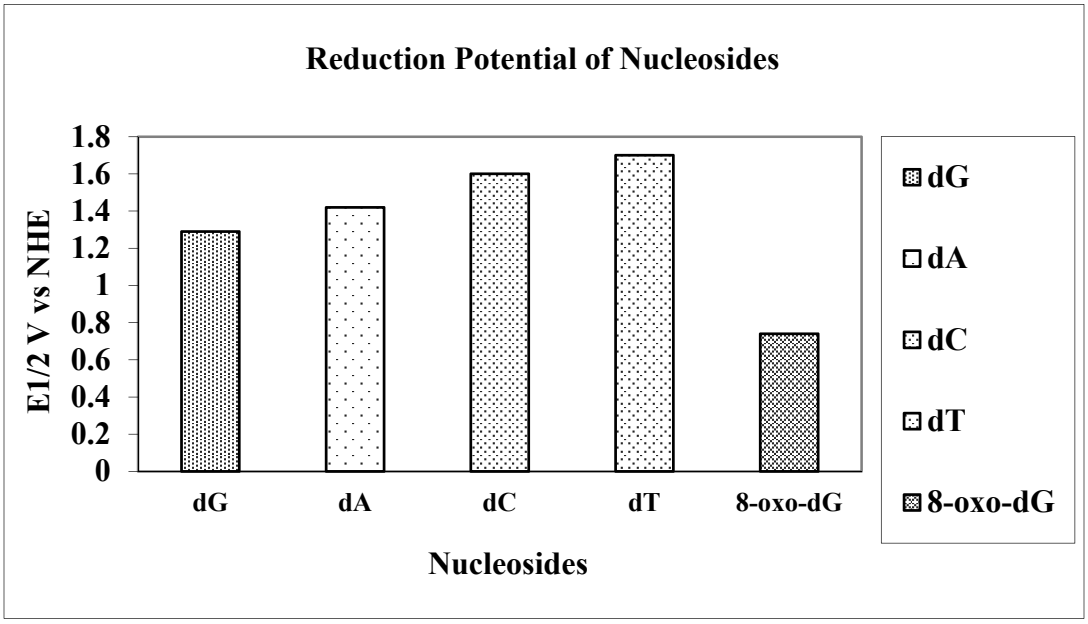

Figure 1.2. The redox potential of the four nucleosides at pH 7 vs. NHE. The redox potential of 8-oxo-G, the most common oxidation product is lower than G.

products is both pH and sequence context dependent.[34, 35, 37, 38] dGh is a major oxidation product in duplexes or in reactions at lower pH (<5.8) whereas in nucleosides and G-quadruplex, dSp is the major oxidation product, as it is at high pH (>5.8) (Scheme 1.1).[37, 39-41] These hydantoin lesions have also been observed as oxidation products of dG or 8-oxo-dG with various radicals such as $^{\bullet}OH$, $CO_3^{\bullet-}$, $^1O_2$ and high valent transition-metal species.[26, 34, 35, 37, 40, 42]

dSp was first detected in *Escherichia coli,*[43] whereas both dSp and dGh have been quantified in mouse model of inflammation leading to colon cancer.[44] These lesions result in G to C and G to T transversion mutations if left unrepaired in a cell and are 100% mutagenic.[45-47] The hydantoin lesions exist as two diastereomers that can be separated and purified by HPLC.[48] Recently, the *R* and *S* absolute configurations for the dSp diastereomers were assigned using enzymatic, chemical, spectroscopic, and computational methods in the Burrows laboratory.[49]

DNA repair to prevent lesion persistence

Measurement of these oxidation products is the most common method of assessing oxidative stress. It has been suggested that cell death is a potential source of 8-oxo-dG or 8-oxo-G in urine excretion. Some reports suggest an increase in urine excretion of 8-oxo-dG because of exposure to radiotherapy or chemotherapy.[50-52] The presence of oxidation products in extracellular fluids alludes to the enzyme activity involved in repair pathways or oxidation of the nucleoside pool. The conservation of genetic information despite the presence of damaged bases has propelled scientists to discover DNA damage-specific repair enzymes. The main oxidative damage repair pathway is the base excision repair

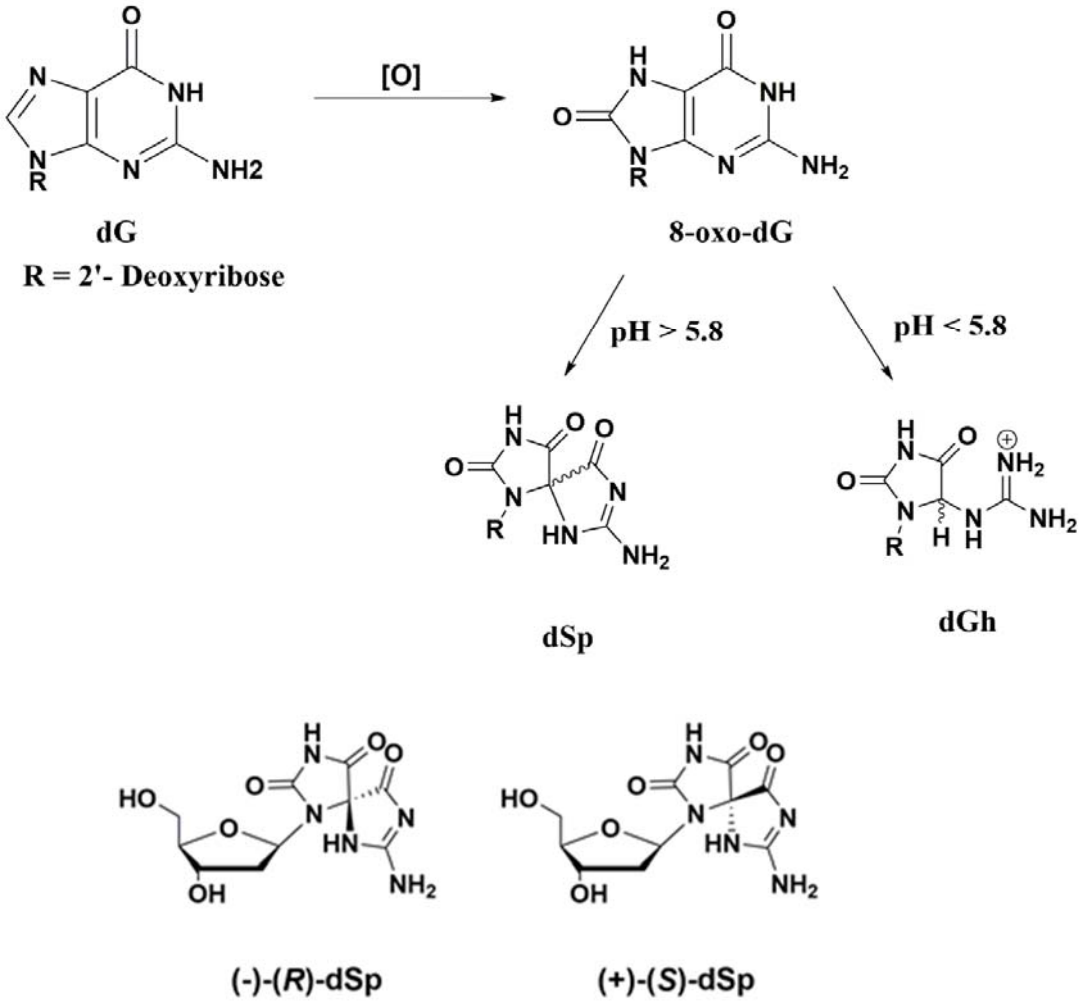

Scheme 1.1. The two-electron oxidation of dG to form 8-oxo-dG, a biomarker of oxidative stress. 8-oxo-dG further oxidizes to hydantoin lesions, dSp and dGh based on pH and sequence contexts. The diastereomers of dSp are also shown.

(BER) that confirms the discovery and use of specific glycosylases that cleave the damaged base from the DNA. The role of nucleotide excision repair (NER) is more complex and entails removal of lesion-containing longer DNA strands.

BER is a highly conserved repair pathway in both prokaryotes and eukaryotes and results in removal of a majority of damaged bases including oxidized, depurinated, deaminated, alkylated bases, and strand breaks in DNA.[53, 54] The BER pathway has been studied in detail in chromatin, and in telomeres, and it also plays an important role in gene regulation and posttranslational modifications. Since the discovery of the first DNA glycosylase enzyme by Lindahl, uracil-DNA glycosylases (UDG) that removes uracil from DNA, BER is a significant repair pathway studied.[55] Among the four steps in BER (Figure 1.3), the first step involves search for the damaged base or lesion in DNA by the DNA glycosylases.[56, 57] So far, several DNA glycosylases have been discovered that remove oxidative lesions, and most are bifunctional (except NEIL3), meaning they not only cleave the damaged base, but also cleave the DNA backbone leaving an α,β-unsaturated aldehyde or a phosphate at the 3'-end of the nick. The sugar is removed by phosphodiesterase activity of an apurinic endonuclease (APE1) and the phosphate group added by polynucleotide kinase (PNK) that adds 3'-phosphate. DNA polymerase β (Pol β) also has lyase activity that can beta remove the remaining uncleaved sugar attached to the 5'-phosphate. After the gap is filled using pol β, it is sealed by a DNA ligase.

There are structural and functional homologs of DNA glycosylases that repair oxidative base damage in both bacteria and humans.[58, 59] We will mainly focus on the enzymes in BER associated with the removal of 8-oxo-G and Sp diastereomers. Oxidation to 8-oxo-G in DNA can result in disruption of Watson-Crick (WC) base pairing (bp), 8-

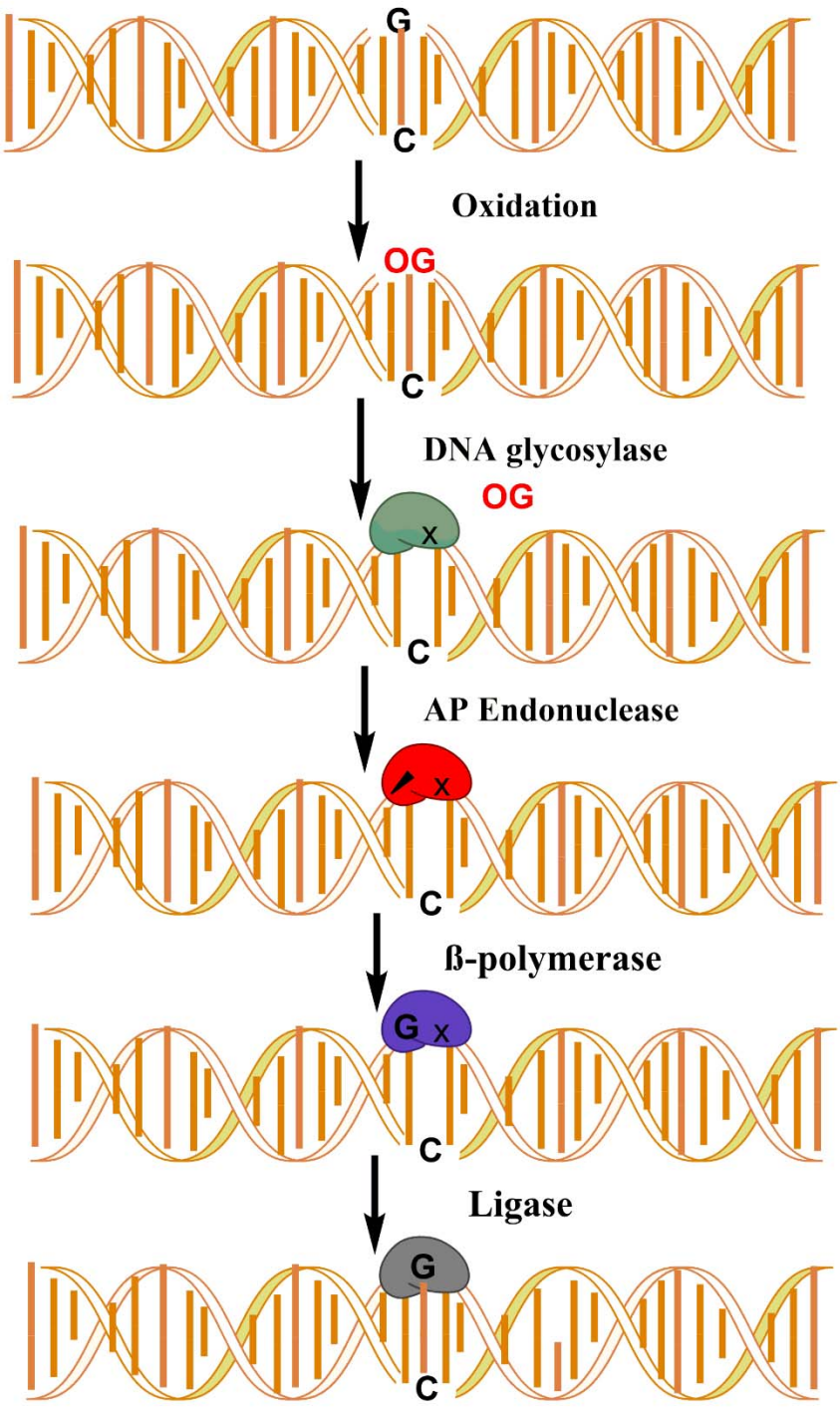

Figure 1.3. A representation of BER pathway involved in the identification and excision of damaged bases. The different color coded globules on the dsDNA indicate different enzymes involved in BER that are mentioned along the arrow before its function.

oxo-G in the *syn* confirmation mimics T and pairs with A(*anti*), whereas the 8-oxo-G(*anti*) forms a stable bp with C(*anti*). The crystal structure of DNA polymerase I fragment (BF) from *B. stearothermophilus* indicates that a 8-oxo-G(*syn*)•A(*anti*) bp is inaccurately bypassed as it mimics a normal bp, whereas 8-oxo-G(*anti*)•C(*anti*) disrupts the template and polymerase during replication.[60] The glycosylases Fpg, MutY, and MutT in *E. coli*[61] and MUTYH, OGG1, and MTH1 in humans[62] constitute the 8-oxo-G repair pathway. Hydrolysis and removal of 8-oxo-G occurs by MutT (or MTH1), that prevents incorporation of damage by DNA polymerase. MutM (or OGG1) glycosylases excise 8-oxo-G from 8-oxo-G•C bp whereas Fpg (or MUTY) intercepts 8oxo-G•A bp and removes A. Structural studies show that 8-oxo-G containing oligomers in pol-β of eukaryotes accommodates the 8-oxo-G•C bp better than 8-oxo-G•A mismatch that is opposite of what is found for the bacterial polymerase BF.[63]

The hydantoin lesion Sp is known to be a substrate for *E. coli* Fpg (MutM); however, the excision of Sp opposite A was less than that opposite C, though greater than removal of 8-oxo-G in these base pairs.[64] Endonuclease VIII (Nei), a bacterial DNA glycosylase, can also remove the hydantoin lesions that have a WC hydrogen-bonding face.[65] Sp was detected on chromate oxidation of repair-deficient (Nei^{-}) *E. coli* by mass spectrometry. Mammalian orthologs of *E. coli* Nei are called Nei-like (NEIL) and include a family of enzymes consisting of NEIL1, NEIL2, and NEIL3.[66-68] NEIL1 and NEIL2 operate on lesions in ssDNA, dsDNA, and bubbled structures to remove the hydantoin lesions.[69, 70] NEIL3 is found in cancerous or proliferating cells where its expression is thought to increase in S-phase.[71] All crystallographic studies done on glycosylases so far

indicate identification of the damaged base and flipping the base out of the helix into the substrate binding pocket followed by cleavage of the N-glycosidic bond.[72-74]

NER is generally a repair pathway for bulky adducts of cyclobutane pyrimidine dimers, DNA-protein crosslink (DPC), and bulky alkylated adducts as it removes short DNA strands containing lesions.[75] However, they seem to act as a 'back up' repair mechanism to mediate excision of 8-oxo-G in mouse cells lacking OGG1.[76, 77] NER is a major repair pathway in neurons that requires TFIIH transcription-repair complex with helicase activity that unwinds the DNA for repair.[78] The UvrABC proteins initiate and function in a coordinated fashion in prokaryotes to locate and excise lesion-containing DNA by NER.[79, 80] It was found that both the 8-oxo-G, hydantoin products and the bulky Sp-amine adducts were recognized by UvrABC in NER (Figure 1.4).[81] Thus, these oxidation products are reminiscent of both NER and BER pathways.

Detection methods

Several biological and chemical methods have been used to detect or quantify the damaged nucleobases and nucleosides. The biological methods include the comet assay,[82] ELISA,[83] and ^{32}P post -labelling methods.[84] In the comet assay, the DNA with strand breaks migrates faster than normal DNA to form a comet-like streak on a gel, and this was first observed using fluorescence.[85, 86] The ^{32}P postlabeling method involves enzymatic digestion of DNA to nucleoside-3'-monophosphates that are radioactively labeled by T4-polynucleotide kinase and [γ^{32}P]-ATP. The nucleoside-3',5'-biphosphate adducts formed are separated by thin-layer chromatography (TLC).[87] Other methods include electrochemical detection (EC), GC-MS,[88] LC-MS, and HPLC coupled to tandem mass

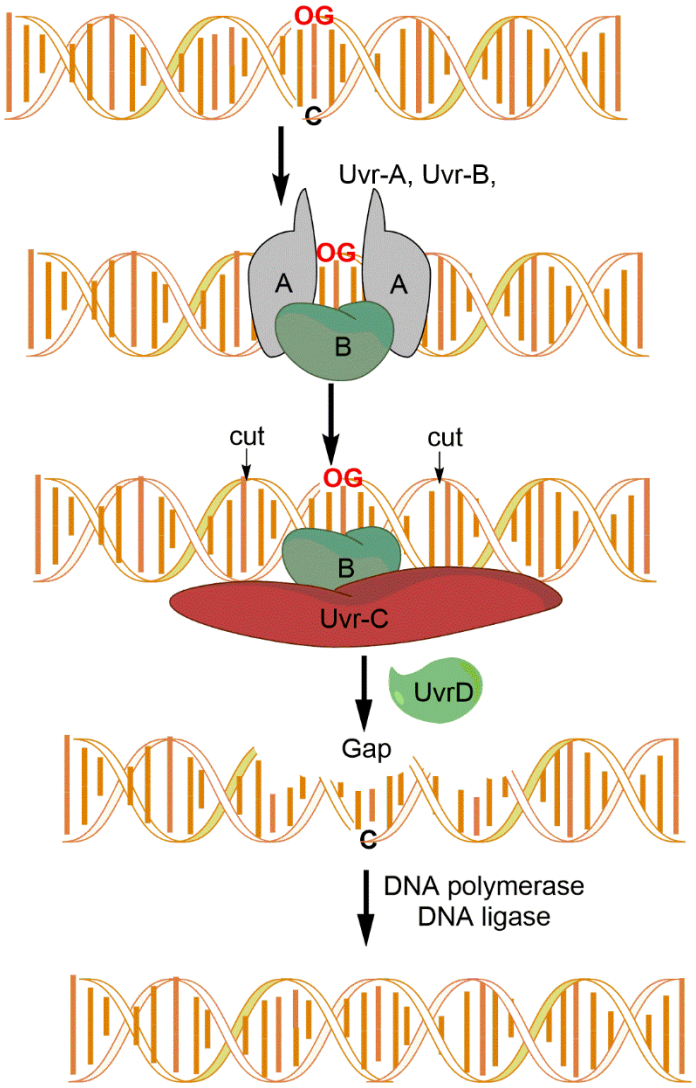

Figure 1.4. A representation of the NER pathway involved in the identification and excision of damaged bases. The labels A and B indicate UvrA dimer and UvrB protein units involved in the detection.

spectrometry (MS/MS) as a sensitive and selective method used in detection of lesions.[89] Recently, fluorescent probes that recognize 8-oxo-dG have been developed.[90-92]

Antibodies have been used for detection; however, they have certain limitations with respect to the timeline of generation and the requirement of animal or cell lines for discovery, and production and also develop an immunological response. Antibodies can be derivatized with small-molecule dyes using an amine linkage and these antibodies can differ in their properties from one lot to another or require secondary antibodies as an alternative for detection. Antibodies are byproducts of an animal's immune response, and therefore, have batch-to-batch variations. Recently, Trevigen has launched a mouse anti-8-oxo-dG monoclonal antibody that can detect 8-oxo-dG in DNA at very low nM concentrations.

A controlled combinatorial method using nucleic acids might be advantageous for detection. Nucleic acids are robust binding agents with great shelf-life and easy production and they do not require an animal host in production, and can be derivatized easily, unlike antibodies.

SELEX technology and aptamers

Nucleic acids are versatile macromolecules that function as carriers of genetic information, gene regulation, or catalysis and therefore have garnered a great deal of attention in recent years.[93-96] These nucleic acids have a propensity to fold in a specific and intricate three-dimensional manner. The structure, variability, and adaptability of these molecules define their functional diversity. Nature has not disregarded this biomolecular recognition, as it is known from the discovery of naturally occurring riboswitches.[97]

Riboswitches are known to regulate gene expression by a change in conformation mediated by binding to a metabolite, in response to physiological conditions.[98, 99] The sparked interest toward these macromolecules is due to an ever-increasing number of discoveries with catalytic or binding function. These so called "functional nucleic acids" are also derived by *in vitro* selection.

An iterative method for *in vitro* selection of functional nucleic acids was introduced and called 'systematic evolution of ligands by exponential enrichment' (SELEX). SELEX experiments were first performed in 1989-1990 by three different groups Oliphant et al.,[100] Ellington and Szostak,[101] and Tuerk and Gold,[102] separately. The products of selection were called 'aptamers' (aptus means 'to fit' and meros means 'piece or part'). The first RNA aptamer was developed by Tuerk et al. for bacteriophage T4 DNA polymerase (a protein) and by Ellington for organic dyes (small molecules). The first DNA aptamer was reported for adenosine and ATP (K_D 6 μM).[103] The choice of either an RNA or DNA aptamer depends on practical considerations and final applications of the system.

The aptamer functionality is based on the 3D-structures characterized by stems, loops, bulges, hairpins, pseudoknots, triplexes, or quadruplexes formed by interaction with a target. The intermolecular interaction or binding between the aptamer and the target results from structural compatibility, complementarity in shape, stacking interactions between aromatic groups, electrostatic interactions between charged groups, van der Waals interactions, and hydrogen bonding or a combination of these effects.[104-108]

Aptamers have been selected for a wide variety of targets that include small molecules and large proteins to a whole cell of interest.[109, 110] Initially, aptamers were developed mostly for small molecules that include metal ions,[111-113] organic dyes,[102] amino

acids,[114-117] antibiotics,[118-120] and nucleotides.[103, 121, 122] Larger targets include co-factors,[123-126] proteins,[127-129] cells,[130-132] viruses,[133-135] and bacteria.[136, 137] According to an aptamer database, most aptamers are developed as RNA aptamers with preference for large targets, especially proteins. These macromolecules with various amino acids have more functional groups and structural motifs that resulting in a higher probability of finding sequences that can interact with target via various interactions (Figure 1.5). Despite this trend, there is an urge to pursue small molecule-binding aptamers. These smaller targets play an important role in biological process and can help understand several intricate physiological process. Aptamers for detection of carcinogens and metal ions might have several applications that will be discussed towards the end of this chapter. The smallest known molecular target for an aptamer selection is ethanolamine (K_D of 6 nM); however, recently aptamers have also been selected for various cations.[138]

A typical SELEX process is universally characterized by repetition of five steps: binding, partitioning, elution, amplification, and conditioning (Figure 1.6). Four important factors are involved in designing the pool, namely: type of randomization, length of randomization, benefit of constant regions, and chemistry of the pool.[139] The most successful aptamers have been selected from 1 in 10^9 to 1 in 10^{13} molecules from a starting random library.[140, 141] Each oligonucleotide has a random region with 20-80 nt that is flanked by regions of fixed sequences of 15-20 nt and that are primer binding sites during amplification. The shorter randomized libraries are manageable and cost effective for synthesis. However, the larger randomized libraries provide sequence and structural diversity.[139] Since the library is commercially synthesized, a large-scale amplification of the starting library is mostly recommended before initiating the SELEX process in order to

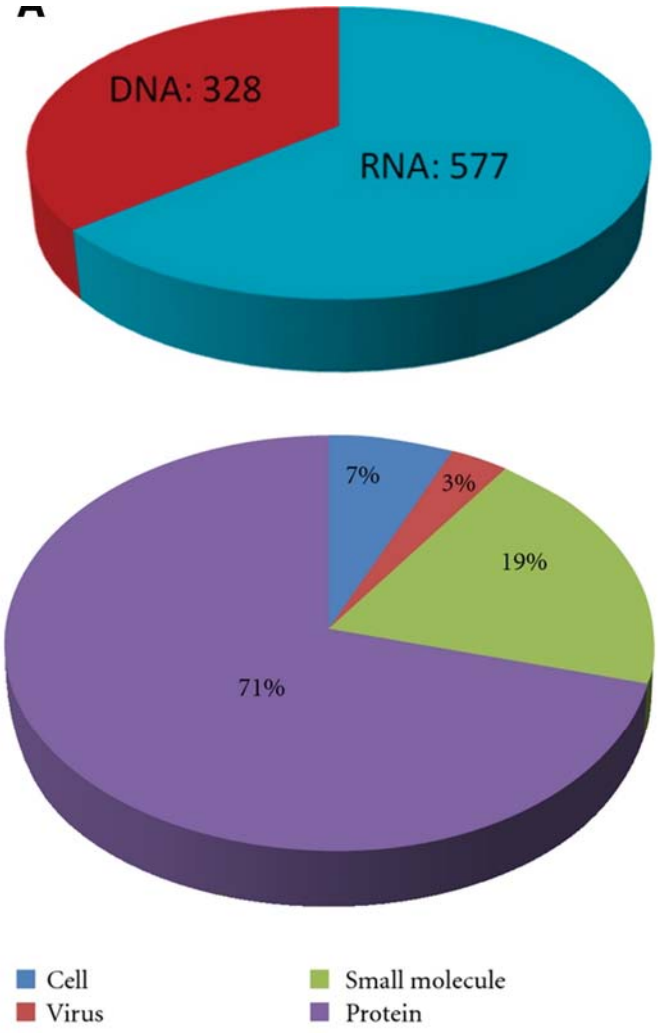

Figure 1.5. The breakdown of aptamers into DNA and RNA (above) and the distribution of targets (below) chosen for aptamer selection collected from the aptamer database.

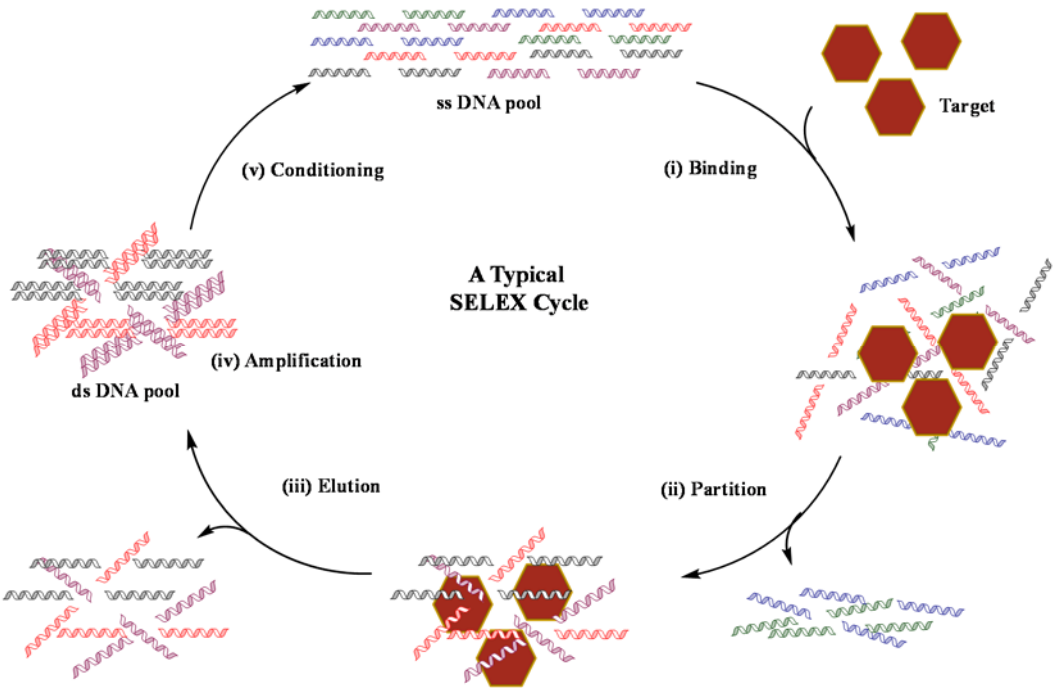

Figure 1.6. A typical SELEX cycle showing five steps: (i) binding to the target, (ii) partition of the bound and unbound sequences, (iii) elution of the bound sequences, (iv) amplification of eluted strands by PCR, and (iv) conditioning of dsDNA to convert to ssDNA pool to be used in next cycle.

eliminate damaged DNA synthesis products. Initial amplification of the pool also provides multiple copies of the original sequence that can serve as templates. The dsDNA is either transcribed to RNA by T7 RNA polymerase for RNA SELEX or converted to ssDNA and used for DNA SELEX. Because amplification by PCR introduces some level of mutation, the term "evolution" aptly describes the selection and mutation process.

The pool or library is incubated with a target under specific buffer, temperature conditions, and incubation time that depends on the requirements for the particular target. The presence of monovalent cations in the buffer reduces nonspecific binding, and for some targets, divalent cations are important to form the complex. The selection starts with a low ratio of library to target in order to bind all ligand molecules to target. The initial rounds are less stringent and have long incubation times with the target.

Negative selection is done in the absence of target to eliminate nonspecific binders or the background strands.[142] The nonspecific binders are predominant in the initial rounds and hence, multiple rounds of SELEX are performed to eliminate these background strands.[143] Later rounds are made more stringent to obtain specific binders by changing buffer composition, incubation times, or decreasing target concentrations. There is an exponential increase in selected sequences as specific binders during the later rounds of SELEX.[144, 145] This justifies the term "exponential" as there is an exponential increase in binding affinity in the SELEX acronym.

After incubation, separation of the bound aptamer-target complex is done from unbound sequences by various partitioning methods. The conventional method used for partition included affinity chromatography using agarose or sepharose[146] or ultrafiltration by nitrocellulose membranes.[143] Several modifications have been done to partitioning

methods in SELEX depending on the target.[110] Some of the most common ones include: capillary electrophoresis (CE)-SELEX where partition is done using CE,[147] covalent SELEX where the aptamers containing reactive groups link covalently to a target,[148] and cell-SELEX generates aptamers for a specific cell of interest especially cancer cell lines.[149] FluMag SELEX is recently developed where the target is bound to magnetic beads and the library is modified with fluorophore for quantification purposes[150] and structure-switching SELEX that immobilizes the library on the column instead of a target.[151] Recently, next generation SELEX was done using a designed library that tiles through mRNA sequence.[152]

The bound sequences are eluted from the column by using denaturing conditions like heat treatment[150] or adding denaturing reagents like urea,[153] sodium dodecyl sulfate (SDS),[154] or EDTA[155]. These eluted rare strands are amplified by PCR and the amplicons are further conditioned to purify the relevant single-stranded sequences. The amplified pool needs to be prepared for the next cycle, and conditioning involves converting these dsDNA to form RNA or ssDNA. Transcription is done for conversion of dsDNA to RNA aptamers, whereas, separation of dsDNA is done to generate ssDNA aptamers. This can be achieved in several ways that have been developed and widely used. The biotinylation of an unwanted or antisense strand can aid in removing this strand on the streptavidin column.[156] Another method involves using a 3'-terminus ribose residue (rU) in the antisense primer that cleaves the dsDNA using NaOH (Figure 1.7).[157] Denaturing PAGE is the most commonly used method to convert the dsDNA into ssDNA and is based on detectable differential migration of two strands by UV shadowing.[158, 159] This principle can also be applied to fluorescent labeled sense primer that are used in PCR and strand separation can be detected by fluorescence.[150] The antisense strand in such cases has a hexaethyleneglycol

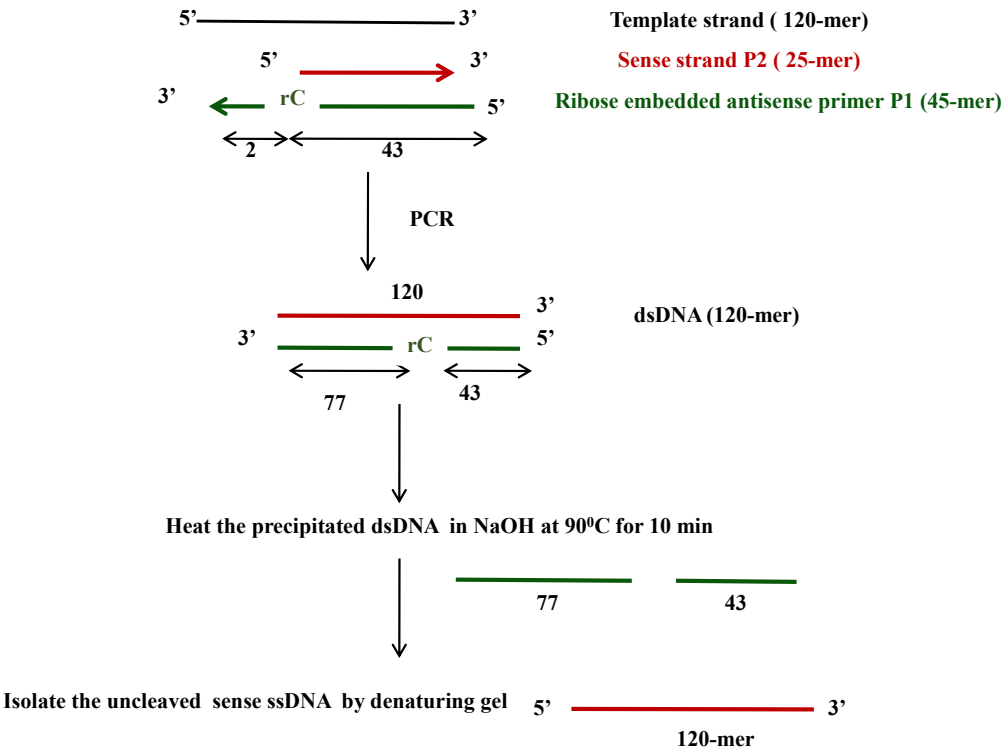

Figure 1.7. The pictorial representation of the one of the several methods of conditioning that uses ribonucleoside (rC) and treatment with NaOH to further purify the ssDNA pool by denaturing PAGE.

(HEGL) spacer poly-A_{20} tail to increase the length and aid in separation of the strands.[160] Another method involves the use of lambda exonuclease that uses a 5'-phosphorylated antisense strand of dsDNA as a substrate (Figure 1.8).[161]

After 6-15 iterative rounds of selection, amplification, and conditioning, the target-binding ligands are enriched and the complexity of the starting library is greatly reduced. The final pool is PCR amplified, cloned into a vector, and the colonies are sequenced. Sequences for around 50 colonies are identified and sequence alignment is done to determine the homology in sequences. The aptamers are grouped based on most identical sequences. The analysis of secondary structure of aptamers by M-fold can provide information on the relevant structures for binding.

Subsequently binding studies are performed to determine the affinity of the aptamers to the target. The dissociation constant (K_D) is an important and characteristic parameter for an aptamer that does not depend on size, quantity, or complexity of the target. A lower K_D value for an aptamer indicates high binding affinity to the target. Several methods for determining the K_D have been developed that include separation-based methods,[162-164] spectroscopy-based methods,[165-168] and mass-sensitive surface-based methods.[169, 170] Most of the separation-based and mass-sensitive methods are challenging to use for the smaller targets as they have less effect on the separation of the complex and the aptamer.

The spectroscopy-based methods include fluorescence intensity method where the aptamer or target fluorescence is quenched or increased upon binding.[165] UV-vis absorption is based on the change in wavelength or intensity of absorption of the aptamer or the target upon binding.[167] Melting studies are also conducted to determine K_D.

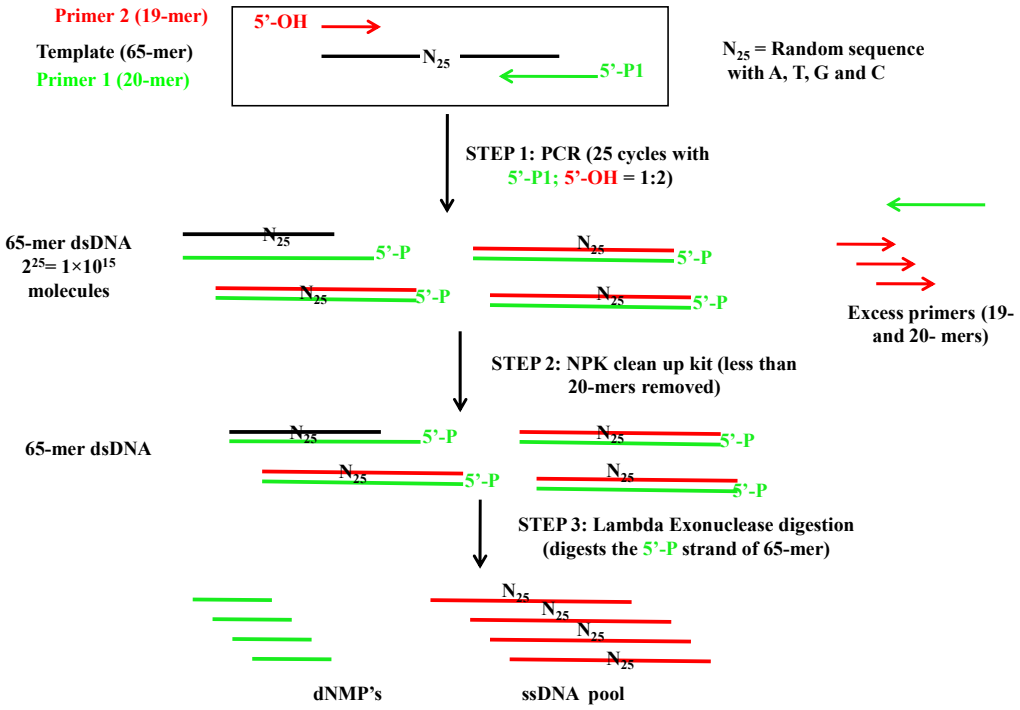

Figure 1.8. The pictorial representation of the one of the several methods used in conditioning the dsDNA pool to convert and purify to ssDNA pool before use in the next round of SELEX.

dichroism (CD) spectra may change significantly because of the difference in conformation upon binding to target.[168] The method used for K_D determination entirely depends on the type of target used, and sometimes several methods need to be tested in order to choose the one that works.

Post-SELEX modifications are done to either increase the stability of the aptamer or optimize binding parameters to the target. Sequences are truncated to narrow down the binding region of the aptamer to the target. The regions that do not account for any direct interaction with the target, or for folding into a structure that binds the target are truncated. There are several examples reported where truncated aptamers have higher binding affinities.[171, 172] An aptamer binding affinity or specificity can be increased by a selection process in which the existing aptamer is modified or mutagenized in order to generate a new diversified library.[122] Mutagenesis can be done by error-prone PCR[173] or random fragmentation on the preselected aptamer.[173]

In order to enhance biostability of RNA aptamers, 2'-OH modifications are done to 2'-F or 2'-NH_2 to protect from nuclease degradation.[174, 175] Locked nucleic acids (LNA) can also be used to prevent nuclease degradation.[176] However, DNA aptamers offer an advantage of stability as compared to RNA aptamers. Exonuclease degradation can be prevented by either 3'-end (inverted dT or streptavidin-biotin) or 5'-end (polyethylene-glycol (PEG), cholesterol, fatty acids) capping.[177, 178]

Aptamers are recently applied for innovative applications in the field of chemical biology.[179, 180] In therapeutics, several aptamers for their targets are being tested. In 2004, Macugen (Pegatnib) became the first and only know FDA approved aptamer-based therapeutic for age-related macular degeneration.[181] A PEGylated form of antivascular

epithelial growth factor (VEGF) aptamer is an active medical component in treatment. Aptamers, because of their small size, can penetrate into cells and tissues easily, and therefore can be used for *in vivo* imaging purposes.[182] They can also be used as molecular detection systems for purification, separation, and quantification of analytes using CE and electrochromatography.[183] Aptamers also play a very important role as biosensors and help in monitoring drug levels in blood, detecting environmental contaminants, or monitoring carcinogens.

Aptamer beacons also called signaling aptamers,[184] aptamers coupled to quantum dots,[185] gold nanoparticles,[186] or electrochemical platform[187] have established the role of aptamers in biosensing. Aptamers can be coupled with other functional moieties without affecting their ability to recognize a cognate target are used to develop regulatory elements called DNAzymes or aptazymes.[188] Allosteric approaches to modular aptamers have been developed for sensing. For example, malachite green (MG) aptamer coupled to a flavin mononucleotide (FMN) aptamer where the fluorescence increases only if FMN is bound to the domain of the coupled aptamer.[184] Intramers, aptamers binding to intracellular protein targets, are important tools in protein-based networks *in vivo*.[189]

Aptamers have limitations in terms of their tertiary structure that is dependent on solution conditions. The other limitations like nuclease degradation and chemical diversity have been combated by using base modifications or spiegelmers. Additionally, there are no immunological responses to aptamers as compared to antibodies. Aptamers can be produced in large scale, easily derivatized regioselectively for detection using dyes, and they are stable indefinitely at room temperature when dry. Aptamers, in the coming years, will have widespread application in the field of therapeutics, diagnostics, and combating

infectious diseases. The understanding of riboswitches is also likely to spur development in the field of aptamers. Since they mimic features of monoclonal antibodies, aptamer technology is developing into a major tool with commercial potential.

The aim of my research initially was to study the products of guanine oxidation using nickel-mediated transition metals. Chapter 2 is aimed at studying damaged guanine oxidation products and to optimize the oxidation conditions to generate 2-Ih as an exclusive product of oxidation of guanine in nucleoside and ssDNA.

The Burrows lab developed various methods for detection of the various damaged bases. One of the methods has been using nanopore technique to study modified bases or damages in the DNA by studying the variations in current-time traces.[190, 191] Aptamers have been used for detection of a wide variety of targets, including nucleosides. The ultimate goal of my research is to select sensors that are selective to the damaged nucleobases that are the products of repair pathways in the cell. The aim was to develop a SELEX method that can be applied to the challenging modified nucleobases and nucleosides.

In Chapter 3, I will discuss in detail, structure-switching SELEX applied to select aptamers for the various damaged guanine oxidation products as targets. The sequences identified and the binding studies of designed sensors are also discussed in this chapter. The concentrations of the target is low: 8-oxo-dG in a cell is about 8 nM, whereas the hydantoin dSp is ~500 nM.[44] All the damaged bases are present in lower concentration than the normal bases and hence the need for new selective methods for detection with high binding affinity (low K_D value).

Sensors are reported for 8-oxo-G as a nucleoside and within a DNA strand. The DNA aptamer identified for 8-oxo-guanine has a K_D of 5.5 μM.[103] Later, an aptamer sensor

was developed to detect 8-oxo-G in a triplex with a detection limit of 5 nM._ENREF_192 Aptamers have not been reported so far for the hydantoin lesions, dSp (both diastereomers) and Sp nucleobase. The structure-switching method is being applied for the first time to develop aptamer sensors against these damaged bases. Through a series of rounds of SELEX and negative selection, we aim to develop aptamers with high binding affinity for these targets.

References

1. Babior, B. M. Phagocytes and oxidative stress. *Am. J. Med.* **2000,** 109, 33-44.
2. Aggarwal, B. B.; Shishodia, S.; Sandur, S. K.; Pandey, M. K.; Sethi, G. Inflammation and cancer: How hot is the link? *Biochem. Pharmacol.* **2006,** 72, 1605-1621.
3. Orient, A.; Donkó, Á.; Szabó, A.; Leto, T. L.; Geiszt, M. Novel sources of reactive oxygen species in the human body. *Neph. Dial. Transplant.* **2007,** 22, 1281-1288.
4. Lacza, Z.; Kozlov, A. V.; Pankotai, E.; Csordás, A.; Wolf, G.; Redl, H.; Kollai, M.; Szabó, C.; Busija, D. W.; Horn, T. F. W. Mitochondria produce reactive nitrogen species via an arginine-independent pathway. *Free Rad. Res.* **2006,** 40, 369-378.
5. Ichinose, M.; Sugiura, H.; Yamagata, S.; Koarai, A.; Shirato, K. Increase in Reactive Nitrogen Species Production in Chronic Obstructive Pulmonary Disease Airways. *Am. J. Resp.Crit. Care Med.* **2000,** 162, 701-706.
6. Closa, D.; Folch-Puy, E. Oxygen Free Radicals and the Systemic Inflammatory Response. *IUBMB Life* **2004,** 56, 185-191.
7. Marnett, L. J. Oxyradicals and DNA damage. *Carcinogenesis* **2000,** 21, 361-370.
8. Wiseman, H.; Halliwell, B. Damage to DNA by reactive oxygen and nitrogen species: role in inflammatory disease and progression to cancer. *Biochem. J.* **1996,** 313, 17-29.
9. Boveris, A. Mitochondrial Production of Superoxide Radical and Hydrogen Peroxide. *Adv. Exp. Med. Biol.* **1997,** 78, 67-82.
10. Papa, S. Mitochondrial Oxidative Phosphorylation Changes in the Life Span. Molecular aspects and Physiopathological Implications. *Biochim. Biophys. Acta* **1996,** 1276.
11. Brown, W. M.; George, M.; Wilson, A. C. Rapid evolution of animal mitochondrial DNA. *Proc. Nat. Acad. Sci.* **1979,** 76, 1967-1971.
12. Zeviani, M.; Moraes, C. T.; DiMauro, S.; Nakase, H.; Bonilla, E.; Schon, E. A.; Rowland, L. P. Deletions of mitochondrial DNA in Kearns-Sayre syndrome. *Neurology* **1988,** 38, 1339-1346.
13. Holt, I. J.; Harding, A. E.; Morgan-Hughes, J. A. Deletions of muscle mitochondrial DNA in patients with mitochondrial myopathies. *Nature* **1998,** 331, 717 - 719.
14. Wallace, D. C.; Singh, G.; Lott, M. T.; Hodge, J. A.; Schurr, G. T.; Lezza, A. M. S.; Elsas Ii, L. J.; Nikoskelainen, E. K. Mitochondrial DNA mutation associated with Leber's hereditary optic neuropathy. *Science* **1988,** 242, 1427-1430.
15. McFarland, R.; Taylor, R. W.; Turnbull, D. M. Mitochondrial Disease—Its Impact, Etiology, and Pathology. In *Curr. Top. Dev. Biol.*, Justin, C. S. J., Ed. Academic Press: 2007; Vol. Volume 77, pp 113-155.
16. Lauritzen, K. H.; Moldestad, O.; Eide, L.; Carlsen, H.; Nesse, G.; Storm, J. F.; Mansuy, I. M.; Bergersen, L. H.; Klungland, A. Mitochondrial DNA Toxicity in Forebrain Neurons Causes Apoptosis, Neurodegeneration, and Impaired Behavior. *Mol. Cell. Biol.* **2010,** 30, 1357-1367.

17. de Souza-Pinto, N. C.; Wilson Iii, D. M.; Stevnsner, T. V.; Bohr, V. A. Mitochondrial DNA, base excision repair and neurodegeneration. *DNA Repair* **2008,** 7, 1098-1109.

18. Gredilla, R.; Bohr, V. A.; Stevnsner, T. Mitochondrial DNA repair and association with aging – An update. *Exp. Gerontol.* **2010,** 45, 478-488.

19. Taylor, R. W.; Turnbull, D. M. Mitochondrial DNA mutations in human disease *Nat. Rev. Genet.* **2005,** 6 389–402.

20. Ames, B. N. Endogenous Oxidative DNA Damage, Aging, and Cancer. *Free Rad. Res.* **1989,** 7, 121-128.

21. Saul, R. L.; Ames, B. N. Background Levels of DNA Damage in the Population. In *Mechanisms of DNA Damage and Repair*, Simic, M.; Grossman, L.; Upton, A.; Bergtold, D., Eds. Springer US: 1986; Vol. 189, pp 529-535.

22. De Bont, R.; van Larebeke, N. Endogenous DNA damage in humans: a review of quantitative data. *Mutagenesis* **2004,** 19, 169-185.

23. Cadet, J.; Sage, E.; Douki, T. Ultraviolet radiation-mediated damage to cellular DNA. *Mutat. Res.* **2005,** 571, 3-17.

24. Cooke, M. S.; Evans, M. D.; Dizdaroglu, M.; Lunec, J. Oxidative DNA damage: mechanisms, mutation, and disease. *FASEB J.* **2003,** 17, 1195-1214.

25. Steenken, S.; Jovanovic, S. V. How Easily Oxidizable Is DNA? One-Electron Reduction Potentials of Adenosine and Guanosine Radicals in Aqueous Solution. *J. Am. Chem. Soc.* **1997,** 119.

26. Ghude, P. S.; Schallenberger, M. A.; Fleming, A. M.; Muller, J. G.; Burrows, C. J. Comparison of transition metal-mediated oxidation reactions of guanine in nucleoside and single-stranded oligodeoxynucleotide contexts. *Inorg. Chim. Acta* **2011,** 369, 240-246.

27. Burrows, C. J.; Muller, J. G. Oxidative Nucleobase Modifications Leading to Strand Scission. *Chem. Rev.* **1998,** 98, 1109-1152.

28. Pratviel, G.; B., M. Guanine Oxidation: One- and Two-Electron Reactions. *Chem. Eur. J.* **2006,** 12, 6018-6030.

29. Matter, B.; Malejka-Giganti, D.; Csallany, A. S.; Tretyakova, N. Quantitative analysis of the oxidative DNA lesion, 2,2-diamino-4-(2-deoxy-β-d-erythro-pentofuranosyl)amino]-5(2H)-oxazolone (oxazolone), in vitro and in vivo by isotope dilution-capillary HPLC-ESI-MS/MS. *Nucleic Acids Res.* **2006,** 34, 5449−5460.

30. Collins, A. R.; Cadet, J.; Möller, L.; Poulsen, H. E.; Viña, J. Are we sure we know how to measure 8-oxo-7,8-dihydroguanine in DNA from human cells? *Arch Biochem Biophys* **2004,** 423, 57-65.

31. David, S. S.; O'Shea, V. L.; Kundu, S. Base-excision repair of oxidative DNA damage. *Nature* **2007,** 447, 941-950.

32. Mangialasche, F.; Polidori, M. C.; Monastero, R.; Ercolani, S.; Camarda, C.; Cecchetti, R.; Mecocci, P. Biomarkers of oxidative and nitrosative damage in Alzheimer's disease and mild cognitive impairment. *Ageing Res. Rev.* **2009,** 8, 285-305.

33. Steenken, S. J., S. V.; Bietti, M.; Bernhard, K. The Trap Depth (in DNA) of 8-Oxo-7,8-dihydro-2‘deoxyguanosine as Derived from Electron-Transfer Equilibria in Aqueous Solution. *J. Am. Chem. Soc.* **2000,** 122 2373−2374.

34. Luo, W.; Muller, J. G.; Rachlin, E. M.; Burrows, C. J. Characterization of Spiroiminodihydantoin as a Product of One-Electron Oxidation of 8-Oxo-7,8-dihydroguanosine. *Org. Lett.* **2000,** 2, 613-616.

35. Luo, W.; Muller, J. G.; Rachlin, E. M.; Burrows, C. J. Characterization of Hydantoin Products from One-Electron Oxidation of 8-Oxo-7,8-dihydroguanosine in a Nucleoside Model. *Chem. Res. Toxicol.* **2001,** 14, 927-938.

36. Rokhlenko, Y.; Geacintov, N. E.; Shafirovich, V. Lifetimes and Reaction Pathways of Guanine Radical Cations and Neutral Guanine Radicals in an Oligonucleotide in Aqueous Solutions. *J. Am. Chem. Soc.* **2012,** 134, 4955-4962.

37. Fleming, A. M.; Muller, J. G.; Dlouhy, A. C.; Burrows, C. J. Structural Context Effects in the Oxidation of 8-Oxo-7,8-dihydro-2′-deoxyguanosine to Hydantoin Products: Electrostatics, Base Stacking, and Base Pairing. *J. Am. Chem. Soc.* **2012,** 134, 15091-15102.

38. Shafirovich, V.; Cadet, J.; Gasparutto, D.; Dourandin, A.; Geacintov, N. E. Nitrogen Dioxide as an Oxidizing Agent of 8-Oxo-7,8-dihydro-2‘-deoxyguanosine but Not of 2‘-Deoxyguanosine. *Chem. Res. Toxicol.* **2001,** 14, 233-241.

39. Gremaud, J. G.; Martin, B. D.; Sugden, K. D. Influence of substrate complexity on the diastereo-selective formation of spiroiminodihydantoin and guanidinohydantoin from chromate oxidation. . *Chem. Res. Toxicol.* **2010,** 23, 379-385.

40. Niles, J. C.; Wishnok, J. S.; Tannenbaum, S. R. Spiroiminodihydantoin and Guanidinohydantoin Are the Dominant Products of 8-Oxoguanosine Oxidation at Low Fluxes of Peroxynitrite: Mechanistic Studies with 18O. *Chem. Res. Toxicol.* **2004,** 17, 1510-1519.

41. Fleming, A. M.; Burrows, C. J. G-Quadruplex Folds of the Human Telomere Sequence Alter the Site Reactivity and Reaction Pathway of Guanine Oxidation Compared to Duplex DNA. *Chem. Res. Toxicol.* **2013,** 26, 593-607.

42. Ye, Y. M., Muller, J. G.; Luo, W.; Mayne, C. L.; Shallop, A. J.; Jones, R. A.; Burrows, C. J. . “Formation of 13C, 15N, and 18O-Labeled Guanidinohydantoin from Guanosine Oxidation with Singlet Oxygen. Implications for Structure and Mechanism.” *J. Am. Chem. Soc.* **2003,** 125, 13926-13927.

43. Hailer, M. K.; Slade, P. G.; Martin, B. D.; Sugden, K. D. Nei Deficient Escherichia coli Are Sensitive to Chromate and Accumulate the Oxidized Guanine Lesion Spiroiminodihydantoin. *Chem. Res. Toxicol.* **2005,** 18, 1378-1383.

44. Mangerich, A.; Knutson, C. G.; Parry, N. M.; Muthupalani, S.; Ye, W.; Prestwich, E.; Cui, L.; McFaline, J. L.; Mobley, M.; Ge, Z.; Taghizadeh, K.; Wishnok, J. S.; Wogan, G. N.; Fox, J. G.; Tannenbaum, S. R.; Dedon, P. C. Infection-induced colitis in mice causes dynamic and tissue-specific changes in stress response and DNA damage leading to colon cancer. *Proc. Natl. Acad. Sci. U.S.A.* **2012,** 109, E1820−E1829.

45. Delaney, S.; Neeley, W. L.; Delaney, J. C.; Essigmann, J. M. The Substrate Specificity of MutY for Hyperoxidized Guanine Lesions in Vivo†. *Biochemistry* **2007,** 46, 1448-1455.

46. Delaney, S.; Delaney, J. C.; Essigmann, J. M. Chemical–Biological Fingerprinting: Probing the Properties of DNA Lesions Formed by Peroxynitrite. *Chem. Res. Toxicol.* **2007,** 20, 1718-1729.

47. Henderson, P. T.; Delaney, J. C.; Muller, J. G.; Neeley, W. L.; Tannenbaum, S. R.; Burrows, C. J.; Essigmann, J. M. The Hydantoin Lesions Formed from Oxidation of 7,8-Dihydro-8-oxoguanine Are Potent Sources of Replication Errors in Vivo. *Biochemistry* **2003,** 42, 9257-9262.

48. Jia, L.; Shafirovich, V.; Shapiro, R.; Geacintov, N. E.; Broyde, S. Spiroiminodihydantoin Lesions Derived from Guanine Oxidation: Structures, Energetics, and Functional Implications†. *Biochemistry* **2005,** 44, 6043-6051.

49. Fleming, A. M.; Orendt, A. M.; He, Y.; Zhu, J.; Dukor, R. K.; Burrows, C. J. Reconciliation of Chemical, Enzymatic, Spectroscopic and Computational Data To Assign the Absolute Configuration of the DNA Base Lesion Spiroiminodihydantoin. *J. Am. Chem. Soc.* **2013,** 135, 18191-18204.

50. Malayappan, B.; Garrett, T. J.; Segal, M.; Leeuwenburgh, C. Urinary analysis of 8-oxoguanine, 8-oxoguanosine, fapy-guanine and 8-oxo-2′-deoxyguanosine by high-performance liquid chromatography–electrospray tandem mass spectrometry as a measure of oxidative stress. *J. Chromatogr. A* **2007,** 1167, 54-62.

51. Evans, M. D.; Olinski, R.; Loft, S.; Cooke, M. S. Toward consensus in the analysis of urinary 8-oxo-7,8-dihydro-2′-deoxyguanosine as a noninvasive biomarker of oxidative stress. *FASEB J.* **2010,** 24, 1249-1260.

52. Roszkowski, K.; Olinski, R. Urinary 8-Oxoguanine as a Predictor of Survival in Patients Undergoing Radiotherapy. *Cancer Epidemiol. Biomarkers Prev.* **2012,** 21, 629-634.

53. Duclos, S.; Doublie, S.; Wallace, S. S. Consequences and repair of oxidative DNA Damage. In *The CellularResponse to the Genotoxic Insult: The Question of Threshold for Genotoxic Carconogens,* , H. Greim, J. J. A. E., Issues in Toxicology: , Ed. The Royal Society of Chemistry, London: 2012; pp 109–152.

54. Krokan, H. E.; Bjørås, M. Base Excision Repair. *Cold Spring Harbor Perspectives in Biology* **2013,** 5.

55. Lindahl, T. An N-Glycosidase from Escherichia coli That Releases Free Uracil from DNA Containing Deaminated Cytosine Residues. *Proc. Nat. Acad. Sci.* **1974,** 71, 3649-3653.

56. Zharkov, D. O.; Grollman, A. P. The DNA trackwalkers: Principles of lesion search and recognition by DNA glycosylases. *Mutat. Res.* **2005,** 577, 24-54.

57. Friedman, J. I.; Stivers, J. T. Detection of Damaged DNA Bases by DNA Glycosylase Enzymes. *Biochemistry* **2010,** 49, 4957-4967.

58. David, S. S.; O'Shea, V. L.; Kundu, S. "Base-excision Repair of Oxidative DNA Damage" *Nature* **2007,** 447, 941-50.

59. Prakash, A.; Doublié, S.; Wallace, S. S. Chapter 4 - The Fpg/Nei Family of DNA Glycosylases: Substrates, Structures, and Search for Damage. *Prog. Mol. Biol.*

Translational Sci., Paul, W. D., Ed. Academic Press: 2012; Vol. Volume 110, pp 71-91.

60. Hsu, G. W.; Ober, M.; Carell, T.; Beese, L. S. Error-prone replication of oxidatively damaged DNA by a high-fidelity DNA polymerase. . *Nature* **2004,** 431, 217–221.

61. Francis, A. W.; David, S. S. Escherichia coli MutY and Fpg Utilize a Processive Mechanism for Target Location. *Biochemistry* **2002,** 42, 801-810.

62. Sidorenko, V. S.; Zharkov, D. O. Correlated Cleavage of Damaged DNA by Bacterial and Human 8-Oxoguanine-DNA Glycosylases. *Biochemistry* **2008,** 47, 8970-8976.

63. Krahn, J. M.; Beard, W. A.; Miller, H.; Grollman, A. P.; Wilson, S. H. Structure of DNA Polymerase β with the Mutagenic DNA Lesion 8-Oxodeoxyguanine Reveals Structural Insights into Its Coding Potential. *Structure* **2003,** 11, 121-127.

64. Leipold, M. D.; Muller, J. G.; Burrows, C. J.; David, S. S. Removal of hydantoin products of 8-oxoguanine oxidation by the Escherichia coli DNA repair enzyme, Fpg. . *Biochemistry* **2000,** 39, 14984–14992.

65. Hazra, T. K.; Muller, J. G.; Raymond, C. M.; Burrows, C. J.; Lloyd, R. S.; Mitra, S. Repair of hydantoins, one electron oxidation product of 8-oxoguanine, by DNA glycosylases of Escherichia coli. *Nucl. Acids Res.* **2001,** 29, 1967–1974.

66. Bandaru, V.; Sunkara, S.; Wallace, S. S.; Bond, J. P. A novel human DNA glycosylase that removes oxidative DNA damage and is homologous to Escherichia coli endonuclease VIII. *DNA Repair (Amst.)* **2004,** 1, 517-529.

67. Hazra, T. K.; Kow, Y. W.; Hatahet, Z.; Imhoff, B.; Boldogh, I.; Mokkapati, S. K.; Mitra, S.; Izumi, T. Identification and Characterization of a Novel Human DNA Glycosylase for Repair of Cytosine-derived Lesions. *J. Biol. Chem.* **2002,** 277, 30417-30420.

68. Hazra, T. K.; Izumi, T.; Boldogh, I.; Imhoff, B.; Kow, Y. W.; Jaruga, P.; Dizdaroglu, M.; Mitra, S. Identification and characterization of a human DNA glycosylase for repair of modified bases in oxidatively damaged DNA. *Proc. Nat. Acad. Sci.* **2002,** 99, 3523-3528.

69. Hegde, M. L.; Hegde, P. M.; Bellot, L. J.; Mandal, S. M.; Hazra, T. K.; Li, G.-M.; Boldogh, I.; Tomkinson, A. E.; Mitra, S. Prereplicative repair of oxidized bases in the human genome is mediated by NEIL1 DNA glycosylase together with replication proteins. *Proc. Nat. Acad. Sci.* **2013,** 110, E3090-E3099.

70. Banerjee, D.; Mandal, S. M.; Das, A.; Hegde, M. L.; Das, S.; Bhakat, K. K.; Boldogh, I.; Sarkar, P. S.; Mitra, S.; Hazra, T. K. Preferential Repair of Oxidized Base Damage in the Transcribed Genes of Mammalian Cells. *J. Biol. Chem.* **2011,** 286, 6006-6016.

71. Liu, M.; Doublié, S.; Wallace, S. S. Neil3, the final frontier for the DNA glycosylases that recognize oxidative damage. *Mutat. Res.* **2013,** 743–744, 4-11.

72. Wallace, S. S. DNA glycosylases search for and remove oxidized DNA bases. *Environ. Mol. Mutagen.* **2013,** 54, 691-704.

73. Huffman, J. L.; Sundheim, O.; Tainer, J. A. DNA base damage recognition and removal: New twists and grooves. *Mutat. Res.* **2005,** 577, 55-76.

74. Hitomi, K.; Iwai, S.; Tainer, J. A. The intricate structural chemistry of base excision repair machinery: Implications for DNA damage recognition, removal, and repair. *DNA Repair* **2007,** 6, 410-428.

75. Brown, K. L.; Roginskaya, M.; Zou, Y.; Altamirano, A.; Basu, A. K.; Stone, M. P. Binding of the human nucleotide excision repair proteins XPA and XPC/HR23B to the 5R-thymine glycol lesion and structure of the cis-(5R,6S) thymine glycol epimer in the 5′-GTgG-3′ sequence: destabilization of two base pairs at the lesion site. *Nuc. Acids Res.* **2010,** 38, 428-440.

76. Osterod, M.; Larsen, E.; Page, F. L.; Hengstler, J. G.; TJ van der Horst, G.; Boiteux, S.; Klungland, A.; Epe, B. A global DNA repair mechanism involving the Cockayne syndrome B (CSB) gene product can prevent the in vivo accumulation of endogenous oxidative DNA base damage. *Oncogene* **2002,** 21, 8232-8239.

77. Klungland, A.; Rosewell, I.; Hollenbach, S.; Larsen, E.; Daly, G.; Epe, B.; Seeberg, E.; Lindahl, T.; Barnes, D. E. Accumulation of premutagenic DNA lesions in mice defective in removal of oxidative base damage. *Proc. Nat. Acad. Sci.* **1999,** 96, 13300-13305.

78. Rozalski, R.; Winkler, P.; Gackowski, D.; Paciorek, T.; Kasprzak, H.; Olinski, R. High Concentrations of Excised Oxidative DNA Lesions in Human Cerebrospinal Fluid. *Clinic. Chem.* **2003,** 49, 1218-1221.

79. Truglio, J. J.; Croteau, D. L.; Van Houten, B.; Kisker, C. Prokaryotic Nucleotide Excision Repair: The UvrABC System. *Chem. Rev.* **2006,** 106, 233-252.

80. Houxen, B. V.; McCullough, A. Nucleotide Excision Repair in E. Coli. *Ann. N. Y. Acad. Sci.* **1994,** 726, 236-251.

81. McKibbin, P. L.; Fleming, A. M.; Towheed, M. A.; Van Houten, B.; Burrows, C. J.; David, S. S. Repair of Hydantoin Lesions and Their Amine Adducts in DNA by Base and Nucleotide Excision Repair. *J. Am. Chem. Soc.* **2013,** 135, 13851-13861.

82. Collins, A. R.; Dobson, V. L.; Dusinska, M.; Kennedy, G.; Stetina, R. The comet assay: what can it really tell us? *Mutat. Res.* **1997,** 375, 183-193.

83. Yin, B.; Whyatt, R. M.; Perera, F. P.; Randall, M. C.; Cooper, T. B.; Santella, R. M. Determination of 8-hydroxydeoxyguanosine by an immunoaffinity chromatography-monoclonal antibody-based ELISA. *Free Rad. Biol. Med.* **1995,** 18, 1023-1032.

84. Phillip, D. H.; Castegrano, M.; Bartsch, H. Post-labelling. methods for the Detection of DNA Damage. In IARC Scientific Publications, IARC, Lyon: 1993.

85. Singh, N. P.; McCoy, M. T.; Tice, R. R.; Schneider, E. L. A simple technique for quantitation of low levels of DNA damage in individual cells. *Exp. Cell Res.* **1988,** 175, 184-191.

86. Ostling, O.; Johanson, K. J. Microelectrophoretic study of radiation-induced DNA damages in individual mammalian cells. *Biochem. Biophys. Res. Commun.* **1984,** 123, 291-298.

87. Phillips, D. H.; Arlt, V. M. The 32P-postlabeling assay for DNA adducts. *Nat. Protocols.* **2007,** 2, 2772-2781.

88. Jenner, A.; England, T. G.; Aruoma, O. I.; Halliwell, B. Measurement of oxidative DNA damage by gas chromatography-mass spectrometry: ethanethiol prevents

artifactual generation of oxidized DNA bases. *Biochem J.* **1998,** 331 (Pt 2), 365–369.

89. Frelon, S.; Douki, T.; Ravanat, J.-L.; Pouget, J.-P.; Tornabene, C.; Cadet, J. High-Performance Liquid Chromatography−Tandem Mass Spectrometry Measurement of Radiation-Induced Base Damage to Isolated and Cellular DNA. *Chem. Res. Toxicol.* **2000,** 13, 1002-1010.

90. Nakagawa, O.; Ono, S.; Li, Z.; Tsujimoto, A.; Sasaki, S. Specific Fluorescent Probe for 8-Oxoguanosine. *Angew. Chem. Int. Ed.* **2008,** 47, 8983-8983.

91. Taniguchi, Y.; Kawaguchi, R.; Sasaki, S. Adenosine-1,3-diazaphenoxazine Derivative for Selective Base Pair Formation with 8-Oxo-2′-deoxyguanosine in DNA. *J. Am. Chem. Soc.* **2011,** 133, 7272-7275.

92. Nakagawa, O.; Ono, S.; Tsujimoto, A.; Li, Z.; Sasaki, S. Fluorescence detection of 8-oxoguanosine by G-clamp derivatives. *Nucleic Acids Symp. Ser.* **2006,** 50, 21-22.

93. Deigan, K. E.; Ferre-D'Amare, A. R. Riboswitches: Discovery of Drugs That Target Bacterial Gene-Regulatory RNAs. *Accounts of Chem. Res.* **2011,** 44, 1329-1338.

94. Kruger, K.; Grabowski, P. J.; Zaug, A. J.; Sands, J.; Gottschling, D. E.; Cech, T. R. Self-splicing RNA: Autoexcision and autocyclization of the ribosomal RNA intervening sequence of tetrahymena. *Cell* **1982,** 31, 147-157.

95. Stark, B. C.; Kole, R.; Bowman, E. J.; Altman, S. Ribonuclease P: An enzyme with an essential RNA component. *Proc. Nat. Acad. Sci.* **1978,** 75, 3717-3721.

96. Fedor, M. J.; Uhlenbeck, O. C. Substrate sequence effects on "hammerhead" RNA catalytic efficiency. *Proc. Nat. Acad. Sci.* **1990,** 87, 1668-1672.

97. Nahvi, A.; Sudarsan, N.; Ebert, M. S.; Zou, X.; Brown, K. L.; Breaker, R. R. Genetic Control by a Metabolite Binding mRNA. *Chem. Biol.* **2002,** 9, 1043-1049.

98. Mandal, M.; Breaker, R. R. Gene regulation by riboswitches. *Nat. Rev. Mol. Cell Biol.* **2004,** 5, 451-463.

99. Tucker, B. J.; Breaker, R. R. Riboswitches as versatile gene control elements. *Curr. Opin. Struct. Biol.* **2005,** 15, 342-348.

100. Oliphant, A. R.; Brandl, C. J.; Struhl, K. Defining the sequence specificity of DNA-binding proteins by selecting binding sites from random-sequence oligonucleotides: analysis of yeast GCN4 protein. *Mol. Cell. Biol.* **1989.,** 9, 2944–2949.

101. Ellington, A. D.; Szostak, J. W. In vitro selection of RNA molecules that bind specific ligands. *Nature* **1990,** 346, 818-822.

102. Tuerk, C.; Gold, L. Systematic evolution of ligands by exponential enrichment: RNA ligands to bacteriophage T4 DNA polymerase. *Science* **1990,** 249, 505-510.

103. Huizenga, D. E.; Szostak, J. W. A DNA Aptamer That Binds Adenosine and ATP. *Biochemistry* **2002,** 34, 656-665.

104. Hermann, T.; Patel, D. J. Adaptive Recognition by Nucleic Acid Aptamers. *Science* **2000,** 287, 820-825.

105. Patel, D. J. Structural analysis of nucleic acid aptamers. *Curr. Opin. Chem. Biol.* **1997,** 1, 32-46.

106. Patel, D. J.; Suri, A. K.; Jiang, F.; Jiang, L.; Fan, P.; Kumar, R. A.; Nonin, S. Structure, recognition and adaptive binding in RNA aptamer complexes. *J. Mol. Biol.* **1997,** 272, 645-664.

107. Wilson, D. S.; Szostak, J. W. In Vitro Selection of Functional Nucleic Acids. *Ann. Rev. Biochem.* **1999,** 68, 611-647.

108. Rimmele, M. Nucleic Acid Aptamers As Tools and Drugs: Recent Developments. *Chembiochem.* **2003,** 4, 963-971.

109. Stolenburg, R.; Reinemann, C.; Strehlitz, B. SELEX-A (R)-Evolutionary Method to Generate High Affinity Nucleic Acid Ligands. *Biomol. Eng.* **2007,** 24, 381-403.

110. McKeague, M.; DeRosa, M. C. Challenges and Oppurtunities or Small Molecule Aptamer Development. *J. Nucl. Acids* **2012,** 2012, 1-20.

111. Ciesiolka, J.; Yarus, M. Small RNA-divalent domains. *RNA* **1996,** 2, 785-793.

112. Hofmann, H. P.; Limmer, S.; Hornung, V.; Sprinzl, M. Ni^{2+}-binding RNA motifs with an asymmetric purine-rich internal loop and a G-A base pair. *RNA* **1997,** 3, 1289-1300.

113. Rajendran, M.; Ellington, A. D. Selection of fluorescent aptamer beacons that light up in the presence of zinc. *Anal. Bioanal. Chem.* **2008,** 390, 1067-1075.

114. Geiger, A.; Burgstaller, P.; von der Eltz, H.; Roeder, A.; Famulok, M. RNA Aptamers That Bind l-Arginine with Sub-Micromolar Dissociation Constants and High Enantioselectivity. *Nucl. Acids Res.* **1996,** 24, 1029-1036.

115. Connell, G. J.; Illangesekare, M.; Yarus, M. Three small ribooligonucleotides with specific arginine sites. *Biochemistry* **1993,** 32, 5497-5502.

116. Famulok, M. Molecular Recognition of Amino Acids by RNA-Aptamers: An L-Citrulline Binding RNA Motif and Its Evolution into an L-Arginine Binder. *J. Am. Chem. Soc.* **1994,** 116, 1698-1706.

117. Majerfeld, I.; Puthenvedu, D.; Yarus, M. RNA affinity for molecular L-histidine; genetic code origins. *J. Mol. Evol.* **2005,** 61, 226-235.

118. Wallis, M. G.; Streicher, B.; Wank, H.; von Ahsen, U.; Clodi, E.; Wallace, S. T.; Famulok, M.; Schroeder, R. In vitro selection of a viomycin-binding RNA pseudoknot. *Chem. Biol.* **1997,** 4, 357-366.

119. Wallace, S. T.; Schroeder, R. In vitro selection and characterization of streptomycin-binding RNAs: recognition discrimination between antibiotics. *RNA* **1998,** 4, 112-123.

120. Goertz, P. W.; Cox, J. C.; Ellington, A. D. Automated selection of aminoglycoside aptamers. *JALA - J. Assoc.Lab. Automation* **2004,** 9, 150-154.

121. Vaish, N. K.; Larralde, R.; Fraley, A. W.; Szostak, J. W.; McLaughlin, L. W. A novel, modification-dependent ATP-binding aptamer selected from an RNA library incorporating a cationic functionality. *Biochemistry* **2003,** 42, 8842-8851.

122. Huang, Z.; Szostak, J. W. Evolution of aptamers with a new specificity and new secondary structures from an ATP aptamer. *RNA* **2003,** 9, 1456-1463.

123. Lorsch, J. R.; Szostak, J. W. In vitro selection of RNA aptamers specific for cyanocobalamin. *Biochemistry* **1994,** 33, 973-982.

124. Burgstaller, P.; Famulok, M. Isolation of RNA aptamers for biological cofactors by in vitro selection. *Angew. Chem. Int. Ed.* **1994,** 33, 1084-1087.

125. Gebhardt, K.; Shokraei, A.; Babaie, E.; Lindqvist, B. H. RNA aptamers to S-adenosylhomocysteine: Kinetic properties, divalent cation dependency, and comparison with anti-S-adenosylhomocysteine antibody. *Biochemistry* **2000,** 39, 7255-7265.

126. Roychowdhury-Saha, M.; Lato, S. M.; Shank, E. D.; Burke, D. H. Flavin recognition by an RNA aptamer targeted toward FAD. *Biochemistry* **2002,** 41, 2492-2499.

127. Tuerk, C.; MacDougal, S.; Gold, L. RNA pseudoknots that inhibit human immunodeficiency virus type 1 reverse transcriptase. *Proc. Nat. Acad. Sci.* **1992,** 89, 6988-6992.

128. Kubik, M. F.; Stephens, A. W.; Schneider, D.; Marlar, R. A.; Tasset, D. High-affinity RNA ligands to human α-thrombin. *Nucl. Acids Res.* **1994,** 22, 2619-2626.

129. Williams, K. P.; Liu, X.-H.; Schumacher, T. N. M.; Lin, H. Y.; Ausiello, D. A.; Kim, P. S.; Bartel, D. P. Bioactive and nuclease-resistant l-DNA ligand of vasopressin. *Proc. Nat. Acad. Sci.* **1997,** 94, 11285-11290.

130. Morris, K. N.; Jensen, K. B.; Julin, C. M.; Weil, M.; Gold, L. High affinity ligands from in vitro selection: Complex targets. *Proc. Nat. Acad. Sci.* **1998,** 95, 2902-2907.

131. Shangguan, D.; Li, Y.; Tang, Z.; Cao, Z. C.; Chen, H. W.; Mallikaratchy, P.; Sefah, K.; Yang, C. J.; Tan, W. Aptamers evolved from live cells as effective molecular probes for cancer study. *Proc. Nat. Acad. Sci.* **2006,** 103, 11838-11843.

132. Shangguan, D.; Meng, L.; Cao, Z. C.; Xiao, Z.; Fang, X.; Li, Y.; Cardona, D.; Witek, R. P.; Liu, C.; Tan, W. Identification of Liver Cancer-Specific Aptamers Using Whole Live Cells. *Anal. Chem.* **2008,** 80, 721-728.

133. Kumar, P. K. R.; Machida, K.; Urvil, P. T.; Kakiuchi, N.; Vishnuvardhan, D.; Shimotohno, K.; Taira, K.; Nishikawa, S. Isolation of RNA Aptamers Specific to the NS3 Protein of Hepatitis C Virus from a Pool of Completely Random RNA. *Virology* **1997,** 237, 270-282.

134. Misono, T. S.; Kumar, P. K. R. Selection of RNA aptamers against human influenza virus hemagglutinin using surface plasmon resonance. *Anal. Biochem.* **2005,** 342, 312-317.

135. Tang, Z.; Parekh, P.; Turner, P.; Moyer, R. W.; Tan, W. Generating Aptamers for Recognition of Virus-Infected Cells. *Clinical Chem.* **2009,** 55, 813-822.

136. Hamula, C. L. A.; Zhang, H.; Guan, L. L.; Li, X.-F.; Le, X. C. Selection of Aptamers against Live Bacterial Cells. *Anal. Chem.* **2008,** 80, 7812-7819.

137. Floege, J.; Ostendorf, T.; Janssen, U.; Burg, M.; Radeke, H. H.; Vargeese, C.; Gill, S. C.; Green, L. S.; Janjic, N. Novel approach to specific growth factor inhibition in vivo - Antagonism of platelet-derived growth factor in glomerulonephritis by aptamers. *Am.J. Pathol.* **1999,** 154, 169-179.

138. Mann, D.; Reinemann, C.; Stoltenburg, R.; Strehlitz, B. In vitro selection of DNA Aptamers binding ethanolamine. *Biochem. Biophys. Res. Commun.* **2005,** 338, 1928-1934.

139. Marshall, K. A.; D., E. A. In Vitro Selection of RNA Aptamers. *Methods in Enzymol.* **2000,** 318, 193-214.

140. Gold, L. Oligonucleotides as Research, Diagnostic, and Therapeutic Agents. *J. Biol. Chem.* **1995,** 270, 13581-13584.

141. James, W. Aptamers. *Encyclopedia of Analytical Chemistry.* **2000**, 4848–4871.

142. Vant-Hull, B.; Payano-Baez, A.; Davis, R. H.; Gold, L. The mathematics of SELEX against complex targets. *J. Mol. Biol.* **1998,** 278, 579-597.

143. Tuerk, C.; Gold, L. Systematic Evolution of Ligands by Exponential Enrichment: RNA Ligands To Bacteriophage T4 DNA Polymerase. *Science* **1990,** 249, 505-510.

144. Schneider, D.; Gold, L.; Platt, T. Selective Enrichment of RNA species for tight binding to Escherichia Coli rho factor. *FASEB J.* **1993,** 7, 201-207.

145. Djordjevic, M.; Sengupta, A. M. Quantitative Modelling and Data Analysis of SELEX Experiments. *Phys. Biol.* **2006,** 3, 13-28.

146. Tombelli, S.; Minunni, A.; Luzi, E.; Mascini, M. Aptamer-based Biosensors for Detection of HIV-1 Tat Protein. *Bioelectrochem.* **2005,** 67, 135-141.

147. Mendonsa, S. D.; Bowser, M. T. In Vitro Selection of High-Affinity DNA Ligands for Human IgE Using Capillary Electrophoresis. *Anal. Chem.* **2004,** 76, 5387-5392.

148. Jensen, K. B.; Atkinson, B. L.; Willis, M. C.; Koch, T. H.; Gold, L. Using in vitro selection to direct the covalent attachment of human immunodeficiency virus type 1 Rev protein to high-affinity RNA ligands. *Proc. Nat. Acad. Sci.* **1995,** 92, 12220-12224.

149. Kim, Y.; Liu, C.; Tan, W. Aptamers generated by Cell SELEX for biomarker discovery. *Biomarkers in Med.* **2009,** 3, 193-202.

150. Stoltenburg, R.; Reinemann, C.; Strehlitz, B. FluMag-SELEX as an advantageous method for DNA aptamer selection. *Anal. Bioanal. Chem.* **2005,** 383, 83-91.

151. Nutiu, R.; Li, Y. Structure-Switching Signaling Aptamers. *J. Am. Chem. Soc.* **2003,** 125, 4771-4778.

152. Reid, D. C.; Chang, B. L.; Gunderson, S. I.; Alpert, L.; Thompson, W. A.; Fairbrother, W. G. Next-generation SELEX identifies sequence and structural determinants of splicing factor binding in human pre-mRNA sequence. *RNA* **2009,** 15, 2385-2397.

153. Bianchini, M.; Radrizzani, M.; Brocardo, M. G.; Reyes, G. B.; Gonzalez Solveyra, C.; Santa-Coloma, T. A. Specific oligobodies against ERK-2 that recognize both the native and the denatured state of the protein. *J. Immunol. Methods* **2001,** 252, 191-197.

154. Theis, M. G.; Knorre, A.; Kellersch, B.; Moelleken, J.; Wieland, F.; Kolanus, W.; Famulok, M. Discriminatory aptamer reveals serum response element transcription regulated by cytohesin-2. *Proc. Nat. Acad. Sci.* **2004,** 101, 11221-11226.

155. Weiss, S.; Proske, D.; Neumann, M.; Groschup, M. H.; Kretzschmar, H. A.; Famulok, M.; Winnacker, E. L. RNA aptamers specifically interact with the prion protein PrP. *J Virol.* **1997,** 71, 8790–8797.

156. Naimuddin, M.; Kitamura, K.; Kinoshita, Y.; Honda-Takahashi, Y.; Murakami, M.; Ito, M.; Yamamoto, K.; Hanada, K.; Husimi, Y.; Nishigaki, K. Selection-by-function: Efficient Enrichment of Cathepsin E Inhibitors from a DNA library. *J. Mol. Recognit.* **2007,** 20, 58-68.

157. Walder, R. Y.; Hayes, J. R.; Walder, J. A. USe of PCR primers containing a 3' terminal ribose residuce to prevent cross-contamination of amplified sequences. *Nuc. Acids Res.* **1993,** 21, 4339-4343.

158. Hendry, P.; Hannan, G. Detection and quantitation of unlabeled nucleic acids in polyacrylamide gels. *Biotechniques* **1996** 20, 258-64.

159. Fitzwater, T.; B., P. A SELEX Primer. *Methods Enzymol.* **1996,** 267, 275-300.

160. Williams, K. P.; Bartel, D. P. PCR product with strands of unequal length. *Nuc. Acids Res.* **1995,** 23, 4220-4221.

161. Avci-Adali, M.; Paul, A.; Wilhelm, N.; Ziemer, G.; Wendel, H. P. Upgrading SELEX Technology by Using Lambda Exonuclease Digestion for Single-Stranded DNA Generation *Molecules* **2010,** 15, 1-11.

162. McKeague, M.; Bradley, C. R.; Girolamo, A. D.; Visconti, A.; Miller, J. D.; DeRosa, M. C. Screening and Initial Binding Assessment of Fumonisin B1 Aptamers. *Int. J. Mol. Sci.* **2010,** 11, 4864-4881.

163. Drabovich, A. P.; Berezovski, M.; Okhonin, V.; Krylov, S. N. Selection of Smart Aptamers by Methods of Kinetic Capillary Electrophoresis. *Anal. Chem.* **2006,** 78, 3171-3178.

164. Turgeon, R. T.; Fonslow, B. R.; Jing, M.; Bowser, M. T. Measuring Aptamer Equilibria Using Gradient Micro Free Flow Electrophoresis. *Anal. Chem.* **2010,** 82, 3636-3641.

165. Flinders, J.; DeFina, S. C.; Brackett, D. M.; Baugh, C.; Wilson, C.; Dieckmann, T. Recognition of Planar and Nonplanar Ligands in the Malachite Green–RNA Aptamer Complex. *ChemBioChem* **2004,** 5, 62-72.

166. Cruz-Aguado, J. A.; Penner, G. Fluorescence Polarization Based Displacement Assay for the Determination of Small Molecules with Aptamers. *Anal. Chem.* **2008,** 80, 8853-8855.

167. Guédin, A.; Lacroix, L.; Mergny, J.-L. Thermal Melting Studies of Ligand DNA Interactions. In *Drug-DNA Interaction Protocols*, Fox, K. R., Ed. Humana Press: 2010; Vol. 613, pp 25-35.

168. Lin, P.-H.; Chen, R.-H.; Lee, C.-H.; Chang, Y.; Chen, C.-S.; Chen, W.-Y. Studies of the binding mechanism between aptamers and thrombin by circular dichroism, surface plasmon resonance and isothermal titration calorimetry. *Colloids and Surfaces B: Biointerfaces* **2011,** 88, 552-558.

169. Sultan, Y.; Walsh, R.; Monreal, C.; DeRosa, M. C. Preparation of Functional Aptamer Films Using Layer-by-Layer Self-Assembly. *Biomacromolecules* **2009,** 10, 1149-1154.

170. Win, M. N.; Klein, J. S.; Smolke, C. D. Codeine-binding RNA aptamers and rapid determination of their binding constants using a direct coupling surface plasmon resonance assay. *Nucl. Acids Res.* **2006,** 34, 5670-5682.

171. Burke, D. H.; Scates, L.; Andrews, K.; Gold, L. Bent Pseudoknots and Novel RNA Inhibitors of Type 1 Human Immunodeficiency Virus (HIV-1) Reverse Transcriptase. *J. Mol. Biol.* **1996,** 264, 650-666.

172. Wilson, C.; Szostak, J. W. Isolation of Fluorophore-specific DNA Aptamer with Weak Redox Activity. *Chem. Biol.* **1998,** 5, 609-617.

173. Bittker, J. A.; Brian, V. E.; Liu, D. R. Nucleic acid evolution and minimization by nonhomologous random recombination. *Nat. Biotech.* **2002,** 20, 1024-1029.

174. Green, L. S.; Jellinek, D.; Bell, C.; Beebe, L. A.; Feistner, B. D.; Gill, S. C.; Jucker, F. M.; Janjić, N. Nuclease-resistant nucleic acid ligands to vascular permeability factor/vascular endothelial growth factor. *Chem. & Biol.* **1995,** 2, 683-695.

175. Rhodes, A.; Deakin, A.; Spaull, J.; Coomber, B.; Aitken, A.; Life, P.; Rees, S. The Generation and Characterization of Antagonist RNA Aptamers to Human Oncostatin M. *J. Biol. Chem.* **2000,** 275, 28555-28561.

176. Petersen, M.; Wengel, J. LNA: a versatile tool for therapeutics and genomics. *Trends Biotech.* **2003,** 21, 74-81.

177. Dougan, H.; Lyster, D. M.; Vo, C. V.; Stafford, A.; Weitz, J. I.; Hobbs, J. B. Extending the lifetime of anticoagulant oligodeoxynucleotide aptamers in blood. *Nucl. Med. Biol.* **2000,** 27, 289-297.

178. Klussmann, S. *The Aptamer Handbook. Functional Oligonucleotides and Their Applications*. Wiley-VCH Verlag GmbH & Co., KGaA, Weinheim: 2006.

179. Hamula, C. L. A.; Guthrie, J. W.; Zhang, H.; Li, X.-F.; Le, X. C. Selection and analytical applications of aptamers. *TrAC Trends in Anal. Chem.* **2006,** 25, 681-691.

180. Tombelli, S.; Minunni, M.; Mascini, M. Analytical applications of aptamers. *Biosensors and Bioelectronics* **2005,** 20, 2424-2434.

181. Tucker, C. E.; Chen, L.-S.; Judkins, M. B.; Farmer, J. A.; Gill, S. C.; Drolet, D. W. Detection and plasma pharmacokinetics of an anti-vascular endothelial growth factor oligonucleotide-aptamer (NX1838) in rhesus monkeys. *J. Chromatogr. B.* **1999,** 732, 203-212.

182. Hicke, B. J.; Stephens, A. W. Escort aptamers: a delivery service for diagnosis and therapy. *J. Clin. Invest.* **2000,** 106, 923-928.

183. Ravelet, C.; Grosset, C.; Peyrin, E. Liquid chromatography, electrochromatography and capillary electrophoresis applications of DNA and RNA aptamers. *J. Chromatogr. A* **2006,** 1117, 1-10.

184. Stojanovic, M. N.; Kolpashchikov, D. M. Modular Aptameric Sensors. *J. Am. Chem. Soc.* **2004,** 126, 9266-9270.

185. Levy, M.; Cater, S. F.; Ellington, A. D. Quantum-Dot Aptamer Beacons for the Detection of Proteins. *ChemBioChem* **2005,** 6, 2163-2166.

186. Liu, J.; Lu, Y. Fast Colorimetric Sensing of Adenosine and Cocaine Based on a General Sensor Design Involving Aptamers and Nanoparticles. *Angew. Chem. Int. Ed.* **2006,** 118, 96-100.

187. Cheng, A. K. H.; Sen, D.; Yu, H.-Z. Design and testing of aptamer-based electrochemical biosensors for proteins and small molecules. *Bioelectrochemistry* **2009,** 77, 1-12.

188. Win, M. N.; Liang, J. C.; Smolke, C. D. Frameworks for Programming Biological Function through RNA Parts and Devices. *Chem. & Biol.* **2009,** 16, 298-310.

189. Famulok, M.; Blind, M.; Mayer, G. Intramers as promising new tools in functional proteomics. *Chem. & Biol.* **2001,** 8, 931-939.

190. Schibel, A. E. P.; An, N.; Jin, Q.; Fleming, A. M.; Burrows, C. J.; White, H. S. Nanopore Detection of 8-Oxo-7,8-dihydro-2′-deoxyguanosine in Immobilized Single-Stranded DNA via Adduct Formation to the DNA Damage Site. *J. Am. Chem. Soc.* **2010,** 132, 17992-17995.

191. An, N.; Fleming, A. M.; White, H. S.; Burrows, C. J. Crown ether–electrolyte interactions permit nanopore detection of individual DNA abasic sites in single molecules. *Proc. Nat. Acad. Sci.* **2012,** 109, 11504-11509.

192. Zhang, Q.; Wang, Y.; Meng, X.; Dhar, R.; Huang, H. Triple-Stranded DNA Containing 8-Oxo-7,8-dihydro-2′-deoxyguanosine: Implication in the Design of Selective Aptamer Sensors for 8-Oxo-7,8-dihydroguanine. *Anal. Chem.* **2012,** 85, 201-207.

CHAPTER 2

COMPARISON OF TRANSITION METAL-MEDIATED OXIDATION OF GUANINE IN NUCLEOSIDE AND SINGLE-STRANDED OLIGODEOXYNUCLEOTIDE CONTEXTS

Introduction

Chemical modification of guanine (G), the most readily oxidized nucleobase in DNA, has been linked to aging, cancer, and degenerative diseases.[1-4] The constant attack by endogenous and exogenous oxidants on guanine generates various oxidation products (Figure 2.1).[5] Among these products, 8-oxo-7,8-dihydroguanine (8-oxo-G), guanine-derived 2,6-diamino-4-hydroxy-formamidopyrimidine (FAPy-G),[6-8] spiroiminodihydantoin (Sp),[9] and oxazolone (Z)[10] have been found *in vivo*. The normal level of 8-oxo-G, the most common oxidation product of guanine, is 0.3 - 4 lesions per 10^6 dG nucleosides,[11] and it has been used as a biomarker of oxidative stress in cells.[12]

The various oxidation products formed are due to hydroxylation or perhydroxylation at the C-5 or C-8 positions of G. For example, the C-5 pathway involves loss of one electron from guanine leading to the formation of the guanine radical cation ($G^{\bullet+}$) that has a pK_a of 3.9;[13] $G^{\bullet+}$ undergoes rapid deprotonation in the nucleoside form, although its lifespan may be prolonged in duplex DNA .[14] The neutral guanine radical ($G^{\bullet}$)[15-17] is attacked by molecular oxygen [18-20] or superoxide anion ($O_2^{\bullet-}$)[17, 21, 22] and results

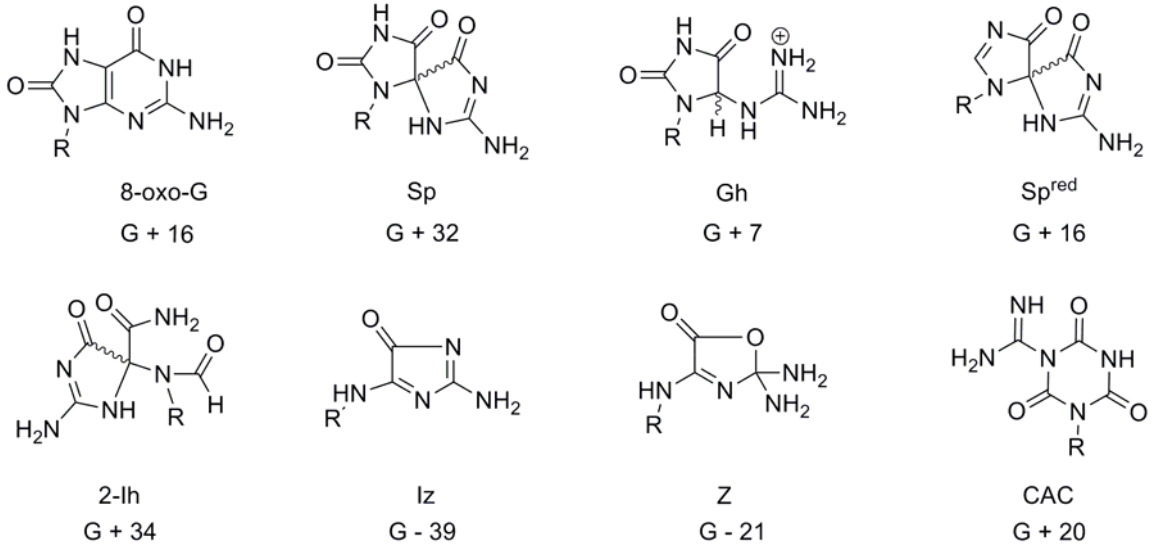

Figure 2.1. Oxidation products of 2',3',5'-tri-*O*-acetyl-guanosine, where R= 2',3',5'-tri-*O*-acetylribose.

in a cascade of decomposition reactions leading to formation the of imidazolone (Iz) and eventually oxazolone (Z) products (Scheme 2.1).[23-25]

On the other hand, the guanine radical cation ($G^{\bullet+}$) can be trapped by H_2O at C-8,[13] followed by the deprotonation and formation of an intermediate adduct (8-OH-$G^{\bullet}$)[26] that is prone to further oxidation and tautomerization leading to 8-oxo-G. Under reducing conditions, one-electron reduction of 8-OH-$G^{\bullet}$ followed by ring opening leads to FAPy-G. Both 8-oxo-G and FAPy-G are formed during radiation damage to DNA.[4,8] 8-Oxo-G has a reduction potential of 0.74 V versus NHE,[27] and because this is ~0.55 V lower than that of G (E = 1.29 V vs. NHE at pH 7), further oxidation can readily occur yielding the spirocyclic base Sp as well as guanidinohydantoin (Gh).[27,28] Both of the hydantoin lesions are known to be highly mutagenic (Scheme 2.2).[28-30]

A wide range of aqueous oxidation systems, from reactive oxygen species (ROS)[31] and photochemical oxidants[32] to transition metals, [25, 33-36] are known to react with the electron-rich guanine (Table 2.1). Among the sulfoxyl radicals, the sulfate radical anion ($SO_4^{\bullet-}$) is the most potent oxidant with a redox potential of 2.43 V vs. NHE at pH 7, and acts by a one-electron abstraction mechanism.[37] Another relevant oxidant is singlet oxygen formed by photoexcitation of photosensitizers such as Rose Bengal (RB).[32] The quantum yield of RB for singlet oxygen production is 0.76 in water.[38] Singlet oxygen can potentially act by four-electron oxidation of G, bypassing 8-oxoG to yield hydantoin products directly.[39]

Furthermore, several transition metal ions act as promoters of nucleic acid oxidation. The simplest of the oxidant mechanistically is hexachloroiridate, $IrCl_6^{2-}$, a water-soluble, one-electron oxidants with a redox potential of 0.9 V vs. NHE.[40] In the presence

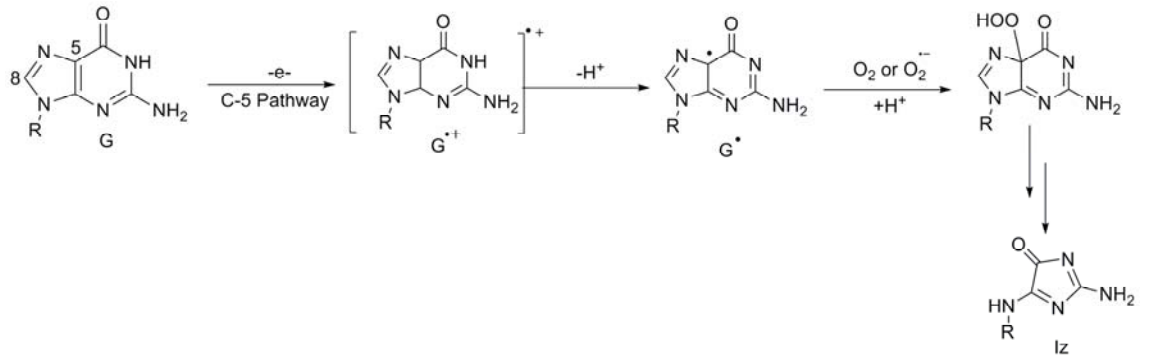

Scheme 2.1. C-5 pathway for oxidation of 2',3',5'-tri-*O*-acetyl-guanosine.

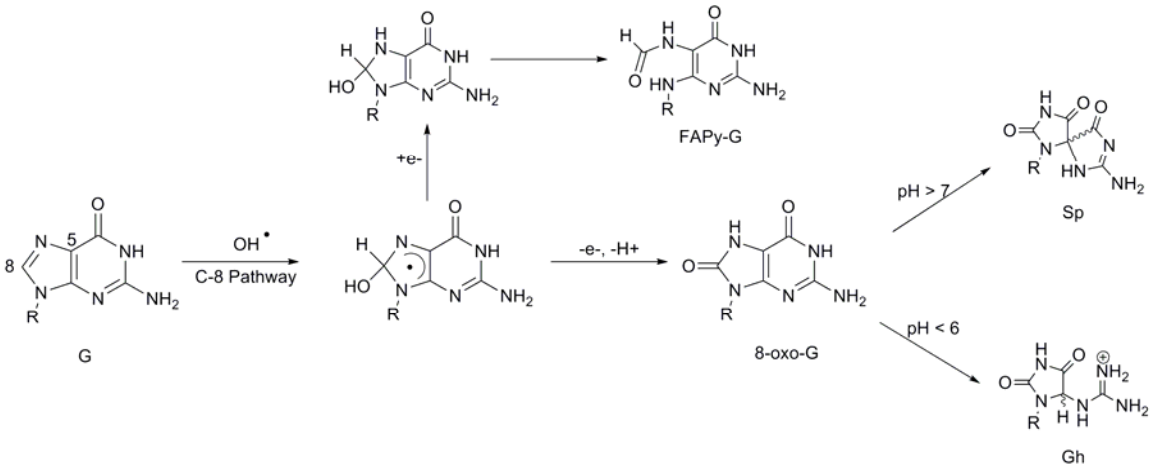

Scheme 2.2. C-8 pathway for oxidation of 2',3',5'-tri-*O*-acetyl-guanosine.

Table 2.1. Aqueous oxidation systems and their reduction potentials vs NHE at pH 7.

Oxidation System	Oxidant	$E_{1/2}$ (V vs. NHE) at pH 7
Na_2IrCl_6	e^-	0.9
$K_2S_2O_8$/ *hv* (256 nm)	$SO_4^{\cdot -}$	2.43
Rose Bengal/ *hv* (360 nm)	$^1O_2$	NA
$CoCl_2$/ $KHSO_5$	$SO_4^{\cdot -}$	>2.0
Ni(II)CR/ $KHSO_5$	L_4-Ni-O-$SO_3^{\cdot}$	>2.0
Fe(II)EDTA/ H_2O_2	$OH^{\cdot}$	1.9

of transition metals such as cobalt (II) and nickel (II), oxone ($KHSO_5$) causes site-specific guanine oxidation.[41-43] Metal-catalyzed decomposition of $KHSO_5$ generates $SO_4^{\cdot -}$ that is responsible for the oxidation of G.[41] $CoCl_2/KHSO_5$ generates highly diffusible sulfate radicals that induce guanine-specific modification in bulges, loops, and single-stranded DNA (ssDNA).[34]

It has been reported that simple nickel salts combined with H_2O_2 result in the formation of 8-oxo-G as the oxidation product.[44, 45] Specifically, nickel (II) complexes that are four-coordinate, and square planar allow nickel binding to chromatin and are known for their toxicity and carcinogenicity.[46, 47] These complexes can facilitate oxidization of the DNA, causing strand breaks, oxidative base damage, and DNA-protein crosslinks.[48, 49] The nickel complexes, however, do not deform the nucleic acids' structure in the process of recognition.[50] Certain ligands, like peptides, coordinate to nickel (II) to enhance the metal reactivity by stabilizing the +3 oxidation state of the metal to promote oxidation.[51-53] The ligand surrounding the metal and the redox properties of the metal play an important role in the determination of oxidation by these nickel macrocycles. Nickel tetraazamacrocyles that possess strong in-plane donor ligands and vacant coordination sites mediate oxidative damage of guanine with peracids like $KHSO_5$.[35] NiCR is a square planar complex with a +2 charge and is a 14-membered macrocycle with nitrogens present as pyridine or imine groups. NiCR, unlike nickel peptides, does not react in the minor groove under low salt concentrations.[54] Base damage occurs in regions where guanines are solvent accessible and hence NiCR acts as a probe in the determination of the three-dimensional folded structures of DNA and RNA.[53, 54]

NiCR is thought to prefer oxidation at exposed Gs by binding to the most basic site,

N7 in guanine, thus delivering the oxidant to the exposed base by direct metal coordination (Figure 2.2).[35, 55] The intermediate is proposed to be an octahedral nickel (III)-bound sulfate radical, in which the two additional ligands, guanine and oxidant, are *cis*-coordinated (Scheme 2.3). Subsequent reductive elimination of these groups results in an oxidized G in DNA that leads to strand scission upon treatment with hot piperidine.[35, 50, 56] The flexibility of the macrocyclic ring is important for *cis*-coordination of the guanine and oxidant around the metal ion. A bifunctional oxidant containing both a ligand (sulfate) and an oxygen atom donor might be effective to bind and stabilize the nickel (III). NiCR differs from $CoCl_2/KHSO_5$ in its mechanism of oxidation and guanine recognition. NiCR coordinates to N7 of guanine whereas Co (II) interacts with the π- face of the purine ring. The difference in mode of recognition is attributed to free $SO_4^{\cdot-}$ induced by $CoCl_2$ as compared to nickel-coordinated $SO_4^{\cdot-}$. [34]

Square planar nickel peptide complexes, Ni^{II}Gly-Gly-His and Ni^{II}Arg-Gly-His, appear to generate a similar reactive complex with SO_4^{2-} radical via autoxidation of sulfite. In this mechanism, Ni(II) catalyzes the formation of HSO_5^- via autoxidation of HSO_3^-. Curiously, the product of G oxidation by the Ni^{II}Gly-Gly-His/ HSO_3^-/O_2 system appears to be 8-oxo-G, which has not been observed from G oxidation by the NiCR/ $KHSO_5$ system.

Despite its popularity as a structural tool, the $NiCR/KHSO_5$ remained elusive in terms of its eventual chemistry with G. The final product formed by G oxidation in oligodeoxynucleotides, with $NiCR/KHSO_5$ system results in base-specific cleavage upon alkaline treatment.[35] The final product formed had a mass that was higher than that of starting material by 34 and had two possible structures.[57] The transient product, G+16 was thought to be formed by hydroxylation of G.[58] Three other laboratories have also observed

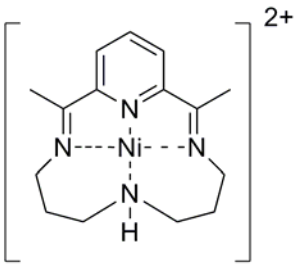

NiCR

Figure 2.2. Structure of NiCR.

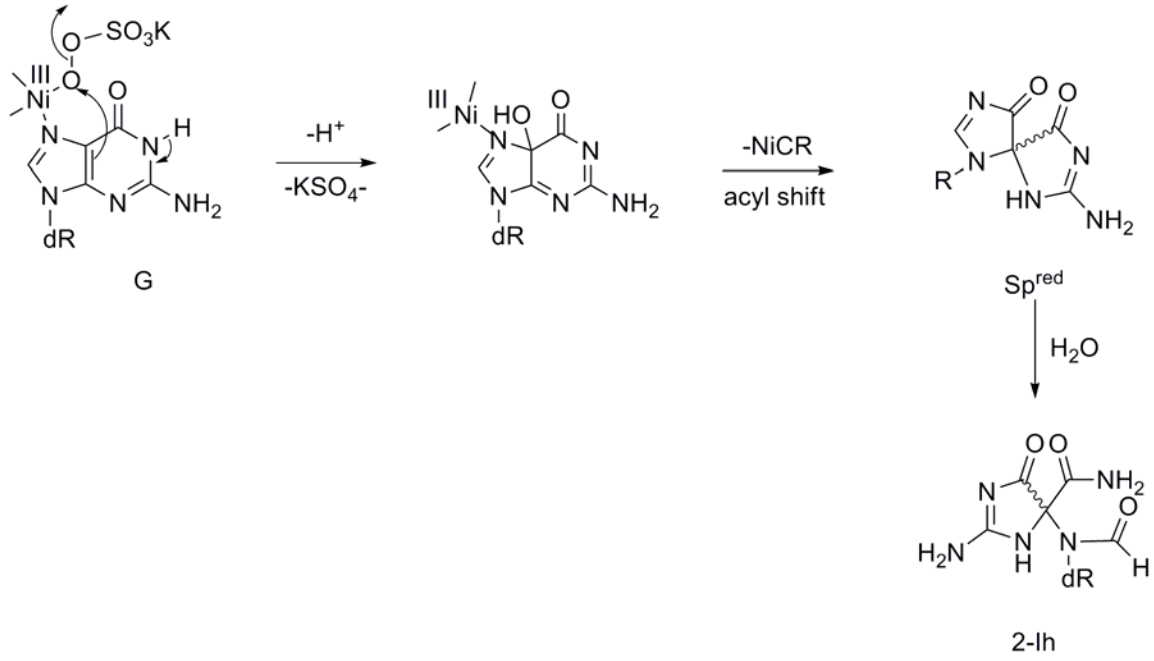

Scheme 2.3. Proposed binding of NiCR/$KHSO_5$ to guanine and formation of 2-Ih.

this mass increase.

Pratviel, Meunier, and coworkers studied the oxidation of G by Mn-TMPyP/$KHSO_5$ and found a minor product that gave the mass increase of G+34.[59, 60] Based on ^{18}O labeling studies in the Burrows laboratory, the new compound G+34 was proposed to be the result of two oxygens being incorporated from H_2O.[60] They suggested that the compound arises from the hydroxylation at C-5 of the $(G)^+$ intermediate, leading to an unstable compound with one labeled oxygen atom from $H_2{}^{18}O$ at C-5. This intermediate was expected to rearrange at physiological pH into a Sp-like structure.[14] The Rokita laboratory also found the mass of G+34 as the major product of DNA oxidation with a dinuclear copper complex, $[Cu_2^{II}(PD`O)(H_2O)_2]^{3+}$ where PD`OH is a pyridylalkylamine containing binucleating ligand.[61] More recently, epoxidation of G by dimethyldioxirane (DMDO) was studied by the Ball laboratory. An oxygen atom transfer reaction gives 5-carboxamido-5-formamido-2-iminohydantoin (2-Ih) as the only product, and its structure was characterized by the Ball laboratory.[62, 63]

In this work, we studied the oxidation chemistry of both a suitably protected nucleoside, namely, 2',3',5'-tri-*O*-acetylguanosine, and a 15-mer ssDNA containing a single 2'-deoxyguanosine site with various oxidants, including NiCR/$KHSO_5$, and the results were compared. Under specific conditions studied, oxidation of G gave 2-Ih as the only isolable product in both nucleoside and ssDNA. Hence, 2-Ih may be considered as a primary DNA lesion generated by several transition-metal oxidants.

Experimental section

Materials

Guanosine hydrate, $KHSO_5$ (oxone), $CoCl_2$, Na_2IrCl_6, Rose Bengal, $K_2S_2O_8$, EDTA, HEPES, sodium chloride, and sodium phosphate were purchased from commercially available sources. NiCR was synthesized by the method of Karn and Busch.[64] The oligodeoxynucleotides (ODNs) were obtained from the DNA Core facility at the University of Utah and were 5'-end labeled using T4 polynucleotide kinase and [γ-^{32}P] ATP following literature protocols.[65] Radioactivity was quantified using a Beckman LS6500 scintillation counter.

Instrumentation

ESI mass spectra were obtained on a Micromass Quattro II spectrometer. HPLC analyses of nucleoside reactions were analyzed on a Beckman System Gold 126NM solvent module attached to a Beckman 168NM diode array detector with a Varian C-18 analytical reversed-phase column (5 μm, 250 mm × 4.6 mm) or Phenomenex Synergi polar reversed-phase column (4 μm, 250 mm × 4.6 mm). All solvents were HPLC-grade that were filtered and sonicated before use. All aqueous solutions were prepared from purified water (Nanopure, Synbron/ Barnsted).

The ODN reactions were HPLC analyzed using a Beckman System Gold 126NM solvent module attached to a Beckman 166NM diode array detector running a Dionex DNAPac PA-100 analytical ion-exchange column (4 mm × 250 mm). Synthesis of 2',3',5'-tri-O-acetyl-guanosine $(OAc)_3G$ was carried out according to the previously published procedures.[66, 67]

Oxidation of $(OAc)_3G$

Oxidation with NiCR/$KHSO_5$: Condition A: 3 mM $(OAc)_3G$ was incubated with 12 μM NiCR and 4 mM $KHSO_5$ in 75 mM sodium phosphate (NaP_i) buffer at pH 7.4 and 37 °C for 30 min. After 30 min, the reaction was quenched with 40 mM HEPES. The reaction mixture was analyzed by HPLC using a polar-reversed- phase column with a linear gradient of 1% solvent B to 70% solvent B over 65 min at 1 mL/min monitored at 245 nm wavelength. Solvent A was 0.1% aqueous CF_3COOH (TFA); solvent B was 0.1% TFA in CH_3CN. Condition B: 3 mM $(OAc)_3G$ was incubated with 60 μM NiCR and 4 mM $KHSO_5$ added in intervals every 3 min in 75 mM NaP_i at pH 7.4 and 37 °C. The reaction was quenched with 40 mM HEPES after 30 min.

Oxidation with $CoCl_2$/$KHSO_5$: 3 mM $(OAc)_3G$ was incubated with 12 μM $CoCl_2$ and 4 mM $KHSO_5$ in 75 mM NaP_i at pH 7.4 and 37 °C for 30 min and the reaction was quenched with 40 mM HEPES.

Oxidation with Na_2IrCl_6: 3 mM $(OAc)_3G$ was treated with 6 mM Na_2IrCl_6 in 75 mM NaP_i at pH 7.4 and 37 °C and was quenched with 60 mM EDTA after 30 min.

Oxidation with singlet oxygen: 3 mM $(OAc)_3G$ was incubated with 300 μM RB in 75 mM NaP_i at pH 7.4 and was irradiated by a sunlamp emitting 360 nm for 30 min at 37 °C at a distance of ~8 cm above the reaction. The RB was removed by passing the reaction mixture through a Nap-25 column following the manufacturer's protocol. The fractions collected were analyzed by HPLC.

Oxidation with $K_2S_2O_8$: 3 mM $(OAc)_3G$ was treated with 70 mM $K_2S_2O_8$ in pH 7.4 and 75 mM NaP_i buffer under 256 nm light for 30 min at a distance of 3 cm.

Each reaction was analyzed by HPLC using a polar-reversed phase column with a

linear gradient of 1% solvent B to 70% solvent B in 65 min at 1 mL/min. Solvent A was 0.1% aqueous TFA; solvent B was 0.1% TFA in CH_3CN. The chromatogram was recorded while monitoring absorbance at 245 nm for product quantification. The reaction mixture was analyzed by LC-MS for product identification.

Oxidation and piperidine-induced cleavage of ODN

The ODN sequence used was a 15-mer with a single G at the eighth position from the 5' end. The sequence was 5'-TTT TTT TGT TTT TTT-3' (5'-T_7GT_7-3'). Oxidation reactions were carried out on 5 μM ODN, 5 μM NiCR with different concentrations of $KHSO_5$ ranging from 5 – 500 μM in 10 mM NaP_i and 100 mM NaCl (pH 7.4). Reactions were quenched with 50 mM HEPES after 30 min. Piperidine cleavage reactions were carried out in 0.4 M piperidine at 90 °C for 30 min. Finally, the smaller DNA fragments were separated by PAGE (20% polyacrylamide/ 7 M urea) and visualized by storage phosphor autoradiography (Molecular Dynamics Storm 840) and quantified with Image QuaNT version 5.2 software.

Oxidation with NiCR/$KHSO_5$: 5 μM ODN was incubated with 5 μM NiCR and then reacted with 250 μM $KHSO_5$ in 10 mM NaP_i and 100 mM NaCl buffer of pH 7.4 at 37 °C for 30 min.

Oxidation with Na_2IrCl_6: 5 μM ODN was allowed to react with 750 μM Na_2IrCl_6 in 10 mM NaP_i and 100 mM NaCl buffer at pH 7.4 at 37 °C for 30 min.

Oxidation with singlet oxygen: 5 μM ODN was incubated with 300 μM RB and irradiated with sunlamp in 10 mM NaP_i and 100 mM NaCl buffer of pH 7.4 at 37 °C for 30 min.

All the above reactions were analyzed by HPLC using an ion-exchange column with a gradient of 15% solvent B to 100% solvent B in 30 min at a flow rate of 1 mL/min. Solvent A is 90% ddH_2O; solvent B is 1.5 M sodium acetate at pH 7 and 10% CH_3CN. The chromatogram was recorded by monitoring absorbance at 260 nm.

Results and discussion

Oxidation of $(OAc)_3G$

The transition metal complex Na_2IrCl_6 is a water-soluble, non-nucleoside binding, outer-sphere, one-electron oxidant.[40] The oxidation of $(OAc)_3G$ with Ir (IV) results in the formation of Sp at pH 7. $CoCl_2$ exists as $[Co(H_2O)_6]^{2+}$ in aqueous solutions, and its higher oxidation state of Co (III) is extremely unstable at pH 7 and this initiates the decomposition of $KHSO_5$ that yields the potent sulfate radical. The freely diffusible $SO_4^{\cdot -}$ results in G-oxidation, yielding Sp as the major product at pH 7, and other oxidants like Gh and Iz as minor products, whereas in the square planar NiCR, two possible roles of Ni(II) have been proposed; one is the redox role where formation of a higher oxidation state is part of the catalytic cycle. The other role is Ni(II) acts as a Lewis acid for the activation of the peracid toward oxidative attack on the G nucleoside. It is well documented that Ni(II) ions bind to the N7 of G.[68] The proposed intermediate is an octahedral Ni (III) species, in which two additional ligands, guanine and an oxidant monopersulfate, are *cis*-coordinated to nickel. The oxidation of $(OAc)_3G$ with NiCR/$KHSO_5$ yielded a mixture of oxidation products that were well separated on the polar-reversed phase column (Figure 2.3). The products 2-Ih, Sp and Gh each exist as two diastereomers.

LC-ESI^+-MS allowed the identification of the products by comparing the retention

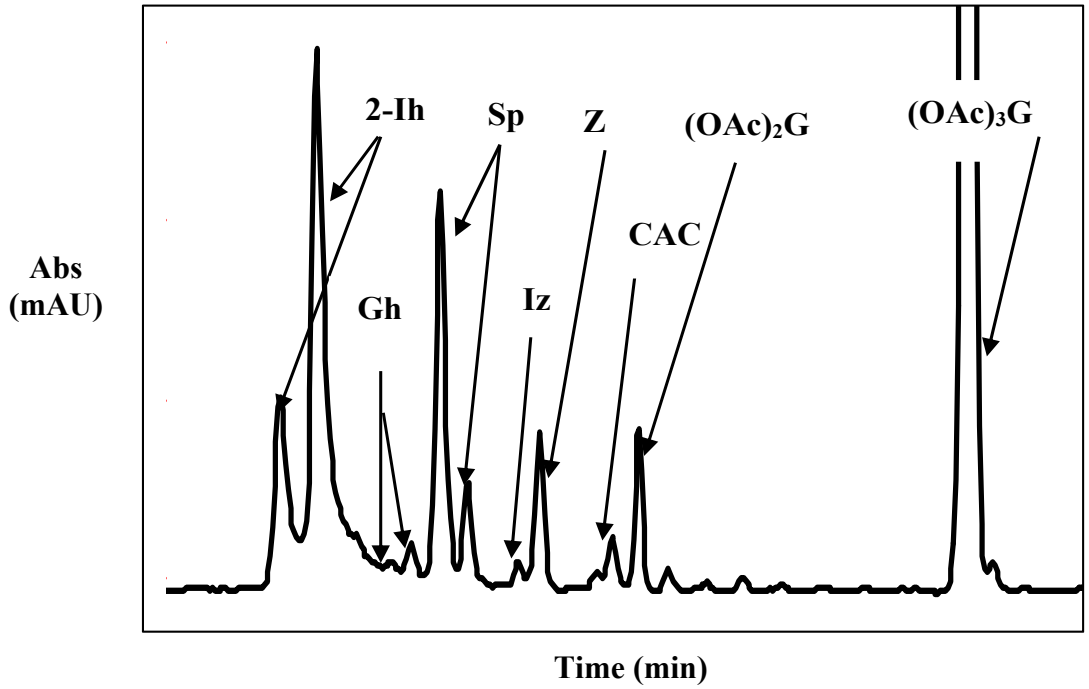

Figure 2.3. HPLC-chromatogram of $(OAc)_3G$ oxidation by $NiCR/KHSO_5$. The products have been identified by LC-ESI^+-MS. The oxidation products 2-Ih, Gh, and Sp give 2 diastereomers. Apart from these the products, Iz, Z, and CAC have also been identified.

time, UV-vis spectra, and mass shown in the Appendix. The masses obtained from oxidation of $(OAc)_3G$ with NiCR/$KHSO_5$ by LC-ESI^+-MS are shown in Table 2.2. Apart from the starting material $(OAc)_3G$ with $[M+H]^+$ of 410.0 amu, $(OAc)_2G$ was also seen with $[M+H]^+$ of 368 amu. All products were quantified by integrating the HPLC peak areas that were normalized through each compound's unique molar extinction coefficients (ε) at 245 nm shown in Table 2.3.[69] The molar extinction coefficient (ε) for 2-Ih was assumed to be similar to Sp at 2.24×10^3 $M^{-1}cm^{-1}$.

Two strategies were employed to form 2-Ih as a major product. The first was to increase the NiCR concentration, and the second was titrating 500 μM $KHSO_5$ at regular intervals of every 3.75 min for a total reaction time of 30 min. The latter yields the 2-Ih product exclusively, and the two diastereomers were well separated on the polar-reversed phase column (Figure 2.4). The two peaks from the reaction of 3 mM $(OAc)_3G$ with 60 μM NiCR and 4 mM $KHSO_5$ (added in aliquots) were collected to determine their mass. Both peaks in the chromatogram increased with increased NiCR concentration and titration of $KHSO_5$ at regular intervals, exclusively yielding the compound with mass of 443.9. 8-Oxo-G was not detected either by $CoCl_2$/ $KHSO_5$ or NiCR/$KHSO_5$ at pH 7.4. Homolytic cleavage of $K_2S_2O_8$ by photolysis generates a clean source of sulfate radical. The oxidation of $(OAc)_3G$ results in formation of 70% Sp, 25% Gh and 5% Iz. Singlet oxygen yields 85% Sp and 25% Gh as the oxidation products of $(OAc)_3G$. Figure 2.5 compares relative product distributions for the oxidation of $(OAc)_3G$ with various oxidants.

Table 2.2. Identification of products by LC-ESI^{+}-MS on oxidation of $(OAc)_3G$ with $NiCR/KHSO_5$.

Oxidation Products	$[M+H]^+$ in amu
Z	389
Gh	416
Sp^{red}	426
CAC	430
Sp	442
2-Ih	444
Iz	371
CA	388

Table 2.3. Molar extinction coefficients for oxidized bases of guanine.

Oxidized base	Molar extinction coefficient (ε) at 245 nm / M^{-1} cm^{-1}
Sp	2.24×10^3
Gh	1.17×10^3
Iz	2.05×10^4
Z	6.00×10^3
CAC	2.00×10^3
2-Ih	2.24×10^3 (assumed similar to Sp)

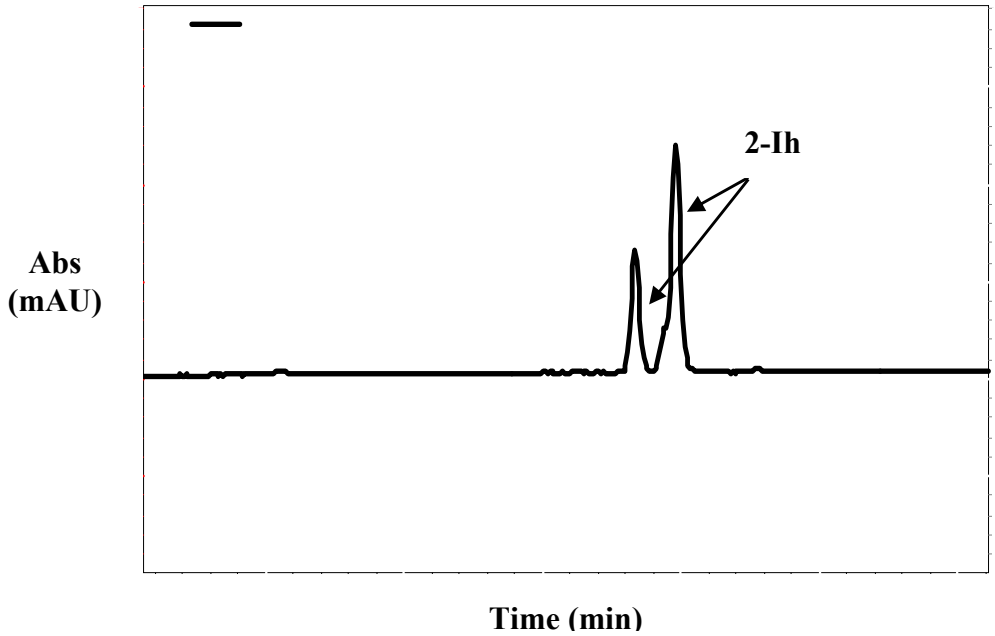

Figure 2.4. HPLC chromatogram of $(OAc)_3G$ oxidation by increased NiCR concentration and $KHSO_5$ titration.

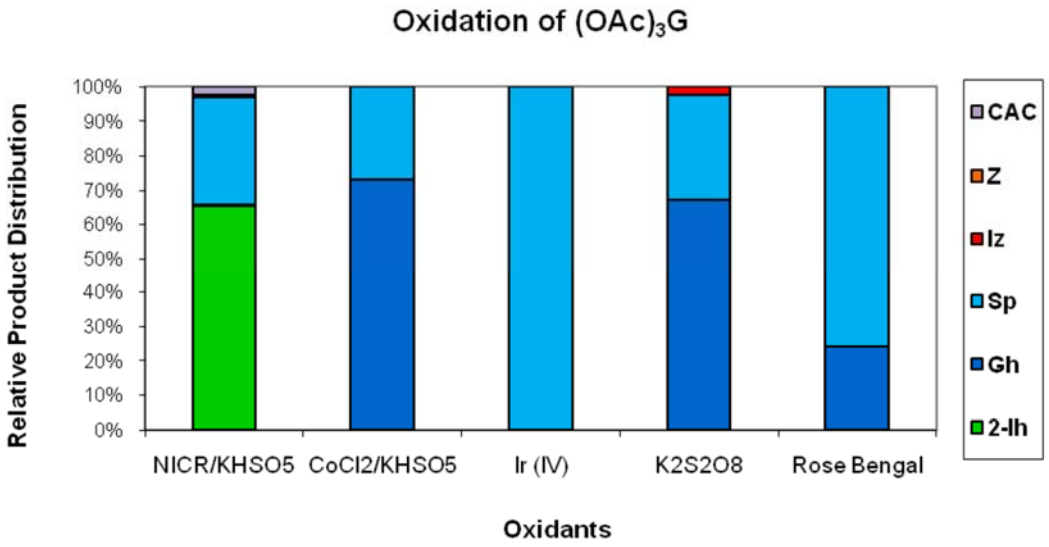

Figure 2.5. Relative product distribution of $(OAc)_3G$ oxidation by various oxidants.

Oxidation of 5'-T_7GT_7-3' ODN

Oxidation of a 15-mer ODN followed by piperidine treatment resulted in exclusive cleavage of the strand at the G site, as analyzed by polyacrylamide gel electrophoresis (Figure 2.6). Lanes 1-6 show the oxidation of 5 μM 5'-T_7GT_7-3' by 5 μM NiCR with increasing concentrations of $KHSO_5$ from 5 to 500 μM. Lane 7 shows a control study without addition of oxidant. Lane 8 is the Maxam-Gilbert G-lane.[70] The G was cleanly oxidized at the concentrations of 125-500 μM.

The reaction of 15-mer with NiCR/$KHSO_5$ was analyzed on an ion-exchange HPLC column and yields 2-Ih as the major product (Figure 2.7). The 2-Ih mass was supported by ESI-MS^+ with the mass of 4558.0 amu for peak 2 corresponding to oxidized ODN. Peak 1 has the mass of 4524.0 for the standard 15-mer.

The 15-mer reaction with iridium (IV) at pH 7.4 and singlet oxygen yielded Sp as the only product and the mass 4556.0 amu was confirmed by ESI^+-MS. The relative product distribution for oxidation of 15-mer with iridium (IV), RB, and NiCR/$KHSO_5$ is shown in Figure 2.8.

Conclusion

The oxidation of $(OAc)_3G$ yields a wide array of products that follow different oxidation pathways. Some oxidants follow the C-8 oxidation pathway and lead to the formation of Sp and Gh, with 8-oxo-G, the most common oxidation product, as an intermediate. The other oxidation pathway starting with C-5 leads to the formation of Iz and 2-Ih. Transition metals play an important role in formation of the oxidative products that depends on the coordination of the oxidant to the metal. The oxidation of the $(OAc)_3G$

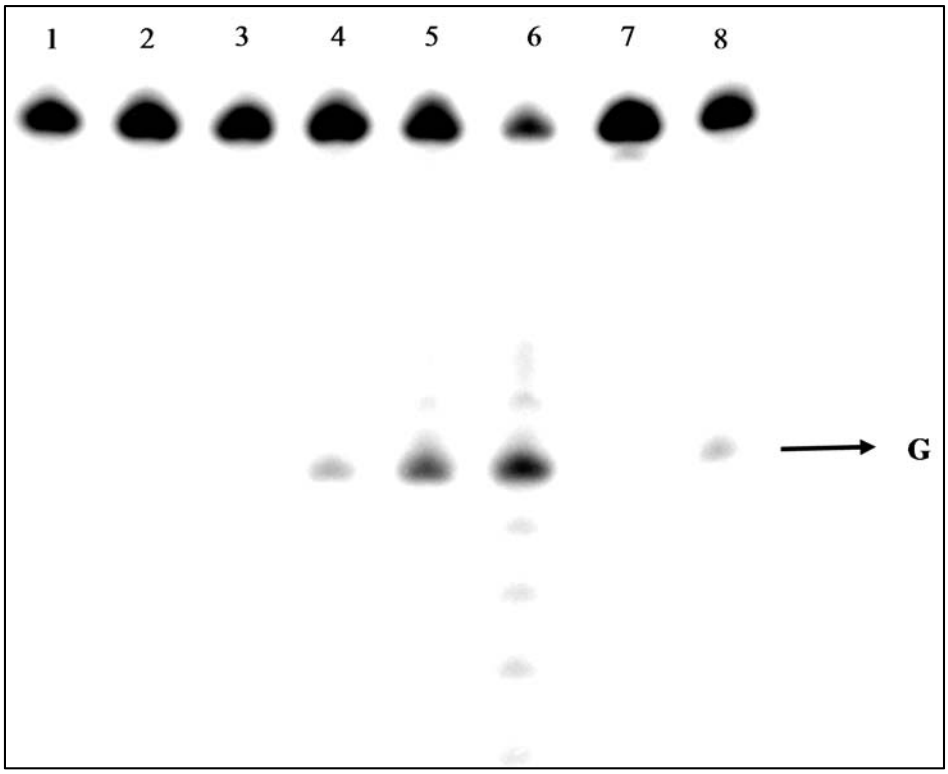

Figure 2.6. Gel analysis for oxidation and piperidine-induced cleavage of 5'-T_7GT_7-3' ODN. All the lanes were piperidine treated. Lanes 1-6: oxidation reactions with 5 μM ODN, 5 μM NiCR and increasing concentration of $KHSO_5$ with lane 1-6 as 5, 25, 50, 125, 250, and 500 μM, respectively. Lane 7: control lane with 5 μM ODN. Lane 8: Maxam-Gilbert G-lane.

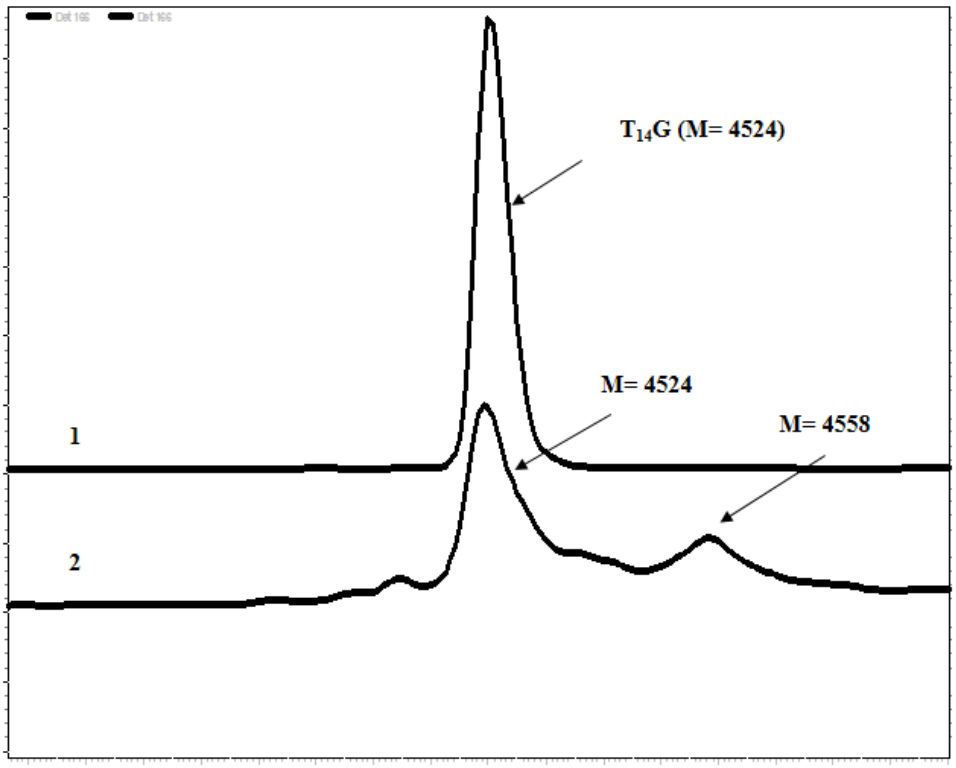

Figure 2.7. HPLC trace for oxidation of 15-mer ODN with NiCR/$KHSO_5$. The HPLC-chromatogram represents a 15-mer standard (1) and reaction of NiCR/$KHSO_5$ with 15-mer yields two peaks (2).

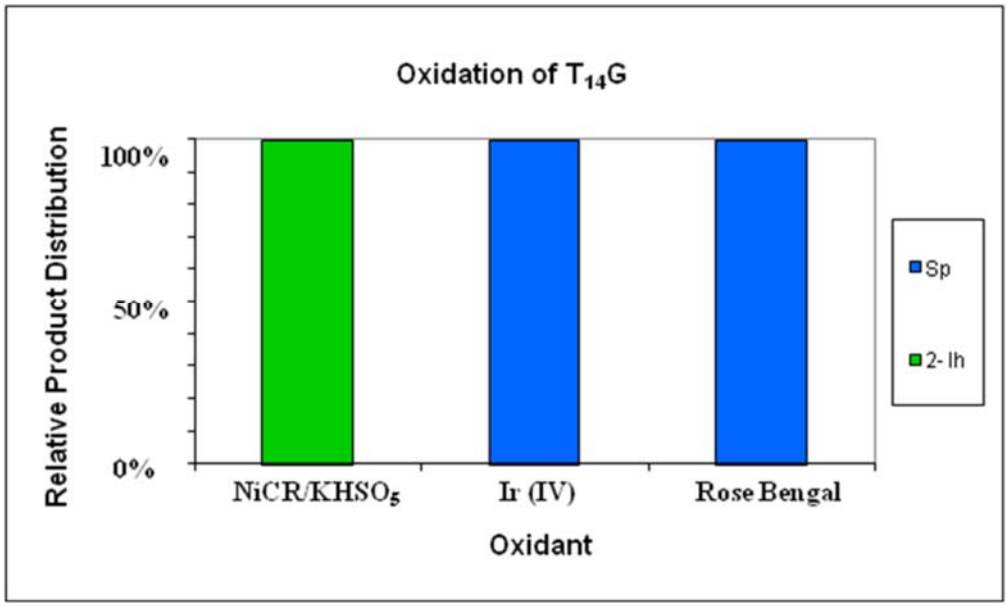

Figure 2.8. Relative product distribution of oxidation of $T_{14}G$ with Ir (IV), Rose Bengal and $NiCR/KHSO_5$.

with NiCR/$KHSO_5$ yielded a wide range of oxidation products with two diastereomers of each Sp, Gh, and 2-Ih.

Since no reducing or anaerobic conditions were used, the product FAPy-G was not observed.[6-8] 2-Ih was formed as the only oxidation product in $(OAc)_3G$ by increasing the concentration of NiCR and adding the $KHSO_5$ in aliquots. The exact mechanism for this is still not clear, but we propose the *cis*-coordinated Ni bound by both sulfate radical and the N7 of G that further results in an acyl ring shift resulting in formation of 2-Ih.

The oxidation of a 15-mer ssDNA containing a single G site also results in formation of exclusively 2-Ih. The NiCR complex was used as a probe for the structure of DNA and the previously unknown product from the piperidine cleavage site with a mass of M+34 can now be confirmed as the oxidation product 2-Ih. Thus, we conclude that 2-Ih is a two-electron oxidation product, whereas Sp and Gh are four-electron oxidation products of G. Furthermore, Sp^{red} can readily be hydrolyzed and the ring opening occurs to give 2-Ih (M+34) and ring opening can result in two possible structures (a) and (b) as shown in Figure 2.9. The structure (a) has been confirmed through NMR studies performed by the Ball Laboratory.[62] Further studies have been carried out in our laboratory on oxidation of dG with copper-mediated Fenton chemistry in the presence of reductants such as ascorbate or N-acetyl-cysteine that are used for reduction of metal ions. It has been shown that 2-Ih is a major product of oxidation in nucleosides, ssDNA and dsDNA, following the C-5 pathway for its formation.[70] Currently, the lab is also conducting experiments with X-rays to understand how ubiquitous is formation of 2-Ih. The formation of 2-Ih as the major product in nucleoside and ssDNA in the presence of redox-active metals suggests that 2-Ih is a primary DNA lesion.

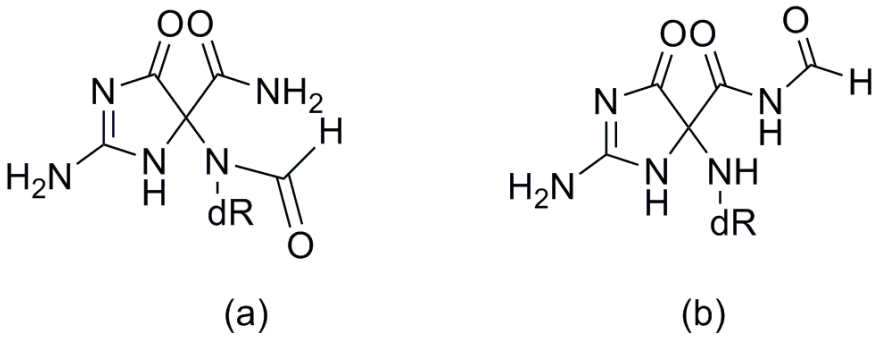

Figure 2.9. 2-Ih as hydrolysis products of Sp^{red}.

References

1. Ames, B. N. Dietary Carcinogens and Anticarcinogens. Oxygen radicals and degenerative diseases. *Science* **1983,** 221, 1256-1264.

2. Wang, D. K., D. A.; Essigmann, J. M. Mutagenicity and Repair of Oxidative DNA Damage: Insights from Studies Using Defined Lesions. *Mutat. Res.* **1998,** 400, 99-115.

3. Ames, B. N.; Shingenaga, M. K.; M., H. T. Oxidants, Antioxidants, and the Degenerative Diseases of Aging. *Proct. Natl. Acad. Sci. USA* **1993,** 90, 7915-7922.

4. Halliwell, B.; Gutteridge, J. M. C. Free Radical, Ageing and Disease. *Free Radicals in Biology and Medicine (Clarendon Press, Oxford)* **1989**.

5. Bjelland, S.; Seeberg, E. Mutagenicity, toxicity and repair of DNA base damage induced by oxidation. *Mutation Research/Fundamental and Molecular Mechanisms of Mutagenesis* **2003,** 531, 37-80.

6. Pouget, J. P.; Douki, T.; Richard, M. J.; Cadet, J. DNA Damage Induced in Cells by Î³ and UVA Radiation As Measured by HPLC/GC-MS and HPLC EC and Comet Assay. *Chem. Res. Toxicol.* **2000,** 13, 541-549.

7. Malins, D. C.; Haimanot, R. Major Alterations in the Nucleotide Structure of DNA in Cancer of the Female Breast. *Cancer Res* **1991,** 51, 5430-5432.

8. Cadet, J.; Sage, E.; Douki, T. Ultraviolet radiation-mediated damage to cellular DNA. *Mutation Research/Fundamental and Molecular Mechanisms of Mutagenesis* **2005,** 571, 3-17.

9. Hailer, M. K.; Slade, P. G.; Martin, B. D.; Sugden, K. D. Nei Deficient Escherichia coli Are Sensitive to Chromate and Accumulate the Oxidized Guanine Lesion Spiroiminodihydantoin. *Chem. Res. Toxicol.* **2005,** 18, 1378-1383.

10. Matter, B.; Malejka-Giganti, D.; Csallany, A. S.; Tretyakova, N. Quantitative analysis of the oxidative DNA lesion, 2,2-diamino-4-(2-deoxy-{beta}-D-erythro-pentofuranosyl)amino]-5(2H)-oxazolone (oxazolone), in vitro and in vivo by isotope dilution-capillary HPLC-ESI-MS/MS. *Nucl. Acids Res.* **2006,** 34, 5449-5460.

11. Gedik, C. M.; Collins, A. F. Establishing the Background Level of Base Oxidation in Human Lymphocyte DNA: Results of an Interlaboratory Validation study. *FASEB J.* **2005,** 19, 82-84.

12. Steenken, S.; Jovanovic, S. V.; Bietti, M.; Bernhard, K. The Trap Depth (in DNA) of 8-Oxo-7,8-dihydro-2'deoxyguanosine as Derived from Electron-Transfer Equilibria in Aqueous Solution. *Journal of the American Chemical Society* **2000,** 122, 2373-2374.

13. Candeias, L. P.; Steenken, S. Structure and acid-base properties of one-electron-oxidized deoxyguanosine, guanosine, and 1-methylguanosine. *J. Am. Chem. Soc.* **1989,** 111, 1094-1099.

14. Pratviel, G. M. B. Guanine Oxidation: One- and Two-Electron Reactions. *Chem. Eur. J.* **2006,** 12, 6018-6030.

15. Stemp, E. D. A.; Arkin, M. R.; Barton, J. K. Oxidation of Guanine in DNA by Ru(phen)2(dppz)3+ Using the Flash-Quench Technique. *J. Am. Chem. Soc.* **1997,** 119, 2921-2925.

16. Schiemann, O.; Turro, N. J.; Barton, J. K. EPR Detection of Guanine Radicals in a DNA Duplex under Biological Conditions: Selective Base Oxidation by Ru(phen)2dppz3+ Using the Flash-Quench Technique. *J. Phys. Chem.* **2000,** 104, 7214-7220.

17. Misiaszek, R.; Crean, C.; Joffe, A.; Geacintov, N. E.; Shafirovich, V. Oxidative DNA Damage Associated with Combination of Guanine and Superoxide Radicals and Repair Mechanisms via Radical Trapping. *J. Biol. Chem.* **2004,** 279, 32106-32115.

18. Cadet, J.; Berger, M.; Buchko, G. W.; Joshi, P. C.; Raoul, S.; Ravanat, J.-L. 2,2-Diamino-4-[(3,5-di-O-acetyl-2-deoxy-.beta.-D-erythro- pentofuranosyl)amino]-5-(2H)-oxazolone: a Novel and Predominant Radical Oxidation Product of 3',5'-Di-O-acetyl-2'-deoxyguanosine. *J. Am. Chem. Soc.* **2002,** 116, 7403-7404.

19. Gasparutto, D.; Ravanat, J.-L.; Gerot, O.; Cadet, J. Characterization and Chemical Stability of Photooxidized Oligonucleotides that Contain 2,2-Diamino-4-[(2-deoxy-Î²-d-erythro-pentofuranosyl)amino]-5(2H)-oxazolone. *Journal of the American Chemical Society* **1998,** 120, 10283-10286.

20. Raoul, S.; Berger, M.; Buchko, G. W.; Joshi, P. C.; Morin, B.; M.;, W.; J., C. 1H, 13C and 15N Nuclear Magnetic Resonance Analysis and Chemical Features of the Two Main Radical Oxidation Products of 2'-Deoxyguanosine: Oxazolone and Imidazolone Nucleosides. *J. Chem. Soc. Perkin Trans. 2* **1996,** 2, 371-381.

21. Luo, W.; Muller, J. G.; Burrows, C. J. The pH-Dependent Role of Superoxide in Riboflavin-Catalyzed Photooxidation of 8-Oxo-7,8-dihydroguanosine. *Org. Lett.* **2001,** 3, 2801-2804.

22. Shafirovich, V.; Dourandin, A.; Huang, W.; Geacintov, N. E. The Carbonate Radical Is a Site-selective Oxidizing Agent of Guanine in Double-stranded Oligonucleotides. *J. Biol. Chem.* **2001,** 276, 24621-24626.

23. Kasai, H.; Yamaizumi, Z.; Berger, M.; Cadet, J. Photosensitized formation of 7,8-dihydro-8-oxo-2'-deoxyguanosine (8-hydroxy-2'-deoxyguanosine) in DNA by riboflavin: a nonsinglet oxygen-mediated reaction. *J. Am. Chem. Soc.* **2002,** 114, 9692-9694.

24. Vialas, C.; Pratviel, G.; Claparols, C.; Meunier, B. Efficient Oxidation of 2'-Deoxyguanosine by Mn-TMPyP/$KHSO_5$ to Imidazolone dIz without Formation of 8-Oxo-dG. *J. Am. Chem. Soc.* **1998,** 120, 11548-11553.

25. Vialas, C.; Claparols, C.; Pratviel, G.; Meunier, B. Guanine Oxidation in Double-Stranded DNA by Mn-TMPyP/$KHSO_5$: 5,8-Dihydroxy-7,8-dihydroguanine Residue as a Key Precursor of Imidazolone and Parabanic Acid Derivatives. *J. Am. Chem. Soc.* **2000,** 122, 2157-2167.

26. Shukla, L. I.; Adhikary, A.; Pazdro, R.; Becker, D.; Sevilla, M. D. Formation of 8-oxo-7,8-dihydroguanine-radicals in γ-irradiated DNA by multiple one-electron oxidations. *Nucl. Acids Res.* **2004,** 32, 6565-6574.

27. Steenken, S.; Jovanovic, S. V.; Bietti, M.; Bernhard, K. The Trap Depth (in DNA) of 8-Oxo-7,8-dihydro-2'deoxyguanosine as Derived from Electron-Transfer Equilibria in Aqueous Solution. *J. Am. Chem. Soc.* **2000,** 122, 2373-2374.

28. Luo, W.; Muller, J. G.; Rachlin, E. M.; Burrows, C. J. Characterization of Spiroiminodihydantoin as a Product of One-Electron Oxidation of 8-Oxo-7,8-dihydroguanosine. *Org. Lett.* **2000,** 2, 613-616.

29. Luo, W.; Muller, J. G.; Rachlin, E. M.; Burrows, C. J. Characterization of Hydantoin Products from One-Electron Oxidation of 8-Oxo-7,8-dihydroguanosine in a Nucleoside Model. *Chem. Res. Toxicol.* **2001,** 14, 927-938.

30. Neeley, W. L.; Essigmann, J. M. Mechanisms of Formation, Genotoxicity, and Mutation of Guanine Oxidation Products. *Chem. Res. Toxicol.* **2006,** 19, 491-505.

31. Lloyd, D. R.; Phillips, D. H.; Carmichael, P. L. Generation of Putative Intrastrand Cross-Links and Strand Breaks in DNA by Transition Metal Ion-Mediated Oxygen Radical Attack. *Chem. Res. Toxicol.* **1997,** 10, 393-400.

32. Foote, C. S. Defination of Type I and Type II Photsensitized Oxidation. *Photochem. Photobiol.* **1991,** 54, 659-659.

33. Vialas, C.; Pratviel, G.; Claparols, C.; Meunier, B. Efficient Oxidation of 2'-Deoxyguanosine by Mn-TMPyP/$KHSO_5$ to Imidazolone dIz without Formation of 8-Oxo-dG. *J. Am. Chem. Soc.* **1998,** 120, 11548-11553.

34. Muller, J. G.; Zheng, P.; Rokita, S. E.; Burrows, C. J. DNA and RNA Modification Promoted by $[Co(H_2O)_6]Cl_2$ and $KHSO_5$: Guanine Selectivity, Temperature Dependence, and Mechanism. *J. Am. Chem. Soc.* **1996,** 118, 2320-2325.

35. Chen, X.; Rokita, S. E.; Burrows, C. J. DNA modification: intrinsic selectivity of nickel(II) complexes. *J. Am. Chem. Soc.* **1991,** 113, 5884-5886.

36. Burrows, C. J.; Muller, J. G. Oxidative Nucleobase Modifications Leading to Strand Scission. *Chem. Rev.* **1998,** 98, 1109-1152.

37. Steenken, S.; Jovanovic, S. V. How Easily Oxidizable Is DNA? One-Electron Reduction Potentials of Adenosine and Guanosine Radicals in Aqueous Solution. *J. Am. Chem. Soc.* **1997,** 119, 617-618.

38. Foote, C. S.; Clennan, E. L. Properties and Reactions of Singlet Dioxygen in Active Oxygen in Chemistry. *Champman and Hall, Bishopbirggs* **1995**.

39. Ye, Y. M., J. G.; Luo, W.; Mayne, C. L.; Shallop, A. J.; Jones, R. A.; Burrows, C. J. "Formation of 13C, 15N, and 18O-Labeled Guanidinohydantoin from Guanosine Oxidation with Singlet Oxygen. Implications for Structure and Mechanism.". *J. Am. Chem. Soc.* **2003,** 125, 13926-13927.

40. Muller, J. M.; Duarte, V.; Hickerson, R. P.; Burrows, C. J. Gel Electrophoretic Detection of 7,8-dihydro-8-oxoguanine and 7,8-dihydro-8-oxoadenine via Oxidation by Ir(IV). *Nucl. Acids Res.* **1998,** 26, 2247-2249.

41. Vieira, A. J. S. C.; Steenken, S. Pattern of hydroxy radical reaction with adenine and its nucleosides and nucleotides. Characterization of two types of isomeric hydroxy adduct and their unimolecular transformation reactions. *J. Am. Chem. Soc.* **2002,** 112, 6986-6994.

42. Kamiya, H.; Miura, H.; Murata-Kamiya, N.; Ishikawa, H.; Sakaguchi, T.; Inoue, H.; Sasaki, T.; Masutanl, C.; Hanaoka, F.; Nishimura, S.; Ohtsuka, E. 8-Hydroxyadenine (7, 8-dihydro-8-Oxoadenine) induces misincorporation in in vitro DNA synthesis and mutations in NIH 3T3 cells. *Nucl. Acids Res.* **1995,** 23, 2893-2899.

43. Jaruga, P.; Dizdaroglu, M. Repair of products of oxidative DNA base damage in human cells. *Nucl. Acids Res.* **1996,** 24, 1389-1394.

44. Kawanishi, S.; Inoue, S.; Yamamoto, K. Site-specific DNA damage induced by nickel(II) ion in the presence of hydrogen peroxide. *Carcinogenesis* **1989,** 10, 2231-2235.

45. Nackerdien, Z.; Kasprzak, K. S.; Rao, G.; Halliwell, B.; Dizdaroglu, M. Nickel(II)- and Cobalt(II)-dependent Damage by Hydrogen Peroxide to the DNA Bases in Isolated Human Chromatin. *Cancer Res.* **1991,** 51, 5837-5842.

46. Kasprzak, K. S. The role of oxidative damage in metal carcinogenicity. *Chem. Res. Toxicol.* **2002,** 4, 604-615.

47. Wetterhahn, K. Environmental metal carcinogens: genotoxicity and altered gene expression by direct metal-mediated and indirect oxidative pathways. *New J. Chem.* **1996,** 20, 199.

48. Ciccarelli, R. B.; Wetterhahn, K. E. Nickel Distribution and DNA Lesions Induced in Rat Tissue by the Carcinogen Nickel Carbonate. *Cancer Res* **1982,** 42, 3544-3549.

49. Ciccarelli, R. B.; Hampton, T. H.; Jennette, K. W. Nickel carbonate induces DNA-protein crosslinks and DNA strand breaks in rat kidney. *Cancer Lett.* **1981,** 12, 349-354.

50. Muller, J. G.; Chen, X.; Dadiz, A. C.; Rokita, S. E.; Burrows, C. J. Ligand effects associated with the intrinsic selectivity of DNA oxidation promoted by nickel(II) macrocyclic complexes. *J. Am. Chem. Soc.* **1992,** 114, 6407-6411.

51. Inoue, S. ESR evidence for superoxide, hydroxyl radicals and singlet oxygen produced from hydrogen peroxide and nickel(II) complex of glycylglycyl-L-histidine. *Biochem. and Biophys. Res. Commun.* **1989,** 159, 445.

52. Datta, K.; Datta, A. K. Effect of nickel(II) and tetraglycine on hydroxylation of the guanine moiety in 2'-deoxyguanosine, DNA, and nucleohistone by hydrogen peroxide. *The Science of the total environment* **1994,** 148, 207.

53. Bal, W.; Lukszo, J.; Kasprzak, K. S. Interactions of Nickel(II) with Histones: Enhancement of 2'-Deoxyguanosine Oxidation by Ni(II) Complexes with CH_3CO-Cys-Ala-Ile-His-NH_2, a Putative Metal Binding Sequence of Histone H3. *Chem. Res. Toxicol.* **1996,** 9, 535-540.

54. Muller, J. G.; Hickerson, R. P.; Perez, R. J.; Burrows, C. J. DNA Damage from Sulfite Autoxidation Catalyzed by a Nickel(II) Peptide. *J. Am. Chem. Soc.* **1997,** 119, 1501-1506.

55. Martin, R. B. Nucleoside sites for transition metal ion binding. *Acc. Chem. Res.* **2002,** 18, 32-38.

56. Muller, J. M.; Chen, X.; Dadiz, A. C.; Rokita, S. E.; Burrows, C. J. Macrocylic Nickel Complexes in DNA Recognition and Oxidation. *Pure & Appl. Chem.* **1993,** 65, 545-550.

57. Luo, W. Characterization of Purine Oxidation Products from One-Electron Oxidants, Superoxide and Singlet Oxygen.

58. Kasprzak, K. S.; Hernandez, L. Enhancement of Hydroxylation and Deglycosylation of 2'-Deoxyguanosine by Carcinogenic Nickel Compounds. *Cancer Res.* **1989,** 49, 5964-5968.

59. Vialas, C.; Claparols, C.; Pratviel, G.; Meunier, B. Guanine Oxidation in Double-Stranded DNA by Mn-TMPyP/$KHSO_5$: 5,8-Dihydroxy-7,8-dihydroguanine Residue as a Key Precursor of Imidazolone and Parabanic Acid Derivatives. *J. Am. Chem. Soc.* **2000,** 122, 2157-2167.

60. Lapi, A.; Pratviel, G.; B., M. Guanine Oxidation in Double-Stranded DNA by MnTMPyP/$KHSO_5$: At Least Three Independent Reaction Pathways. *Metal Based Drugs* **2001,** 8, 47-56.

61. Li, L.; Karlin, K. D.; Rokita, S. E. Changing Selectivity of DNA Oxidation from Deoxyribose to Guanine by Ligand Design and a New Binuclear Copper Complex. *J. Am. Chem. Soc.* **2005,** 127, 520-521.

62. Ye, W.; Sangaiah, R.; Degen, D. E.; Gold, A.; Jayaraj, K.; Koshlap, K. M.; Boysen, G.; Williams, J.; Tomer, K. B.; Ball, L. M. A 2-Iminohydantoin from the Oxidation of Guanine Volume 19, Number 4, April 2006, pp 506-510. *Chem. Res. Toxicol.* **2006,** 19, 887-887.

63. Ye, W.; Sangaiah, R.; Degen, D. E.; Gold, A.; Jayaraj, K.; Koshlap, K. M.; Boysen, G.; Williams, J.; Tomer, K. B.; Mocanu, V.; Dicheva, N.; Parker, C. E.; Schaaper, R. M.; Ball, L. M. Iminohydantoin Lesion Induced in DNA by Peracids and Other Epoxidizing Oxidants. *J. Am. Chem. Soc.* **2009,** 131, 6114-6123.

64. Karn, J. L.; Busch, D. H. Nickel (II) Complexes of the Tetradentate Macrocycle 2,12-Dimethyl-3,7,11,17-Tetraazabicyclo (11.3.1) Heptadeca-1 (17),2,11,13,15-Pentaene. *Nature* **1966,** 211, 160-162.

65. Carey, M. F.; Peterson, C. L.; Smale, S. T. Preparation of 32P-End-Labeled DNA Fragments for Performing DNA-Binding Experiments. *Cold Spring Harbor Protocols* **2013,** 2013, pdb.prot074336.

66. Holmes, R. E.; Robins, R. K. Purine Nucleosides. IX. The Synthesis of 9-beta-D-Ribofuranosyl Uric Acid and Other Related 8-Substituted Purine Ribonucleosides. *J. Am. Chem. Soc.* **1965,** 87, 1772-1776.

67. Matsuda, A.; Shinozaki, M.; Suzuki, M.; Watanabe, K.; Miyasaka, T. A Convenient Method for the Selective Acylation of Guanine Nucleosides. *Synthesis* **1986**, 385-386.

68. Shih, H. C.; Tang, N.; Burrows, C. J.; Rokita, S. E. Nickel-Based Probes of Nucleic Acid Structure Bind to Guanine N7 but Do Not Perturb a Dynamic Equilibrium of Extrahelical Guanine Residues. *J. Am. Chem. Soc.* **1998,** 120, 3284-3288.

69. Suzuki, T.; Friesen, M. D.; Ohshima, H. Identification of Products Formed by Reaction of 3',5'-Di-O-acetyl-2'-deoxyguanosine with Hypochlorous Acid or a Myeloperoxidase $H_2O_2Cl^-$ System. *Chem. Res. Toxicol.* **2003,** 16, 382-389.

70. Maxam, A. M.; Gilbert, W. A new method for sequencing DNA. *Proc. Natl. Acad. Sci. USA* **1977,** 74, 560-564.

.

CHAPTER 3

SELECTION OF DNA APTAMERS FOR OXIDIZED GUANINE LESIONS BY THE STRUCTURE-SWITCHING SELEX METHOD

Introduction

Several modifications have been made to the typical SELEX procedure, since its invention.[1-6] The flexibility offered with respect to methodology is an enormous advantage of SELEX that was explained in Chapter 1. Several alterations have been made either to generate improved aptamers or simplify the SELEX procedure.[7, 8] Some of these refinements include changes to target immobilization, nucleic acid library, selection stringency, amplification, or monitoring the enrichment. Nucleic acids have the propensity to hybridize to complementary oligonucleotides, which has been applied for construction of molecular probes.[9, 10] However, nucleic acids developed as aptamers have also been adapted selectively to undergo "induced fit" conformational change in the presence of cognate ligands.[11] The aptamers can compete and switch from DNA/DNA duplex to DNA/target complex. The duplex is formed between the DNA library or aptamer and a small oligonucleotide moiety complementary to the aptamer. In the presence of a target, the aptamer prefers the aptamer-target complex and a switch in structure occurs. This switch of binding partners for aptamers has been widely studied by various groups and

referred to as structure-switching aptamers (Figure 3.1).[12, 13] These aptamers have also been engineered to transduce this molecular recognition through signaling.[3, 14] It is important to note that not all aptamers can be converted to structure-switching probes, thus one needs to perform structure-switching SELEX for these targets.

The structure-switching principle was applied in our research to select aptamers for the targets. The five targets used for selection are the guanine oxidation products, 8-oxo-dG and its nucleobase (8-oxo-G), dSp nucleoside diastereomers, and one Sp enantiomer (Figure 3.2) that are formed by reaction of various reactive oxygen species (ROS) with guanine.[15-17] These targets are substrates for either BER or NER repair pathways that have been discussed in detail in Chapter 1. The above mentioned oxidation products are small molecules and possess technical challenges with performing SELEX.[4, 18] The most crucial step for a successful aptamer selection involves the separation of target-bound and unbound species.[19] Affinity chromatography, a conventional separation method, is used to immobilize target on column material such as sepharose or agarose.[7, 20] However, chemical modification of the target is required to immobilize it on the column. Another disadvantage to chemical modification is that the library is exposed to the modified target, as opposed to the desired unmodified target, increasing the possibility of selecting sequences that display binding properties toward the linker arm or the modified target. Besides, a substantial amount of modified target is required to be synthesized in order to achieve sufficiently high loading of the column. These challenges along with target solubility issues at high concentrations have led us to use an alternative approach to select the aptamers.

The selection strategy for aptamers is based on the work previously reported by Li,[21] Stojanovic,[22] and Stoltenberg[23]. The main difference in selection was the presentation

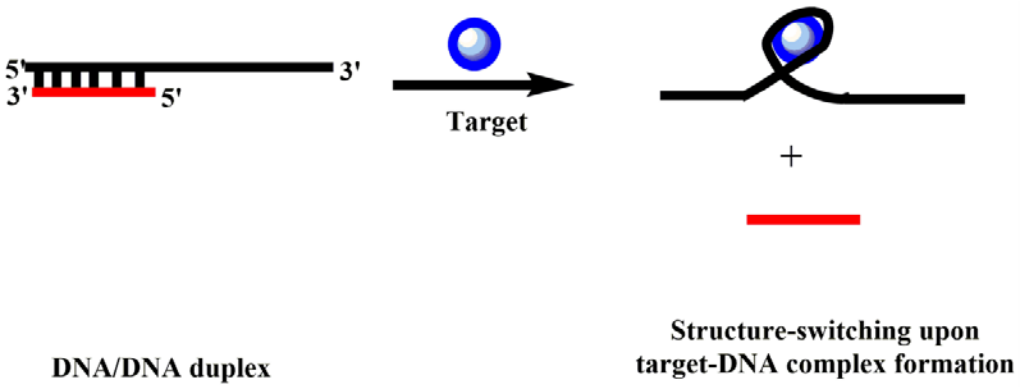

Figure 3.1. The structure-switching process of the aptamer from its complementary DNA/DNA duplex to a more favored DNA-target complex.

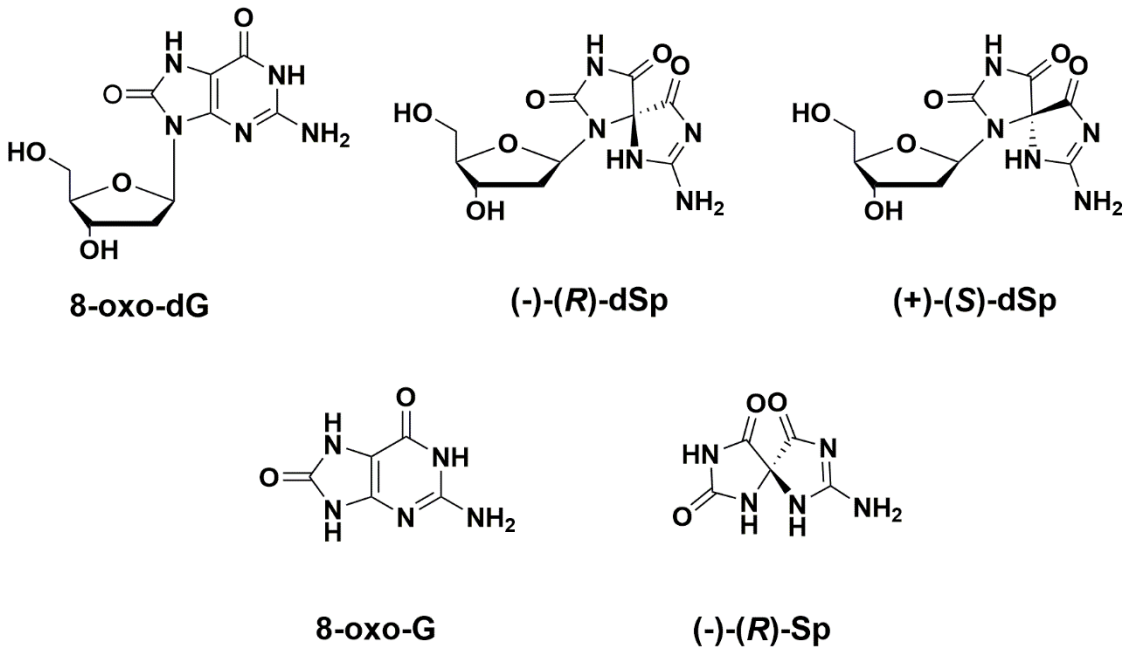

Figure 3.2. Targets used to select aptamers by performing capture-SELEX. All these targets are oxidation products of guanine.

of target and the oligonucleotide library as compared to standard affinity chromatography. A special SELEX library was developed to enable the immobilization of the library instead of the target on the column. In one case, a competitor oligonucleotide complementary to the primer region was utilized (Figure 3.3a) and in another a centralized docking region (Figure 3.4a) was used to capture the library on the column. The two strategies along with different randomized libraries and docking regions are shown in Figures 3.3 and 3.4 and will be henceforth referred to as MS-SELEX, and YL-SELEX, respectively.

MS-SELEX has a special 72-mer ssDNA library that consists of a 30-nucleotide (nt) randomized region that is flanked by primer-binding sequences (PBS). An 18-mer capture or docking strand that is 3'-biotinylated is partially complementary to one of the primer regions (Figure 3.3b). This arrangement permits immobilization of the DNA library on a streptavidin-agarose resin column through DNA hybridization. In the presence of a target, the library sequences undergo structural-switching to form a DNA-target complex. The DNA eluted from the column by this switching mechanism is amplified to dsDNA and further converted to ssDNA library to be used for the next round of selection.

YL-SELEX has a 94-mer ssDNA library that consists of a central 15-nt fixed sequence flanked by two random-sequence domains of 10 and 20-nt, each further flanked by PBS. The capture strand that is 5'-biotinylated with a poly-A linker attaches to the central 15-nt fixed region of the library (Figure 3.4b). Target-binding initiates structural changes and selective library sequences are eluted from the column. PCR amplification of the eluted strands and further conversion to ssDNA was conducted to proceed to the next round. YL-SELEX was used for the selection of aptamers for target 8-oxo-G to compare the aptamers with respect to MS-SELEX. Both MS-SELEX and YL-SELEX libraries were

(a)

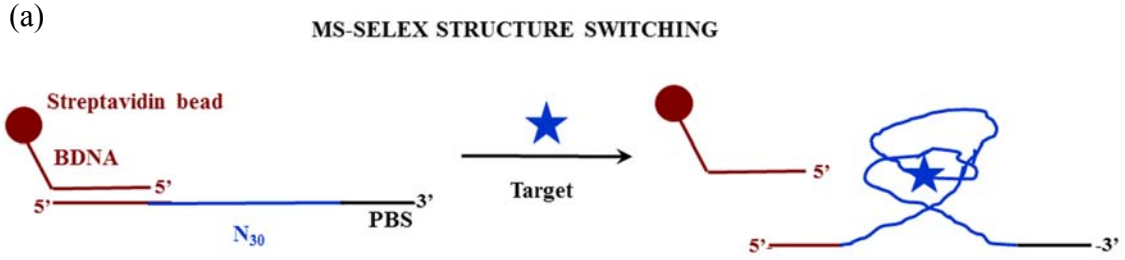

(b)

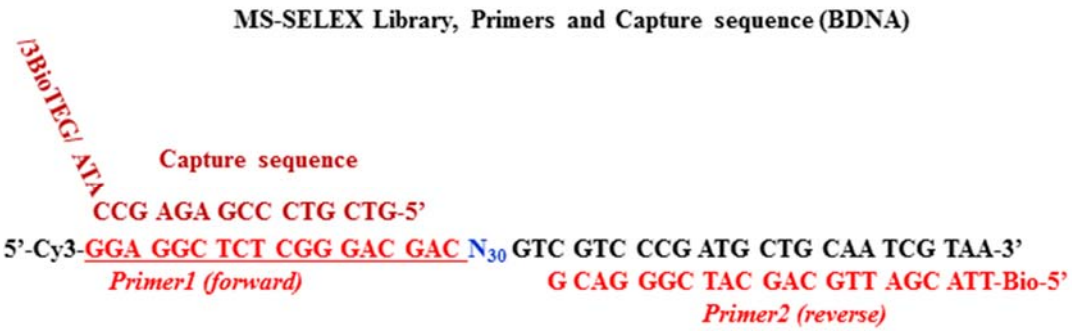

Figure 3.3. Structure-switching strategy in MS-SELEX. (a) A pictorial representation of structure-switching strategy involved in MS-SELEX. (b) The sequences of random library, primers, and capture strands used in MS-SELEX.

(a)

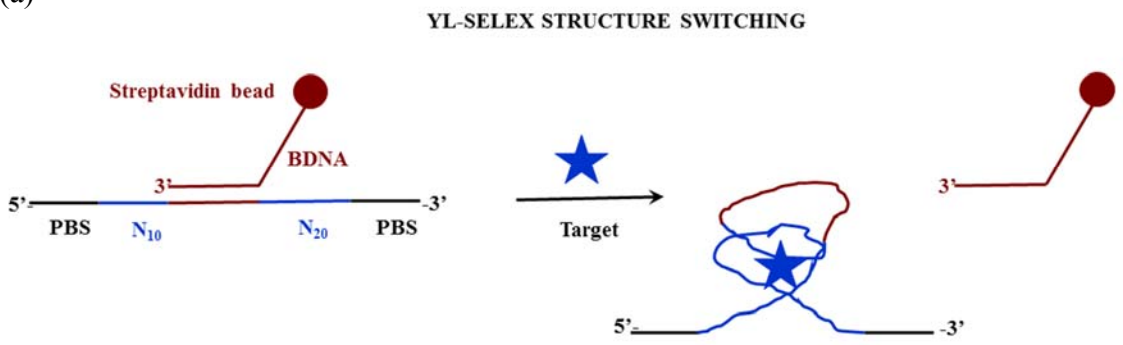

(b)

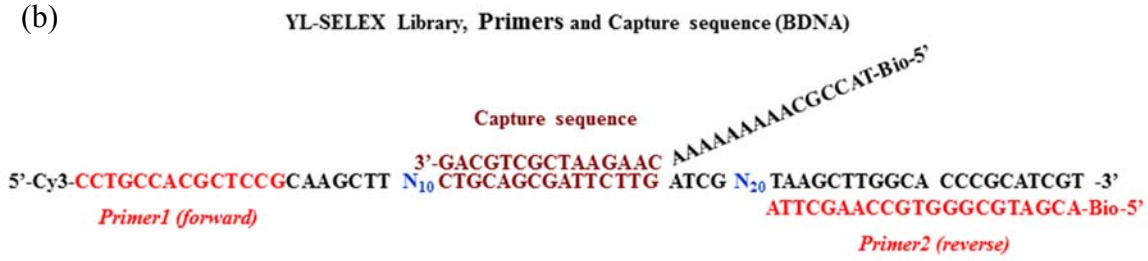

Figure 3.4. Structure-switching strategy in YL-SELEX. (a) A pictorial representation of structure-switching strategy involved in YL-SELEX. (b) The sequences of random library, primers, and capture strands used in YL-SELEX.

fluorescently labeled to monitor the amount of aptamer release from the column during the target binding step.

The amplification of these released aptamers was done by PCR,[24] using a 5'-cy3-forward primer (FP) and a 5'-biotinylated reverse primer (RP). This resulted in 5'-cy3-labeled sense strands and 5'-biotinylated antisense strands. Several methods have been used in literature protocols to convert dsDNA to ssDNA.[25, 26] In our experiments, the conversion of dsDNA to ssDNA was done on the streptavidin agarose resin that captures the antisense strand. The sense strand was eluted from the column using NaOH that denatures the dsDNA, whereas the antisense strand remains on the column, because the biotin streptavidin interaction remains tight during the mild base treatment.

The first few rounds of SELEX were performed in low stringency as individual sequences were not highly represented. In later rounds, as the high copy number of specific binders or functional sequences were obtained, stringent conditions were applied.[27] Several rounds of SELEX with increased stringency results in enrichment of highly-selective functional sequences.[28] Stringency in SELEX was introduced by gradually decreasing the concentration of target in consecutive cycles starting from 100-1 μM. Counter selection was done using similar target structures simultaneously present during detection in the initial and later rounds of SELEX.[29]

Further, the selected binders were cloned to E. coli and sequenced. These selected sequences were aligned in the randomized regions and assigned to different classes based on the similarities. Post-SELEX modifications were done to obtain sequences with enhanced binding and specificity over the original sequences. These include truncating the original sequence and testing these new sequences for their binding affinities to the target.

Binding affinities of the selected sensors toward small molecule targets are measured by various methods.[4] The most commonly used methods are mass sensitive surface-based,[30] separation-based,[31-35] or spectroscopy-based.[36-38] We used a fluorescence-based method to determine the binding affinity of the aptamer to the target. The aptamer served as a molecular recognition element, and the competitor or capture strand served as a signal transduction element. The capture strand was partially complementary and bound to the aptamer. However, in the presence of target, the competitor was displaced and an aptamer-target complex was formed. A signal-on detection scheme was used as shown in Figure 3.5. The fluorescence quenched in the double-stranded capture/aptamer complex was procured when duplex was dissociated upon addition of a target.[10]

Experimental section

Materials

All chemicals, enzymes, and kits used were purchased from commercially available sources. The oligodeoxynucleotides (ODNs) were obtained from the DNA/peptide Core facility at the University of Utah. Sanger sequencing of the plasmids was done at the DNA Core sequencing facility at the University of Utah.

Instrumentation

HPLC analyses of nucleoside reactions were done on a Beckman System Gold 126NM solvent module attached to a Beckman 168NM diode array detector with a C-18 nalytical reversed-phase column (5 μm, 250 × 4.6 mm) and Hypercarb column (5 μm, 150 × 4.6 mm). All solvents were HPLC-grade that were filtered and sonicated before use.

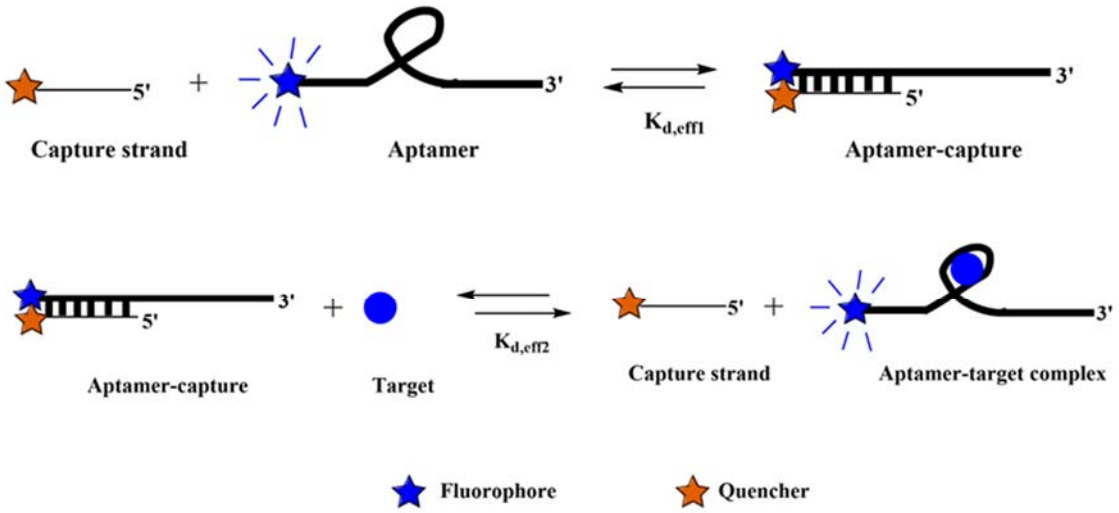

Figure 3.5. Strategy for aptamer-based optical detection by using signal-on detection scheme to determine the binding affinity of the aptamer to the target.

All aqueous solutions were prepared from 18MΩ purified water (Nanopure, Synbron/ Barnsted).

Capture-SELEX Library, capture ODN, and primers design

The ODNs used for MS-SELEX are as follows: (1) A single-stranded random (N_{30}) library (72-mer), 5'-Cy3-GGAGGCTCTCGGGACGACN$_{30}$GTCGTCCCGATGCTGCA ATCGTAA-3'; (2) forward primer (FP, 18-mer), 5'-Cy3-GGAGGCTCTCGGGACGA C-3'; (3) reverse primer (RP, 24-mer) 5'-Btn-TTACGATTGCAGCATCGGGACGAC-3'; (4) biotinylated tetraethylene glycol (TEG) column immobilizing sequence (BtnDNA, 18-mer), 5- GTC GTCCCGAGAGCCATA-btnTEG-3'.

The ODNs used for YL-SELEX are as follows: (1) A single-stranded random (N_{30}) library (94-mer), 5'-Cy3-CCTGCCACGCTCCGCAAGCTTN$_{10}$CTGCAGCGATTCTTG ATGC N$_{20}$TAAGCTTGGCACCCGCATCGT-3'; (2) forward primer (FP, 14-mer), 5'-Cy3-CCTGCCACGCTCCG-3'; (3) reverse primer (RP, 21-mer) 5'-btn-ACGATGCGGG TGCCAAGCTTA-3'; (4) biotinylated-column immobilizing sequence (BtnDNA, 18-mer), 5'-btnTEG-TACCGCAAAAAAAAACAAGAATCGCTGCAG-3'.

Preparation of buffer solutions

The selection buffers or reaction buffers used for both the MS and YL-SELEX had different compositions and were prepared in nuclease-free water. The buffers used were (1) MS-SELEX buffer (100 mM NaCl, 10 mM $MgCl_2$, 20 mM Tris, pH 7.4); (2) YL-SELEX buffer (300 mM NaCl, 50 mM KCl, 10 mM $MgCl_2$, 50 mM Tris, pH 7.4); (3) strand separation buffer (1 M NaCl, 20 mM Tris, pH 7.4).

Control experiments

Four control experiments were conducted before starting the SELEX cycles to determine (a) the amount of streptavidin-agarose resin (1-3 mg biotinylated BSA/ mL of resin) for SELEX on micro bio-spin columns using gravity-flow method, (b) the loading capacity of the resin, (c) the hybridization efficiency of the library to BtnDNA, and (d) the binding efficiency of PCR amplified dsDNA on the resin and the yields of ssDNA eluted from column after strand separation were all determined.

♦ *(a) Amount of resin used for SELEX on the micro biospin columns:* Micro bio-spin polypropylene chromatography columns (Bio-Rad) with a bed volume of 0.8 mL, bed height of 2 cm, and overall length of 3 cm were used for SELEX. The amount of streptavidin agarose resin (Thermo Scientific) used on these micro bio-spin chromatography columns for every SELEX round was determined so the flow rate was consistent using a gravity flow method. Different volumes of resin (50, 100, and 250 µL) were used to check the flow with the same amount of selection buffer (250 µL) through the column.

♦ *(b) Determination of maximum loading capacity of MS- and YL-BtnDNA on the resin:* The streptavidin agarose resin with a binding capacity of 15-25 µg biotin/ mL of settled resin was used for SELEX experiments. The resin was stored in an azide solution as a 50% slurry mixture. Hence, for one mL of settled resin, it was reported that the loading capacity was ~ 0.06 - 0.12 µmol of biotin. We used 50 µL of settled resin (100 µL with slurry) and the calculated loading capacity of biotin to be 3 - 6 nmol.

To precisely determine the maximum loading capacity of the BtnDNA, 50 µL of settled resin (minimum amount of resin) was loaded on two columns each with 6 nmol of

MS- and YL-BtnDNA, respectively. The column was equilibrated by washing with 3 X 100µL of water, and then with 3 X 100 µL of MS- and YL-SELEX buffers, respectively. According to the protocol, the maximum loading capacity of resin, 6 nmol of MS- and YL-BtnDNA were incubated on two columns for 30 min at RT. The eluate was collected and BtnDNA was applied twice on the column, each for 5 min. The last eluate and five washes with buffer were collected separately and used to determine the amount of unbound (UB) BtnDNA for both the MS- and YL-ODNs by UV-measurements using a nanodrop spectrometer (Thermo Scientific). The difference between the total amount of BtnDNA loaded and the amount of BtnDNA collected from the eluate and combined washes gave the amount of BtnDNA loaded, and hence the maximum binding capacity of the resin.

♦ *(c) Hybridization efficiency of the library with capture strand:* To determine the hybridization efficiency of MS- and YL-libraries on the capture strand or BtnDNA, different fractions of the library were added, as compared to 3 nmol of DNA, on 100µL resin. The different fractions were one-fourth, one-fifth, and one-sixth the concentration of MS- and YL-BtnDNA maximum loading capacity with 100 µL of resin. Therefore, for 3 nmol MS- and YL-BtnDNA, 750, 600, and 500 pmol of the respective library was loaded and incubated for 1 h at RT. The eluate was collected separately to determine the amount of UB library. This was followed by 5 X 100 µL washes and 30 min incubation with only 5 X 100 µL MS and YL 1X SELEX buffers to determine the background in each of these ratios. The background was the amount of library that eluted when incubated with 1X SELEX buffer. The fraction of the library that gave the least amount of background and at least 70% binding efficiency to BtnDNA was selected and used for all SELEX experiments

to minimize the background obtained in each cycle. All the measurements were done by fluorescence to measure the absorbance of the cy3-labeled library.

♦ *(d) Determination of binding efficiency of PCR amplified dsDNA on the resin and the yields of ssDNA eluted from the column after strand separation:* The MS- or YL-ssDNA library was amplified by PCR with 5'-biotinylated reverse primers and purified by gel extraction to test the binding of the dsDNA on 200μL of resin. The column was equilibrated by washing with 5 X 200 μL water, and further with 5 X 200 μL strand separation (SS) buffer. 250 pmol of MS- or YL-dsDNA was applied to two columns, respectively, and incubated for 15 min at RT. The eluate was applied twice to the column for 5 min each and was collected to determine the amount of UB dsDNA by nanodrop. The resin was washed with 10 X 200 μL SS buffer and incubated with 200μL of 0.1 M NaOH for 10 min. The eluate was collected and the step was repeated with 100μL of 0.1 M NaOH. The two above fractions from the column were collected, neutralized with 3M NaOAc, and concentrated using centrifugal filters. This determined the amount of ssDNA obtained from the column that was measured using fluorescence by nanodrop microarray that determines the concentration of the cy3-labeled library.

Before starting the SELEX cycles, the targets were synthesized, HPLC purified, and characterized by electronic circular dichroism (ECD) spectroscopy that is discussed in the section below. A 4 mL stock solution of MS- or YL-BtnDNA on the resin was prepared beforehand for each SELEX for a target in order to use uniform concentration of BtnDNA and resin in each cycle. The procedure of binding BtnDNA to the streptavidin resin has been described above.

Synthesis and preparation of target for SELEX

Preparation of 8-oxo-dG and 8-oxo-G solutions: The targets used in this SELEX are shown in Figure 3.2. 8-Oxo-dG and 8-oxo-G were commercially available. A 100 μM stock solution of each target was made in MS- or YL-SELEX buffers.

The procedure for the synthesis of dSp and Sp was conducted as follows: [39,40] dSp nucleosides were prepared in a large volume of 100 mL in 100 mM NaP_i buffer at pH 8. 1 mM dG was reacted with 500 μM methylene blue with a 350 nm light using a 300 W bulb suspended ~ 8 cm above the reaction for 1 h at RT. The photooxidant was removed by passing the mixture through a NAP-25 column (GE Healthcare) following the manufacturer's protocol. Further, the unreacted dG was removed by passing the reaction mixture through a reversed-phase HPLC column. The mixture of dSp diastereomers was then collected from the void volume and the diastereomers were individually purified using a Hypercarb column. The method used for resolving the two diastereomers had line A as ddH_2O with 0.1% acetic acid, and line B as methanol, running with flow rate of 1 mL/min at isocratic gradient of 0%B for 20 min followed by a linear increase in B to 75% over 25 min. The reaction was monitored at 240 nm absorbance and the retention times for (-)-(*R*)-dSp and (+)-(*S*)-dSp were 11 and 16 min, respectively. The yields of these reactions were approximately 15% and was obtained by Beer's Law with the extinction coefficient of dSp at 245 nm. The HPLC traces and ECD spectra are consistent with previously published work on these diastereomers. Finally, a 100 μM stock solution was made for dSp nucleosides in MS-SELEX buffer.

The (*R*)-Sp free-base was synthesized from purified (-)-(*R*)-dSp nucleoside.[41, 42] This was done by adding 40% HF in pyridine to an anhydrous pellet of dSp to give a final

concentration of 10 mg/mL. The sample was incubated at 45 °C for 30 min. Later, the HF was neutralized with 100 mg $CaCO_3$, and the mixture was filtered. The pure Sp enantiomer was purified using a Hypercarb column with 70% yield. The enantiomer purity was confirmed by ECD spectroscopy. Since this enantiomer was HPLC purified with low yields, a stock solution of 100 μM was made in 1X MS buffer.

PCR amplification of initial ssDNA library

A 20 pmol (~10^{13} sequences) sample of both MS- and YL-ssDNA libraries were PCR amplified in a 10 mL PCR reaction using *Taq* DNA polymerase with ThermoPol Buffer (New England Biolabs) and 1 μM primers. PCR protocol for the MS-library consisted of 1 cycle of 95 °C, 2 min, 20 cycles of [95 °C, 15 sec; 60 °C, 30 sec; 72 °C, 45 sec], and 1 cycle of 72 °C, 2 min. Each PCR cycle for the YL-library consisted of 1 cycle of 95 °C, 5 min, 15 cycles of [95 °C, 1 min; 62 °C, 1 min; 72 °C, 1 min], and 1 cycle of 72 °C, 5 min. The PCR amplicons were extracted on 4% agarose gel followed by purification with a QIAEX II gel purification kit (QIAGEN). It is important to mention that this amplified library was used for all the five targets in SELEX. Stochastic effects like loss of Sequemce variants due to random fluctuations are neglected as a consequence of having a large copy numbers of each sequence variant.

General structure-switching or capture-SELEX protocol

The general protocol for capture-SELEX is explained below, with each cycle consisting of 5 main steps (Figure 3.6). The number of cycles, target concentration, and counter SELEX done for each SELEX cycle vary with respect to the target used and will

be mentioned separately in the results and discussion section where each target is discussed separately. The general procedure involved mainly the following 5-steps for capture-SELEX done on five targets.

(1) Immobilization of the library on the resin: The first step involves the attachment of the BtnDNA to the library. As previously mentioned, a large amount of resin (4.5 mL) attached with BtnDNA was made in order to use the resin with the same loading capacity for all rounds of SELEX per target. To prepare such large amounts on the resin, 24nmol of BtnDNA was incubated on the resin for 24 h at RT using the rotor. The resin was centrifuged at low speed of 3000 rpm for 30 sec and the supernatant was collected and nanodrop was done to determine the amount of UB-BtnDNA. The resin was washed several times with 1X SELEX buffer and stored in the same buffer at 4 °C until further use.

In each round, 100 pmol of ssDNA library was loaded on 250 µL BtnDNA resin in micro bio-spin chromatography columns. The ssDNA library was incubated for 1h at RT and the collected mixture was reapplied to the column twice for 15 min each time. The eluate was then collected to determine the amount of UB ssDNA in each cycle by nanodrop. The column was washed with 10 × 250 µL 1X SELEX buffer to remove unbound or loosely bound strands. The background was measured for each cycle by incubating SELEX buffer on the column for 30 min at RT.

(2) Incubation of the target with the library: Incubation allows the target to interact with the library and strongly bound sequences lead to structure-switching. For all the SELEX cycles, the first round had 100 µM target in 250 µL SELEX buffer incubated on the resin for 30 min at RT. This step was repeated twice for 30 min at RT.

(3) Elution of the aptamer from the column: Elute was then collected consisting of

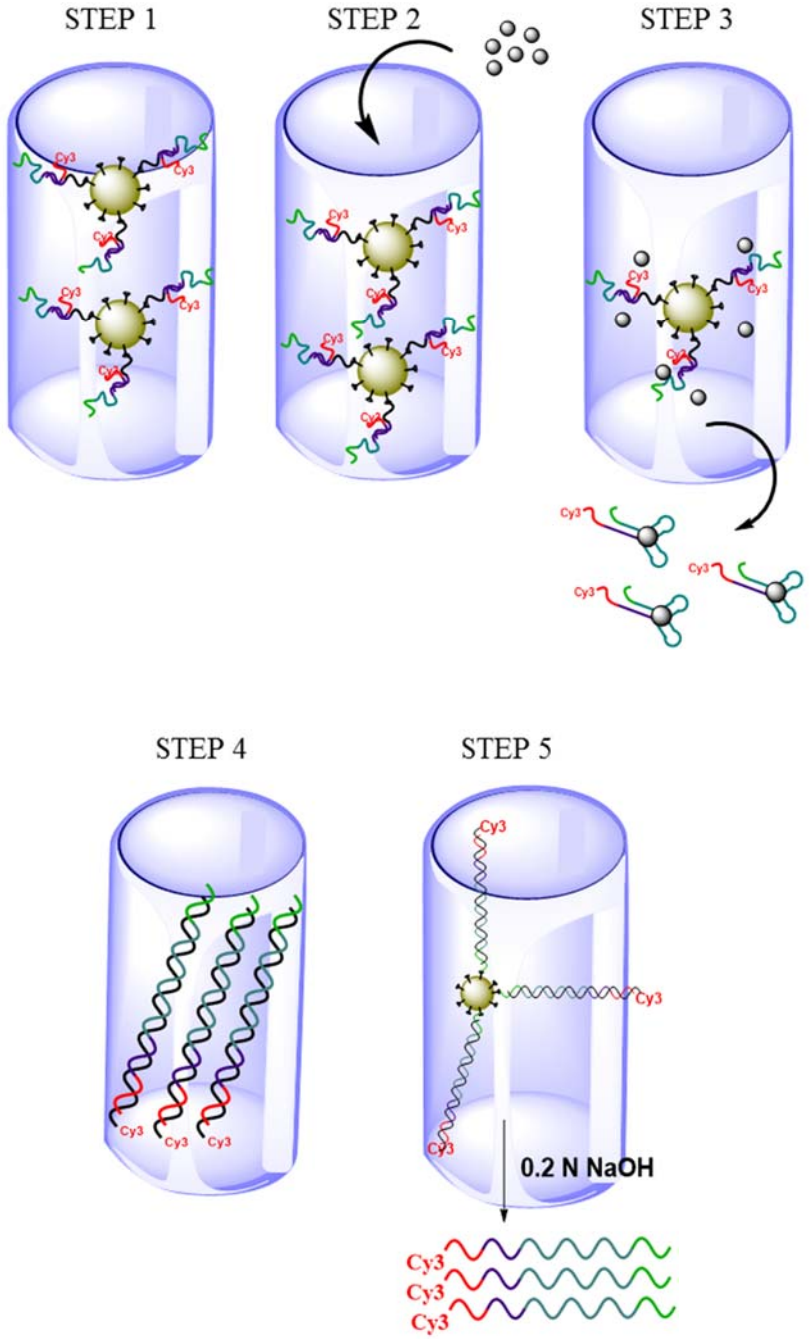

Figure 3.6. The pictorial representation of each of the five steps of capture-SELEX. The brown circle represents streptavidin bead, the black pins are biotin, the ssDNA as cy3-labeled strand and grey beads as targets of interest.

DNA-target complex using 3 × 250 µL of 100 µM target solution (collecting each 250 µL fraction separately). The eluted samples were then used as a template for PCR after concentrating to 100 µL by Amicon Ultra centrifugal filter (Millipore). The concentration of target used for further rounds to increase the stringency of SELEX is mentioned in the results and discussion section as these vary based on the target used. One important point to be made is that elution is strictly carried out using the gravity-flow method without disturbing or centrifuging the spin columns.

(4) Amplification of the elute strands by PCR: The elute strands were amplified after every round with 25 cycles of 40 PCRs was set up with a negative and positive PCR in every cycle using 5'-biotinylated-RP and 5'-Cy-3-FP as controls. A negative PCR reaction consists of all components except the template, whereas a positive PCR reaction consists of the original ssDNA library. The protocol for both MS- and YL-PCR is mentioned in the section above in PCR amplification of the initial ssDNA library.

For a 50 µL PCR reaction, 5 µL 10X buffer, 1 µL each of 50 µM FP and RP, 2 µL dNTPmix, 0.5 µL Taq polymerase, 2.5 µL elute containing ssDNA and 38 µL of nuclease free ddH_2O was used. The dsDNA obtained from PCR was run on 4% agarose gel stained with ethidium bromide (EtBr) in 1X TAE buffer at 70 V for 1 h. The dsDNA bands were cut under UV light using a clean razor and the gel bands were dissolved at 55 °C in agarose dissolving buffer using a gel extraction kit (Zymogen). The amount of pure dsDNA was measured using nanodrop.

(5) Conversion of dsDNA to ssDNA: 200 µL of streptavidin resin was used on micro bio-spin columns at RT. The resin was washed with 5 × 200 µL water followed by 5 × 200 µL SSB. In every round, ~250 pmol of dsDNA was loaded on the resin and

incubated for 15 min at RT. The mixture was reapplied to the column. The UB dsDNA was collected in eluate and measured by nanodrop. The column was washed with 5 × 200 µL of SSB followed by incubation of 200 µL 0.2 M NaOH on the resin at RT for 10 min. A second fraction of 100µL NaOH was applied and eluate consisting of ssDNA was collected. The ssDNA obtained was neutralized by 3M NaOAc and was used for the next round as the initial library.

Fluorescence detection

The ssDNA library was labeled with Cy-3 at the 5'-terminus and the aptamer strands that eluted from each round were amplified using FP with 5'-Cy3. The amount of aptamer released during the target binding step was analyzed by fluorescence detection. The fluorescence measurement was performed on a nanodrop using microarray settings with excitation of Cy3 at 550 nm and emission at 570 nm. The concentration of DNA was determined with respect to fluorescence after every round. The targets did not influence the fluorescence readings.

Cloning and sequencing

The insert-DNA for cloning was prepared using aforementioned PCR conditions, except for the final extension step that was increased to 15 min at 72 °C to add an A-tail effectively for a T/A cloning system. The primers used for amplification in this case did not have any modifications at the 5' or 3'-end. The PCR amplicons were purified as previously mentioned and were directly incorporated into the plasmid vector (pCR 4-TOPO) using TOPO TA cloning kit (Invitrogen) following the manufacturers protocol.

The vector and its linearized form are shown in Figure 3.7. The plasmids were then transformed into one shot TOP10 competent cells (Invitrogen), and the positive clones containing recombinant plasmid were identified by blue/white screening. Each colony was picked and replated for growth on Petri dishes containing LB Agar (MO-BIO) and ampicillin (Sigma). Finally, the individually grown colonies were picked and re-grown in 3 mL of Luria Broth (LB media). This procedure has been represented in Figure 3.8 and is followed for all targets. The cell pellets were obtained and each individual plasmid was extracted using a PureLink Quick Plasmid Miniprep Kit (Invitrogen). Positive clones were confirmed by PCR and Sanger sequencing was performed at the DNA Sequencing facility at University of Utah. The analysis of each electropherogram files (AB1 files) and verification of each error was completed using Chromas Lite. Multiple sequence alignment was carried out using a MultAlin program for the random regions in each SELEX.

Sensor selection for measurement of binding affinities

The sensors were designed after truncating most bases in the primer regions and the secondary structures were determined using Quikfold. A bischromophoric approach was applied where the sensor was labeled with carboxyfluorescein (5-FAM). It folded into a 7-8 base pair (bp) stem region that competes with 13- or 14-mer quencher or capture strand that acts as a complimentary capture strand with 3'-dabcyl modification. Each sensor with a specific 13- and 14-mer was designed to perform fluorescence studies.

All fluorescence measurements were carried out in SELEX buffer. Each sensor was separately incubated with the 13- or 14-mer quencher strands, annealed at 95 °C for 10 min

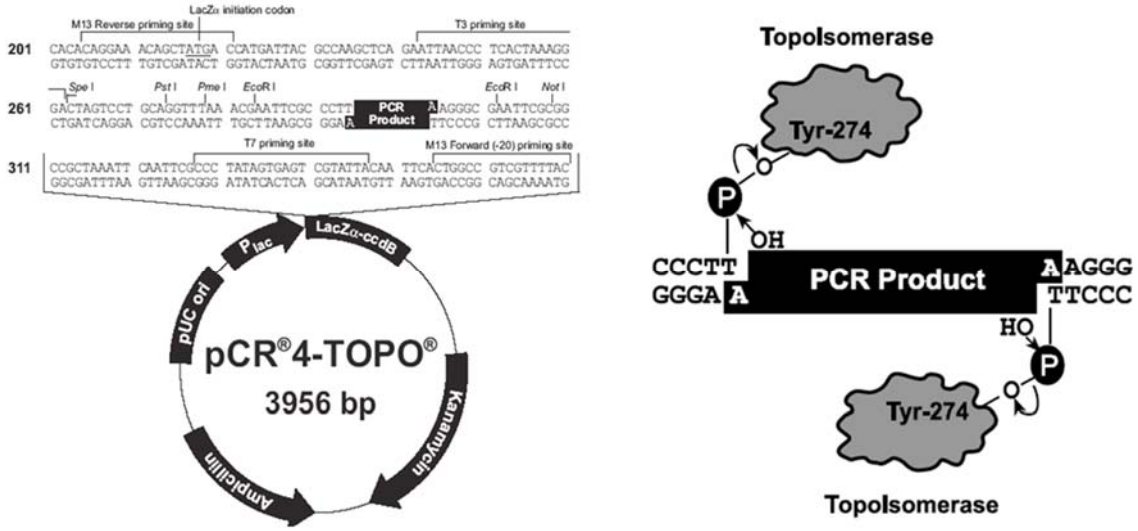

Figure 3.7. The pCR-4 TOPO TA vector and the linearized plasmid used for cloning. The pictures have been adapted from the Invitrogen site for TA cloning vectors (http://www.lifetechnologies.com/order/catalog/product/K204040).

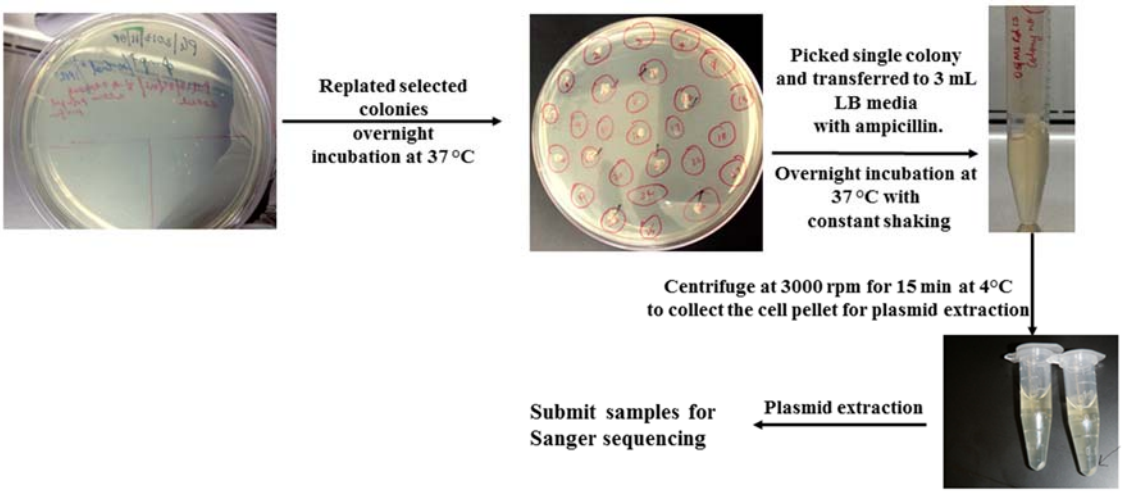

Figure 3.8. General protocol for growing *E. coli* cells with transformed plasmid.

and flash cooled to 4 °C for 10 min and then at RT for 30 min. Each sensor had a constant concentration of 5 nM, whereas the quencher strands ranged from 0-100 nM. The fluorescence was measured on a 96-well black plate (Costar) at excitation wavelength for 5-FAM at 490 nm and emission at 520 nm. The experiments were done in three trials and relative fluorescence units (RFU) were plotted against concentration of quencher strands. This plot determines the K_{deff1} of the quencher by Equation (1) in Scheme 3.1. For each target, at least four different sensor and quencher sequence combinations were used and only one or two of these showed decrease in fluorescence with increase in quencher concentration upon hybridization. The sensor and quenchers ratio that showed 60% quenching was further used for target binding studies to determine the binding affinity (K_{deff2}) of the target measured by Equation (2) in Scheme 3.1. The sensor-quencher strand ratio selected was incubated with target concentrations ranging from 2 nM - 500 μM. The $K_{D,aptamer}$ was determined by Equation (3) in Scheme 3.1. The details of the sensor and capture or quencher sequences tested for every target and the aptamer with their binding affinities are mentioned in the results and discussion.

Results and discussion

Control experiments results

The amount of resin used on the column was determined for every round of SELEX based on the consistent flow-rate for 250 μL of buffer. Since SELEX was performed on micro bio-spin chromatography columns using a gravity-flow method, a consistent flow through the column was necessary to carry out every round of SELEX. Henceforth, 250 μL of resin was used for every round of SELEX. The maximum loading capacity of the

$$K_{d,eff1} = [\text{Capture strand}]\,[\text{Aptamer}]/\,[\text{Capture strand-Aptamer}] \quad (1)$$

$$K_{d,eff2} = [\text{Capture strand}][\text{Aptamer-Target}]/[\text{Aptamer-Capture strand}][\text{Free Target}] \quad (2)$$

$$K_{d,\,aptamer} = [\text{Aptamer}]\,[\text{Target}]/\,[\text{Aptamer-Target}] = K_{d,eff1}/\,K_{d,eff2} \quad (3)$$

Scheme 3.1. Equations for two different affinities of the capture strand (K_{deff1}) and of the target (K_{deff2}) that lead to determining the binding affinity of the aptamer ($K_{d,aptamer}$) to the target.

biotinylated capture strand on 50 μL settled streptavidin resin was determined. It was found that the maximum loading capacity of the resin was 3 nmol of capture strand.

The hybridization efficiency of the library with the capture strand was determined so the least amount of background was observed. This was important for SELEX to be performed as this would decrease the background loss in SELEX. The least amount of background was observed with one-fifth concentration of the library (600 pmol) as compared to the capture strand. The percentage of library that was hybridized and loaded on the column was 80% of the total amount loaded.

The conversion of dsDNA to ssDNA for both the MS- and YL-libraries was determined by loading the dsDNA on streptavidin resin and capturing the biotinylated antisense strand. The amount of ssDNA obtained was measured in concentration by fluorescence as the sense strand was cy3-labeled. For 250 pmol of dsDNA loaded, the amount of ssDNA obtained was 110 pmol.

dSp and Sp HPLC and ECD data

The 2'deoxyspiroiminodihydantoin diastereomers, (-)-(*R*)-dSp and (+)-(*S*)-dSp were synthesized and HPLC-purified as mentioned in the experimental section. The HPLC traces of both 2'deoxy-spiroiminohydantoin diastereomers purified on a Hypercarb column are shown in Figure 3.9. To verify the purity of the diastereomers, we performed electronic circular dichroism of the two diastereomerically-pure dSp samples, (-)-(*R*)-dSp and (+)-(*S*)-dSp (Figure 3.10). The high performance liquid chromatography trace determined by recording at 280 nm and electronic circular dichroism spectrum for the enantiomer (*R*)-Sp are shown in Figure 3.11.

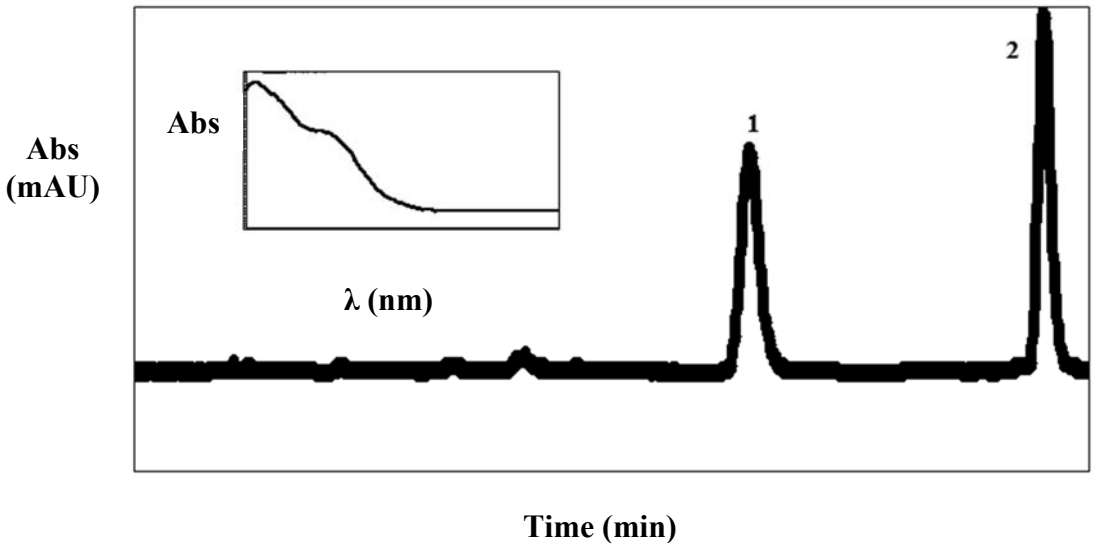

Figure 3.9. HPLC trace for the purification of the dSp diastereomers on a Hypercarb column. Peaks 1 and 2 were purified separately and indicate (-)-(*R*)-dSp and (+)-(*S*)-dSp, the two diastereomers of dSp nucleoside. The inset shows the UV spectra for both nucleosides at recorded over 200-300 nm. The HPLC trace was determined by recording at 240 nm.

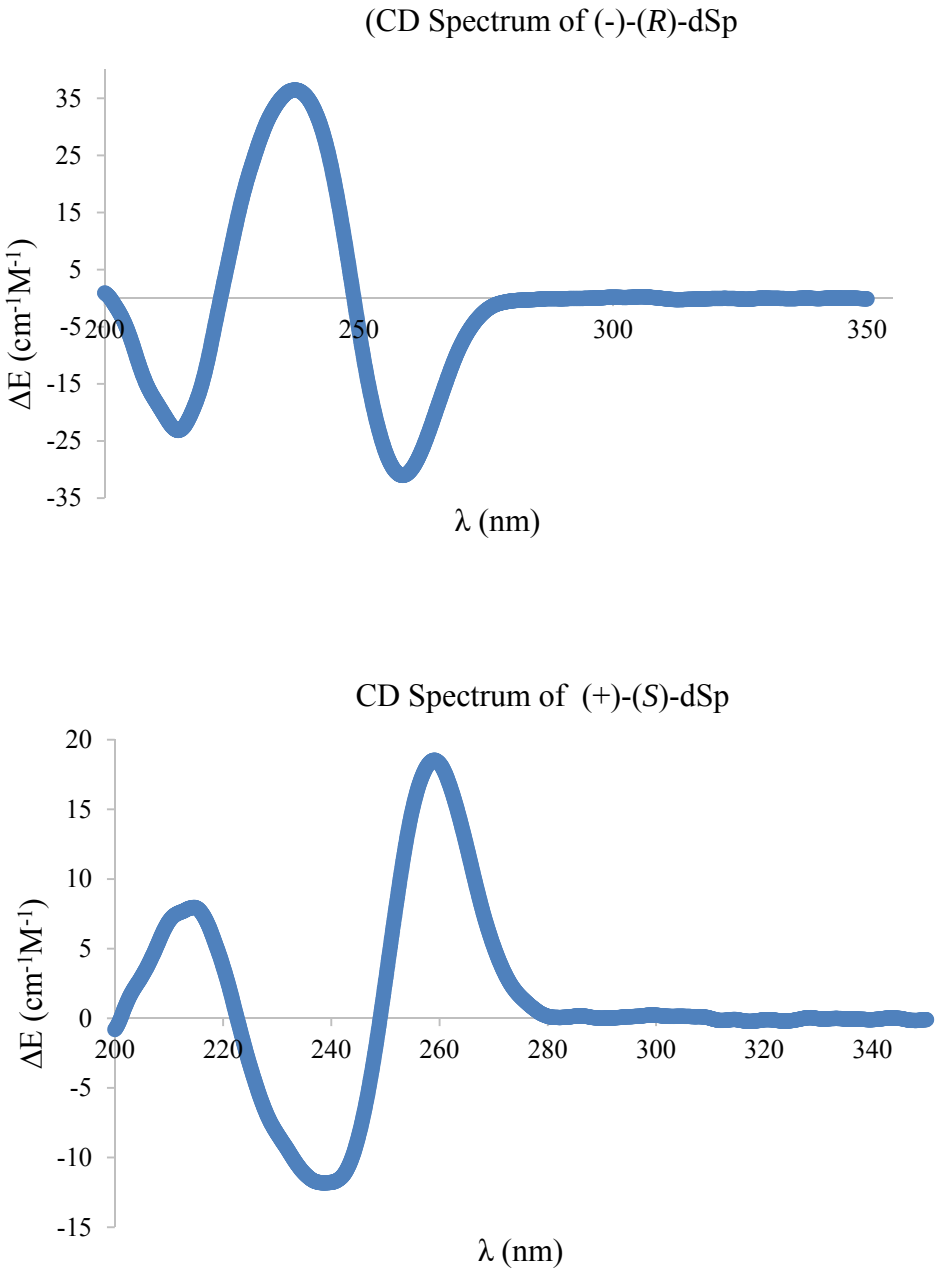

Figure 3.10. ECD spectra of both the purified diastereomers of dSp. The above ECD spectra is for both the purified diastereomer (-)-(*R*)-dSp whereas the bottom one is for (+)-(*S*)-dSp.

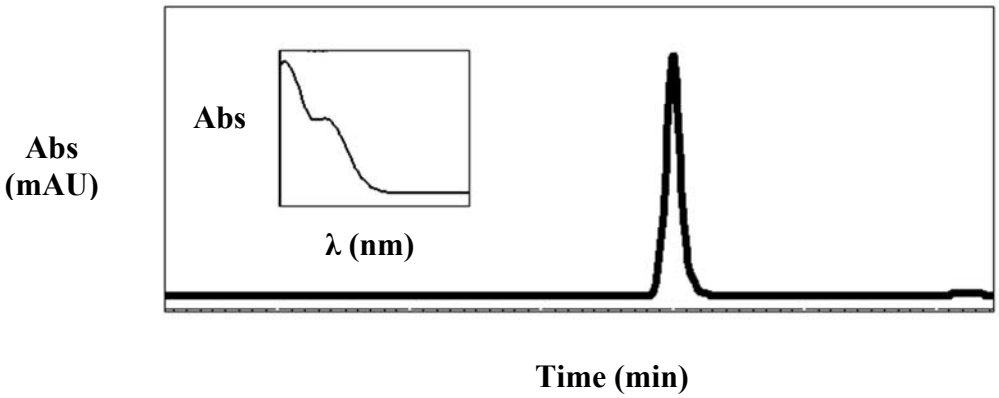

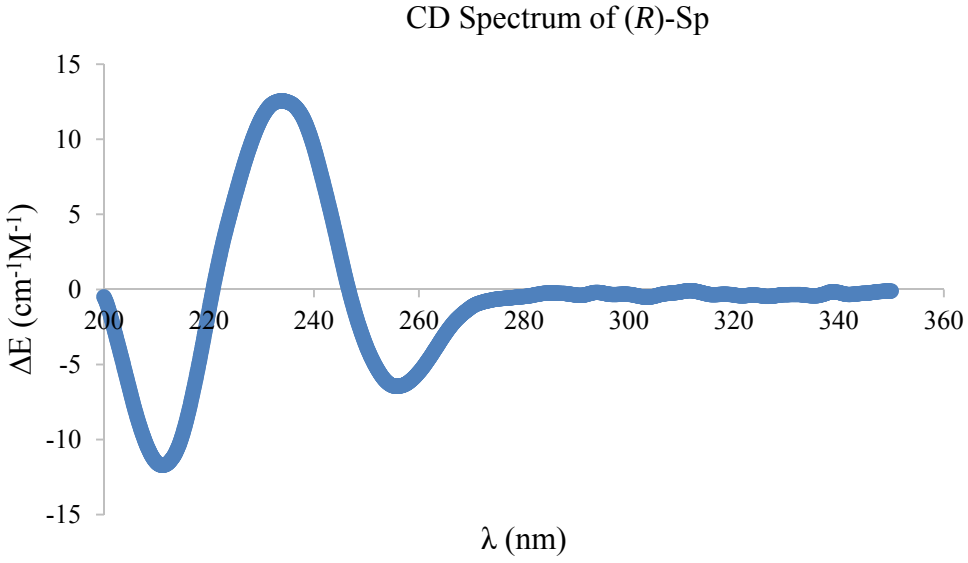

Figure 3.11. HPLC purification spectra on Hypercarb column and ECD spectrum for the purified (*R*)-Sp enantiomer. The inset in the hplc trace shows the UV spectra for the enantiomer at 240 nm.

Capture-SELEX for lesions 8-oxo-G and 8-oxo-dG

Both MS- and YL-SELEX aptamer selections were done for 8-oxo-G, a common biomarker of oxidative stress.[43] 100 pmol of starting library was loaded on the column for each cycle. The concentration of target ranged from 1-100 μM over 13 cycles. Negative selection was done in round 7 with 100 μM dG, dA, dT, dC, and uric acid (UA). UA is a metabolic breakdown product of purine nucleotides. MS-SELEX was carried out on 1-100 μM 8-oxo-dG target concentration over 13 cycles and negative selection was done similarly as outlined above. The details of target concentration for every round and the negative selections are mentioned in Table 3.1 for 8-oxo-G and 8-oxo-dG.

The elution profiles for the background and target in each round of SELEX are shown in Figures 3.12 and 3.13 for 8-oxo-G MS- and YL-SELEX, whereas Figure 3.14 shows an elution profile for 8-oxo-dG MS-SELEX. The amount of ssDNA eluted in pmol was measured by the Cy-3 fluorescence after each round. The elution profiles help monitor the progress of SELEX. In the initial rounds, when only small amount of specifically target-bound ODNs are present in the solution, the ratio of background to target elution equals one.

In later rounds, as successful selection of the aptamers proceeds, the amount of target binders increased and hence the ratio elevates. This was followed by amplifying the binders using PCR with the number of cycles changing depending on the elution profiles in each cycle. 4% Agarose test gels were run on amplicons after every round and scanned on a Typhoon imager are shown in Figure 3.15 (a) and (b) for 8-oxo-G and 8-oxo-dG MS-SELEX and Figure 3.16 (a) and (b) for 8-oxo-G YL-SELEX. After transformation of cloned plasmid, 50 colonies were picked from each SELEX and the sequences obtained

Table 3.1. The details for the number of rounds performed during SELEX and the concentration of 8-oxo-G and 8-oxo-dG in each cycle.

SELEX Round No.	8-Oxo-G concentration (MS and YL-SELEX)	8-oxo-dG concentration
1	100 μM	100 μM
2	100 μM	100 μM
3	100 μM	100 μM
4	100 μM	100 μM
5	100 μM	100 μM
6	100 μM	100 μM
7	100 μM (dA, dT, dG, dC, UA) counter selection 100 μM target	100 μM (dA, dT, dG, dC, UA) counter selection 100 μM target
8	50 μM	50 μM
9	50 μM	50 μM
10	25 μM	25 μM
11	25 μM	25 μM
12	10 μM	10 μM
13	1 μM	1 μM

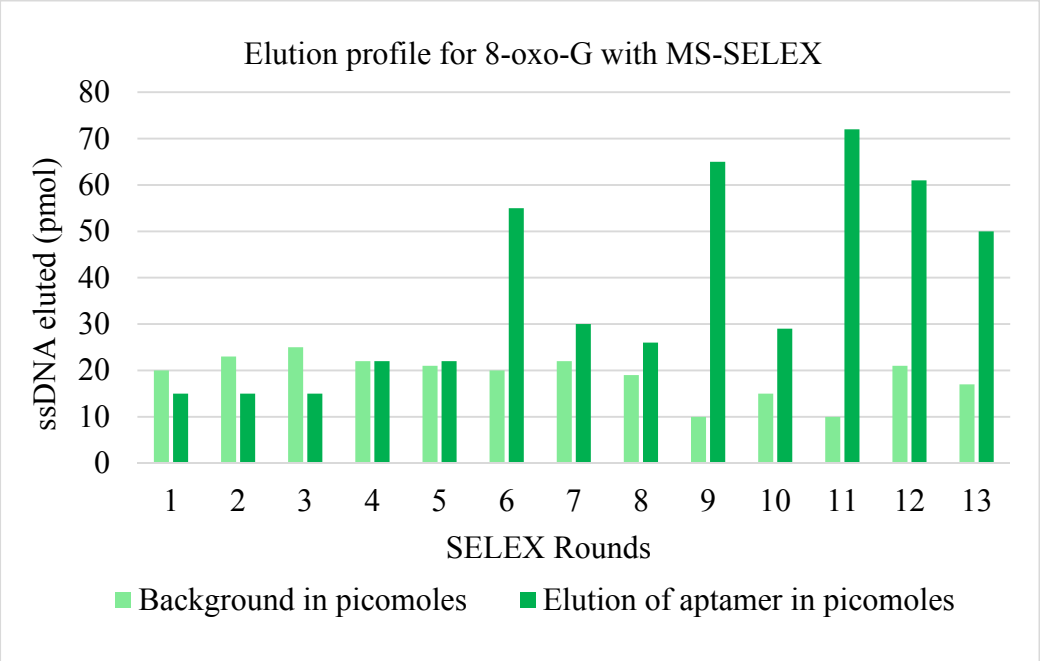

Figure 3.12. Elution profile for the background and aptamer strands for every SELEX round of 8-oxo-G using MS-SELEX.

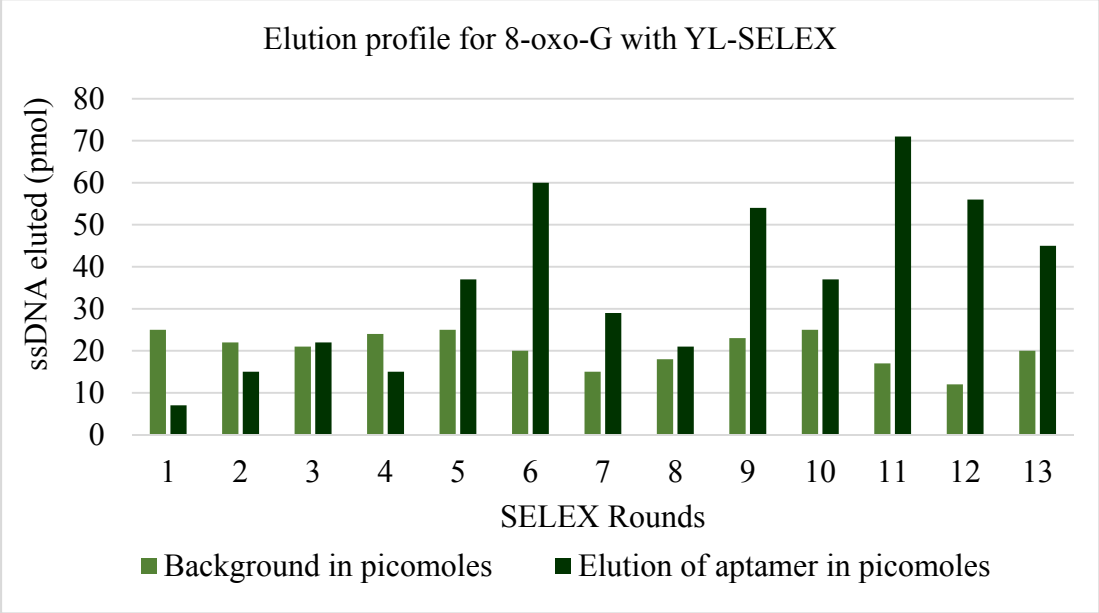

Figure 3.13. Elution profiles for background and aptamer strands eluted in each SELEX round for 8-oxo-G with YL-SELEX.

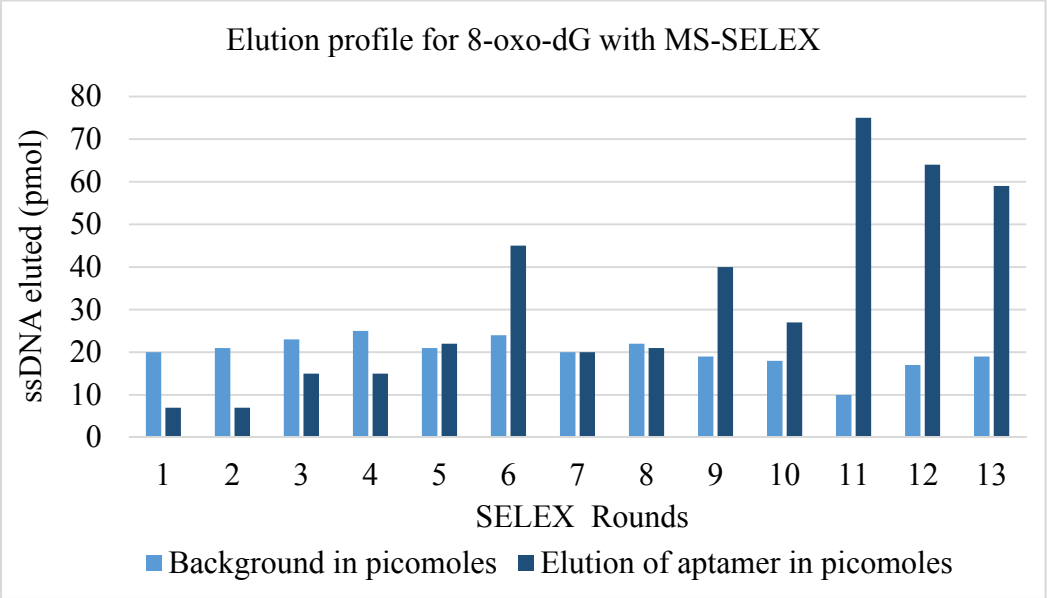

Figure 3.14. Elution profiles of 8-oxo-dG SELEX for every round representing the elution of background and aptamer strands.

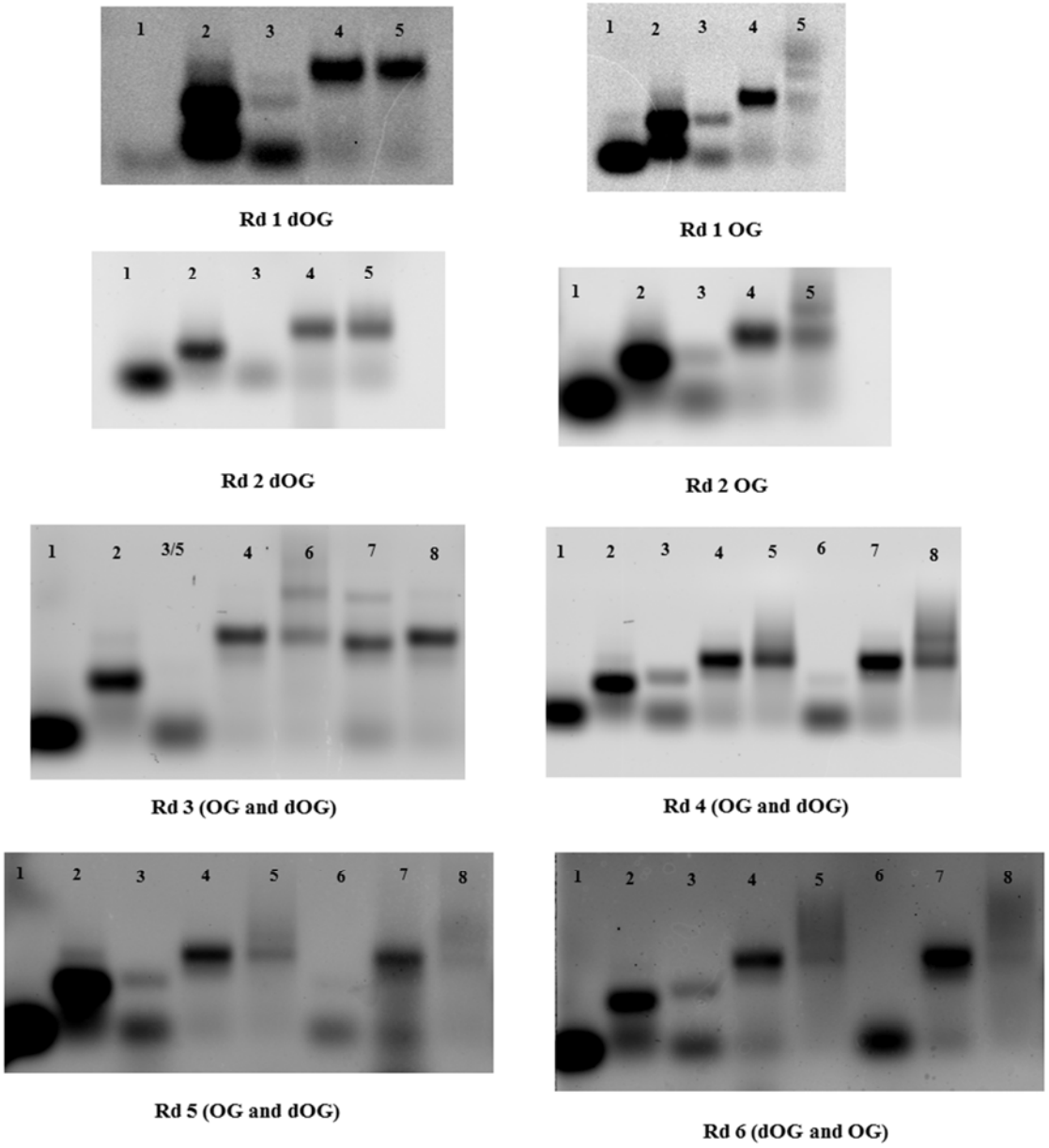

Figure 3.15. 4% Agarose test gels of MS-SELEX for 8-oxo-G and 8-oxo-dG. (a) First 6 rounds. Lanes 1 and 2 represent the forward primer, and ssDNA MS-library. In rounds (Rd) 1 and 2, lanes 3, 4, and 5 represent negative, positive, and elute PCR for that round. However, in rounds 3-6, lanes 3, 4, and 5 represent negative, positive, and elute PCR for that round for 8-oxo-G (labeled as OG above. Lanes 6, 7, and 8 represent negative, positive, and elute PCR for that round for 8-oxo-dG (labeled as dOG). (b) 7-13 rounds. Lane 1 represents ssDNA MS-library. Lanes 2, 3, and 4 as negative, positive, and elute PCR for that round for 8-oxo-G.Whereas, lanes 5, 6, and 7 represent negative, positive, and elute PCR for that round for 8-oxo-dG.

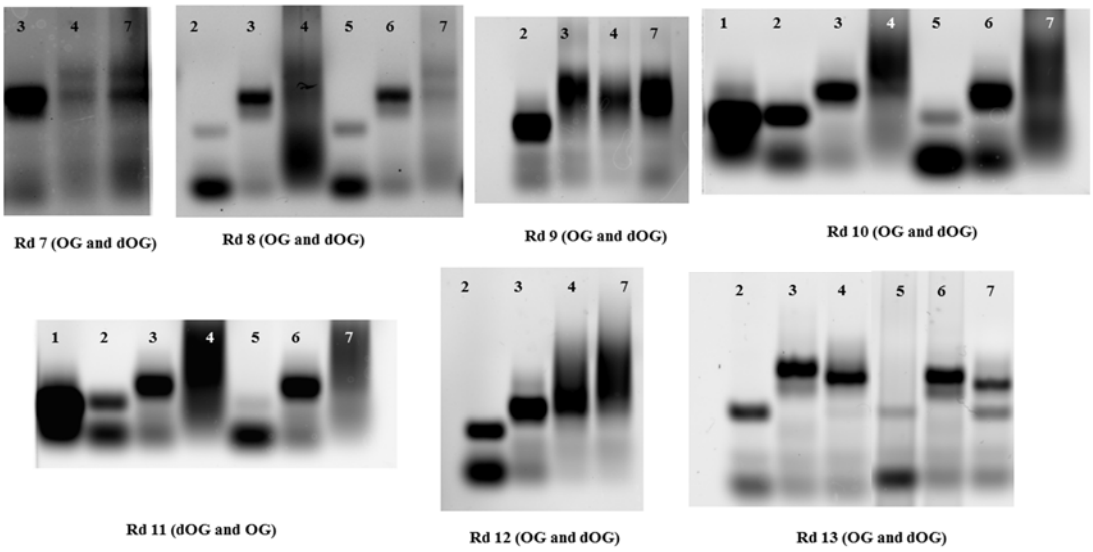

Figure 3.15. Continued

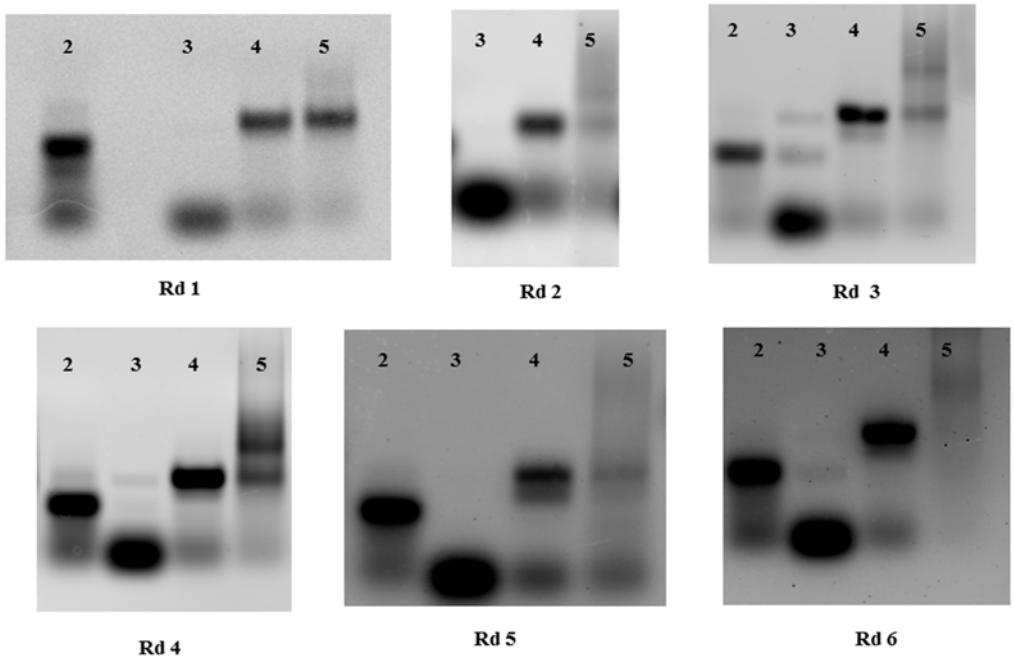

Figure 3.16. 4% Agarose test gels of 8-oxo-G YL-SELEX. (a) For the first six rounds. (b) for the rounds 7-13. Lane 2 represents ssDNA YL-library. Lanes 3, 4, and 5 represent negative, positive, and elute PCR for that round.

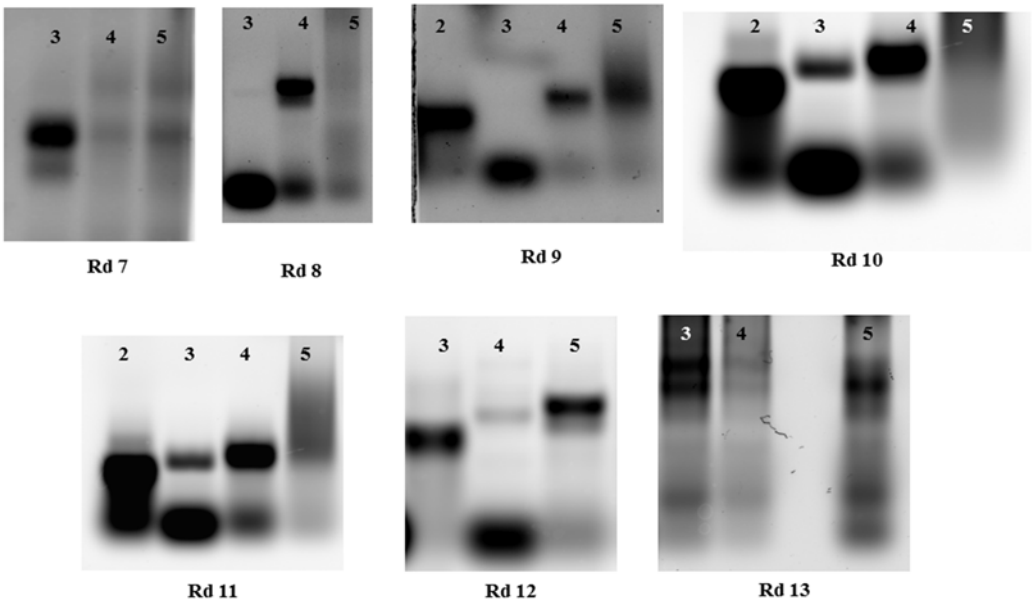

Figure 3.16. Continued

are shown for 8-oxo-G and 8-oxo-dG with MS-SELEX in Table 3.2 and Table 3.3. The sequences obtained for 8-oxo-G for YL-SELEX are shown in Table 3.4. The sequences for 8-oxo-G YL-SELEX had several deletions and mutations in most regions and were not further studied for binding. Each sequence from MS-SELEX was further truncated in the primer regions and post-SELEX modifications to develop sensors and determine the K_D of the aptamer.

Capture-SELEX for diastereomeric dSp and enantiomeric (R)-Sp lesions

The selection of aptamers for the diastereomers of dSp was done using MS-SELEX library. Aptamer selection for (*R*)-Sp, a product of BER removed by hNEIL1 and hNEIL3 DNA glycosylases,[44] was done in 8 rounds of selection using the MS-library. The choice of only (*R*)-Sp for SELEX was based on high HPLC purification yields of this enantiomer as compared to its counterpart. Eight rounds of SELEX were performed individually for each target. Every round was initiated by loading 100 pmol of starting library on the column round of 8-oxo-G using MS-SELEX.

The concentration of target for dSp and Sp varied from 1-100 μM in each round and are shown in Tables 3.5 and 3.6, respectively. Counter SELEX was done in round 2 with 100 μM dG, dA, dT, dC, and UA. Another counter SELEX cycle for dSp nucleosides was done in round 6 with 10 μM 8-oxoG, 8-oxo-dG and the other diastereomer of dSp. The counter selection was done rounds apart to enrich the pool in consecutive cycles, to prevent the loss of strong affinity aptamers. The elution profiles for the background and target after every round of SELEX are shown in Figures 3.17, 3.18, and 3.19 for (-)-(*R*)-dSp, (+)-(*S*)-dSp, (*R*)-Sp, respectively.

Table 3.2. The insert sequences obtained (labeled M) from cloning for 8-oxo-G by MS-SELEX. The N_{30} random regions are only indicated here. Number of sequences represent the number of times this sequence has appeared during cloning and sequencing.

Sequence name	Random regions of insert library obtained for 8-oxo-G MS-SELEX	No. of sequences
M1	AGCCAGTTGTTAGAATGGTTGAACCCGTGA	1
M3	AGGGGAGAGACTCCTAGCGGTAAATCTCCT	1
M4	GGGGTCCTCCGTTCAAATTGACGTGGGTGT	1
M6	AGGTGAGAGACTCCTAGCGGTAAATCTCCT	1
M7	GAAACCGGTTAATCTAGGATCAAATTGGAT	1
M13	AACTGTGATAGTACCGTTACTTAAGTATTG	1
M5	CTCAGAGACTCCTAGCGGTAAATCTCCTGT	1
M9	AAACAAGCCGGTTGTGGAATCATGCGATT	3
MS1	ACCGGTCAGCGGTAGCCTGTCGTCCCGAGA	1
M2	TCTATCCGAGATGCCGACTTTACGAATATC	2
M12	ACACGAGAGACTCCGGATTGCGGTCGCAAC	3
M15	ACGGATCGGAGATGCCGACTTTACAATATC	1

Table 3.3. The insert sequences obtained (labeled dMS) from cloning for 8-oxo-dG by MS-SELEX. The N_{30} random regions are only indicated here. Number of sequences represent the number of times this sequence has appeared during cloning and sequencing.

Sequence name	Random regions of the insert library obtained for 8-oxo-dG MS-SELEX	No. of sequences
dMS2	TAATGCCTTGGTCCGAAGTTCATTTGGTAG	1
dMS7_2	AGTGTACAAAACAAATAAGAATAAGGTCAA	1
dMS10	GGCCCATGAGAGACTCCTTAGCCGCGTGCT	1
dMS12	GTCCCGATGCTGCAATCGTAAAACGGATGA	2
dMS19	AGCCCATGAGAGCCGACAACAAGGACCGCA	2
dMS32	GACCAGAGAGACTCCCGCGGACACATGACT	1
dMS26	ATGTTCCGTGTTACTACTCCATGAAATCTT	1
dMS23	AGAGCTTGATGAATCATTTAATAAGGTCTA	1
dMS2	TAATGCCTTGGTCCGAAGTTCATTTGGTAG	2
dMS7	GGGGTTCCTGCTGATATAGGTCCGTCGTAG	2
dMS8	TAGGATTTTCAGCTCTCCTGCCAGGGGCCC	3
dMS9	GAGTGACTCCTGGAGTGTAACATGTCTATA	1
dMS14	GGGGTTCCTGCTGATATAGGTCCGTCGTAG	1

Table 3.4. The sequences obtained (labeled Y) after 8-oxo-G YL-SELEX. The sequences obtained from this type of library were less in number and often involved deletions in primer, random, and capture strand regions. The blue regions indicate primer sites, whereas the red regions indicate capture strand and the black regions indicate N_{10} and N_{20} random regions.

Sequence Name	Sequences obtained from 8-oxo-G YL-SELEX after cloning.
Y2_OG	CCTGCCACGCTCCGCAAG***GGGGTGGC**CTG***CGATTCTTG ACCG CCTGTAGATTGGCCAGCGGTTAAGCTTGGCACCCGCATCGT
Y4_OG	CCTGCCACGCTCGCAGC**CAACGGAGACCTGCAGCGATTATCG ***G GCATTGCGTTTCACCGCT*TTAAGCTTGGCACCCGCATCGT
Y12_OG	CCTGCCACGCTCCGCAAGGCTTTAGCCACTGGCTGCAGTGATCCTTGATCG ATTTGGCATATTCCCTGAACTAAGCTTGGCACCCGCATCGT
Y15_OG	CCTGCCACGCTCCGCAAGGCTTTAGCCACTGGCTGCAGTGATCCTTGATCG ATTTGGCATATTCCCTGAACTAA GCT TGG CAC CCG CAT CGT
Y16_OG	CCTGCCACGCTCCGCAAGGCTTGCACGAGGCGCTGCAGTGATTCTTGATCG CAATTCTGGCCAACGACTAG TAAGCTTGGCACCCGCATCGT

Table 3.5. The concentration of (-)-(*R*)-dSp and (+)-(*S*)-dSp used for every round of MS-SELEX.

SELEX Round No.	(-)-(*R*)-dSp concentration (MS-SELEX)	(+)-(*S*)-dSp concentration (MS-SELEX)
1	100 μM	100 μM
2	100 μM (dA, dT, dG, dC, UA) counter selection 100 μM target	100 μM (dA, dT, dG, dC, UA) counter selection 100 μM target
3	50 μM	50 μM
4	25 μM	25 μM
5	25 μM target	25 μM target
6	10 μM (8-oxo-G, 8-oxo-dG, (+)-(*S*)-dSp) counter selection 10 μM target	10 μM (8-oxo-G, 8-oxo-dG, (-)-(*R*)-dSp) counter selection 10 μM target
7	10 μM	10 μM
8	1 μM	1 μM

Table 3.6. The concentration of (*R*)-Sp used for every round of MS-SELEX.

SELEX Round No.	(*R*)-Sp concentration (MS-SELEX)
1	100 μM
2	50 μM (dA, dT, dG, dC, UA) counter selection 50 μM target
3	50 μM
4	25 μM
5	25 μM
6	10 μM (8-oxo-G, 8-oxo-dG, (-)-(*R*)-dSp, (+)-(*S*)-dSp) counter selection 10 μM target
7	10 μM
8	1 μM

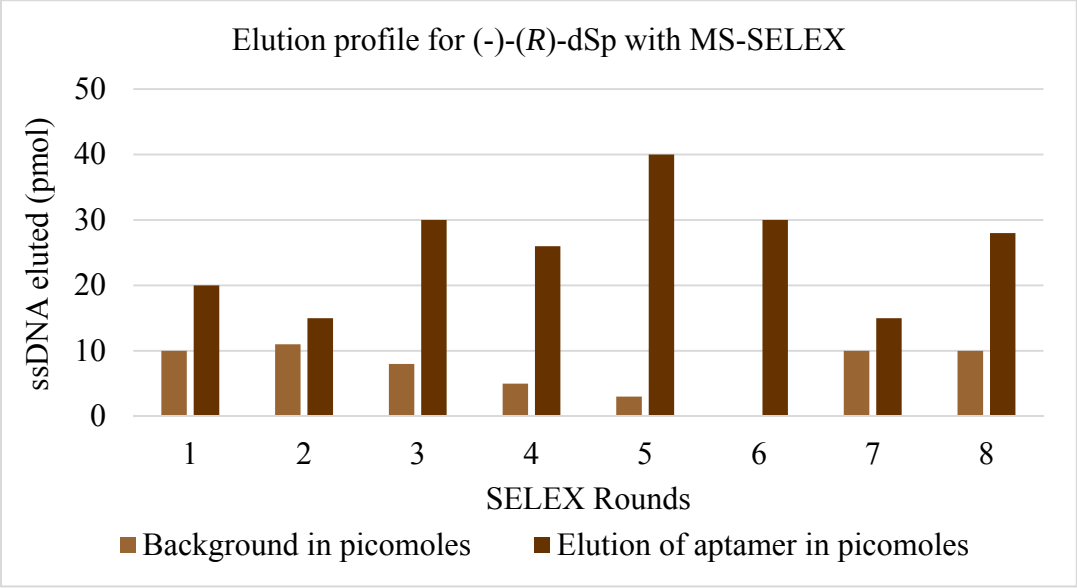

Figure 3.17. Elution profiles of background and aptamer strands for every round of (-)-(*R*)-dSp MS-SELEX.

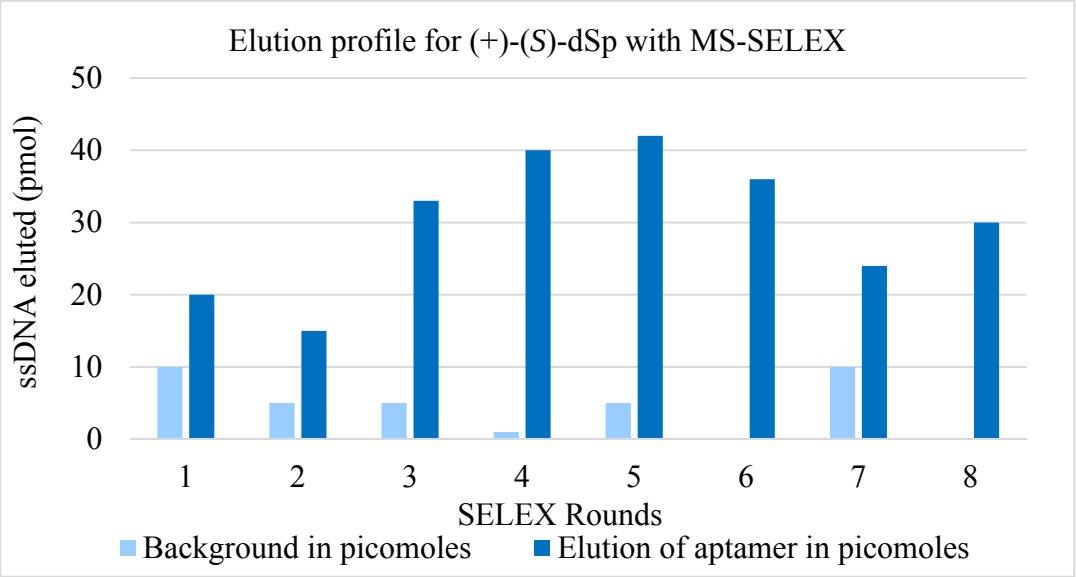

Figure 3.18. Elution profiles of background and aptamer strands for every round of (+)-(*S*)-dSp MS-SELEX.

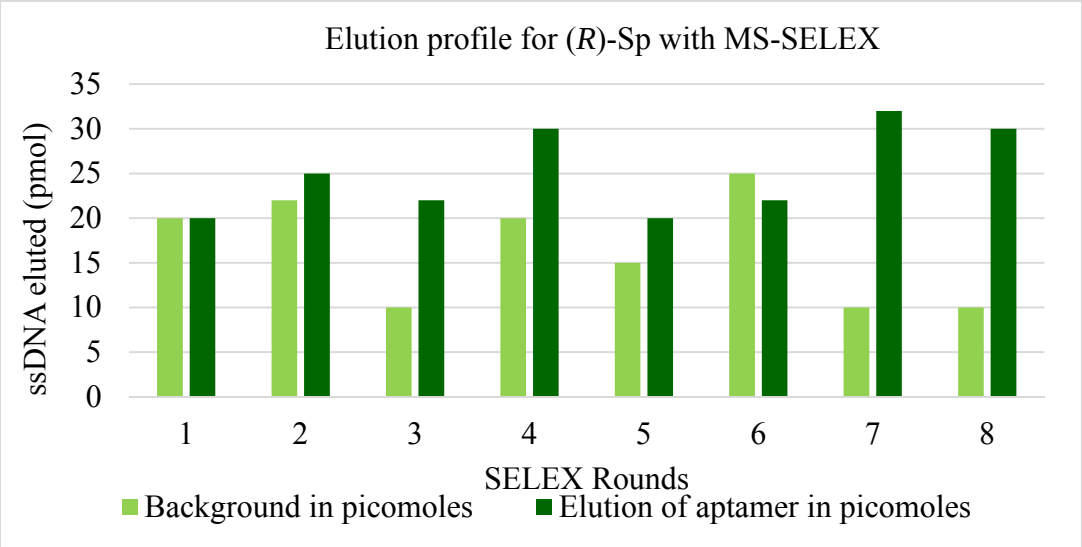

Figure 3.19. Elution profiles of background and aptamer strands for every round of (*R*)-Sp MS-SELEX.

The concentration of eluted ssDNAs was measured by the Cy-3 fluorescence. After each round of selection and amplification, agarose test gels were scanned on an imager for fluorescence as shown in the Figures 3.20 (a) and (b) for (-)-(*R*)-dSp, (+)-(*S*)-dSp and Figures 3.21 (a) and (b) for (*R*)-Sp, respectively. Upon transformation of cloned plasmid, 50 colonies were picked and sequenced. The insert DNAs are listed in Tables 3.7, 3.8, and 3.9 for (-)-(*R*)-dSp, (+)-(*S*)-dSp, and (*R*)-Sp, respectively.

The post-SELEX modifications of selected sequences were done by truncating primer regions and designing sensors for studying binding affinities of the sensors to the respective targets. At least four sequences, obtained from cloned plasmid, PCR amplified, and converted to ssDNA where tested with the respective target for their elution and the sequences that showed highest elution were further used for designing sensors and testing binding to the target in a signal-on detection method explained in the introduction of this chapter.

Binding studies or K_D measurements

Different sensors were designed for every SELEX round and selected based on predicted M-fold structures. There were mainly four types of structures obtained in all SELEXs for all targets: three-way junctions (3WJ), hairpin loops, and stem loops with one or more symmetric internal loops. The M-fold structures are shown in Figure 3.22. The sensor and capture sequences were designed based on using a 7-8 bp stem loop for sensor and 13- and 14-mer capture or competitor strands complementary to the sensor region are shown in Tables 3.10, 3.11, 3.12, 3.13, and 3.14. for 8-oxo-G, 8-oxo-dG, (-)-(*R*)-dSp, (+)-(*S*)-dSp, and (*R*)-Sp, respectively. The number in brackets at the end of every sequence in table indicates the predicated melting temperature of the strands using Quikfold and oligo

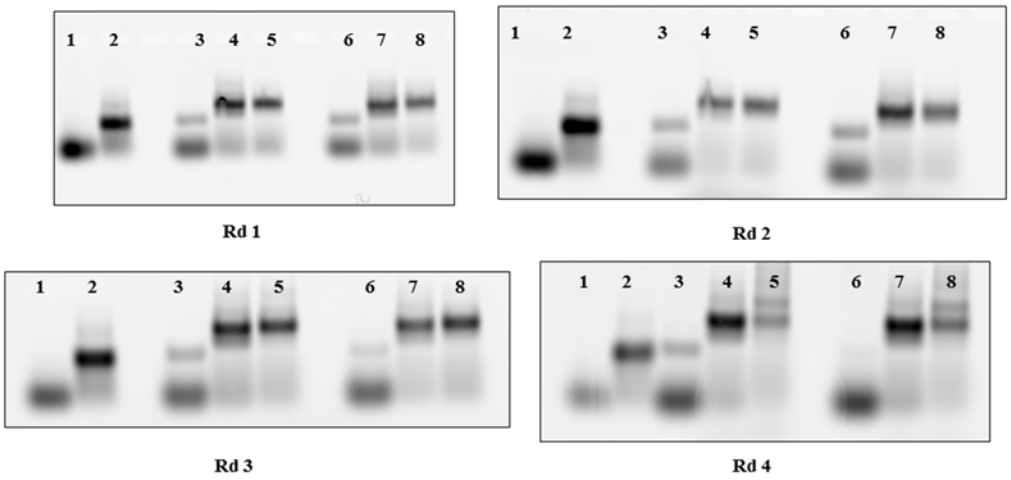

Figure 3.20. 4% Agarose gels of MS-SELEX for dSp nucleosides. (a) The first four rounds of SELEX. (b) rounds 5-8 of MS-SELEX. Lanes 1 and 2 represent forward primer, and ssDNA library. Lanes 3, 4, and 5 refer to negative, positive PCR, and elute PCR, respectively for that cycle of (-)-(*R*)-dSp. Lanes 6, 7, and 8 represent negative, positive PCR, and elute PCR, respectively, for that cycle of (+)-(*S*)-dSp.

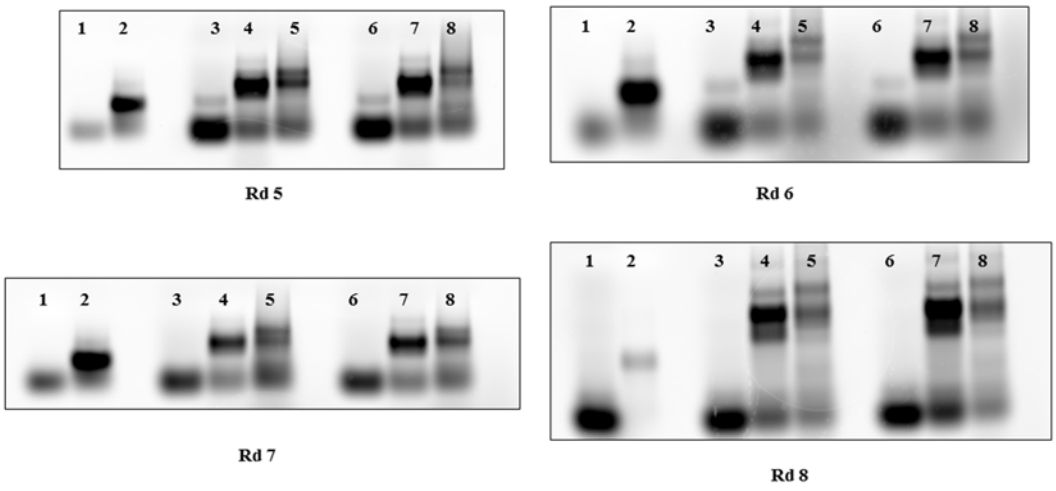

Figure 3.20. Continued

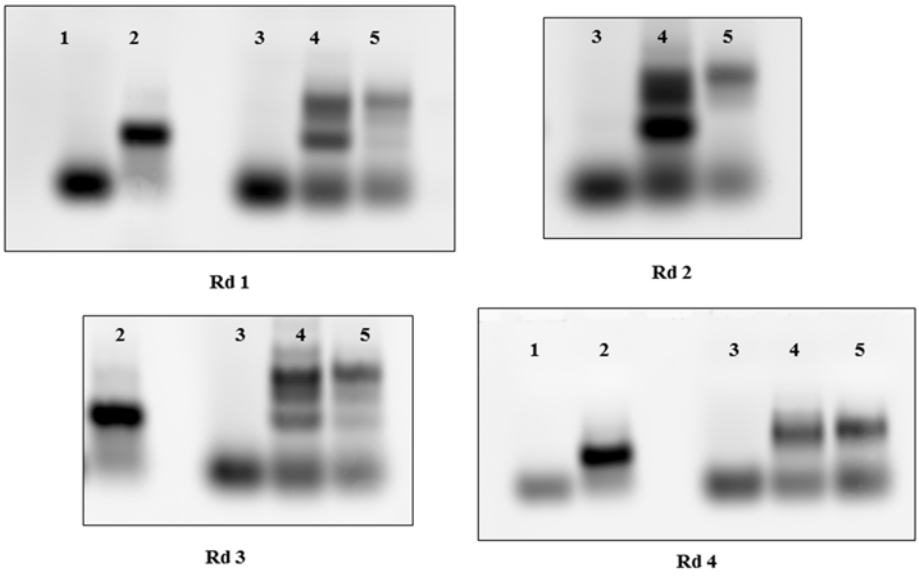

Figure 3.21. 4% Agarose test gels of MS-SELEX for (*R*)-Sp. (a) The first four rounds of SELEX. (b) Rounds 6-9 of SELEX. Lanes 1 and 2 represent forward primer, and ssDNA library. Lanes 3, 4, and 5 refer to negative, positive PCR, and elute PCR, respectively, for that cycle of (*R*)-Sp.

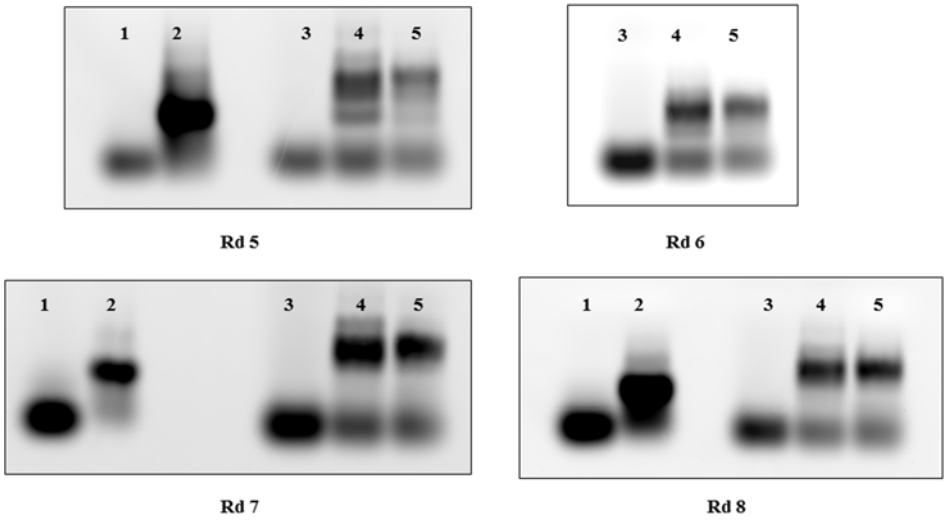

Figure 3.21. Continued

Table 3.7. Insert DNA sequences (labeled dSpA) for (-)-(*R*)-dSp MS-SELEX obtained after cloning. The random N_{30} regions of the library are shown here and the number of sequences represents the number of times the sequence has appeared in cloning and sequencing.

Sequence name	Random regions of insert library obtained for (-)-(*R*)-dSp MS-SELEX	No. of sequence
dSpA8_1	GTCCAGTAAGGCTTTTAATTTTTTCAGTCC	1
dSpA8_2	TAAGATCTGACAGACGAACAGATTCTTTTT	1
dSpA8_4	TAATACCTCACTACCCACATAGCATGTCTA	2
dSpA8_7	GATAGAGGTACATAGGCTGCACCTAAACTA	1
dSpA8_8	AGCGAAAGTAACCGGATGTGTTCCTAGACT	2
dSpA8_9	GGCCCGCGACCGATCTCCACCTAACGGCCT	2
dSpA8_10	ACCATCGGGTATTTGAACAGCCACTCCAAT	2
dSpA8_19	GGCCTTTGCCCATAGCGGTAAGTACTACCG	3
dSpA7_3	AAAGCGTGACTTCCTTCTGATAGCCCCTCT	1
dSpA7_9	TAGTAGCGCCTGTGTACAACACGTGCAATT	1
dSpA7_13	AGGAGAGTCGTTAGGTACTAAGACCGAAAA	2

Table 3.8. Insert DNA sequences (labeled dSpB) for (-)-(*S*)-dSp SELEX obtained after cloning. The random N_{30} regions of the library are shown here and the number of sequences represents the number of times the sequence has appeared in cloning and sequencing.

Sequence name	Random regions of insert library obtained for (+)-(S)-dSp MS-SELEX	No. of sequence
dSpB8_4	AGGCGGTCTGAGACACCGACACAAGCCTG	2
dSpB8_7	GGTTAGGGACGGATTAAAAGGACCGACACG	1
dSpB7_7	TAATACCTCACTACCCACATAGCATGTCTA	2
dSpB7_17	TTGACGATTTTCTAAGGCTTCCAAACGTCT	1
dSpB8_3	TAAACCAGTGGCAGCCCAGCTACCCGGAAA	2
dSpB8_12	CCAGTCACGGCGTAGGCATACACCCCGAGA	2
dSpB8_9	GCGAATCTCAGTTAGCTTTGAGATTTTGAA	2
dSpB8_17_2	GGGTAGCCAAGCCAGGGGCATGCCAACACT	1

Table 3.9. Insert DNA sequences (labeled SpA) for (*R*)-Sp MS-SELEX obtained after cloning. The random N_{30} regions of the library are shown here and the number of sequences represents the number of times the sequence has appeared in cloning and sequencing.

Sequence name	Random regions of insert library obtained for (*R*)-Sp MS-SELEX	No. of sequences
SpA8_8	CGAATCTAGCTATCGGGAGTCTCATCGGGT	3
SpA8_10	CTGAATATGCGCTAGAACTGCCGTAGAACT	1
SpA8_20	GAGCCTAGGGGAATAACATAATGGCTTAAA	1
SpA8_42	CCTGGGGCTAGTTTATGAAACATACCTCGG	1
SpA8_9	GACCAGTTGATCTAGATCAGCGCCCGTACT	1
SpA8_3	GAAAACACGTATACCTAGCTTAGTAGTCGA	2
SpA8_11	GGGTACCGGCGGACCAGGCCTCCCGATCGG	1
SpA8_40	AGGTGAGAGACTCCTAGCGGTAAATCTCCT	2
SpA8_14	CGAATCTAGCTATCGGGAGTCTCATCGGGT	1
SpA8_23	TCCGTGAGAGCCCGACCTAGGGAAGTCACA	1
SpA8_24	GGTCCCCAGTAGGGACTGGGTGGTGCGACT	1
SpA8_25	GATGTCAACCGGTAAATAGGAGTCTCTCGT	1
SpA8_31	AGGTACTAATTATGGAGTAAGGTAAGTCCA	1
SpA8_36	ACCTGAGAGACTCCCGATAAAGTCGCGACT	2
SpA8_37	ACCTGAGAGACTCCGCAATTAGAATGGCAT	3
SpA8_47	ACCCGATGAGACTCCCGATAGCTAGATTCG	1

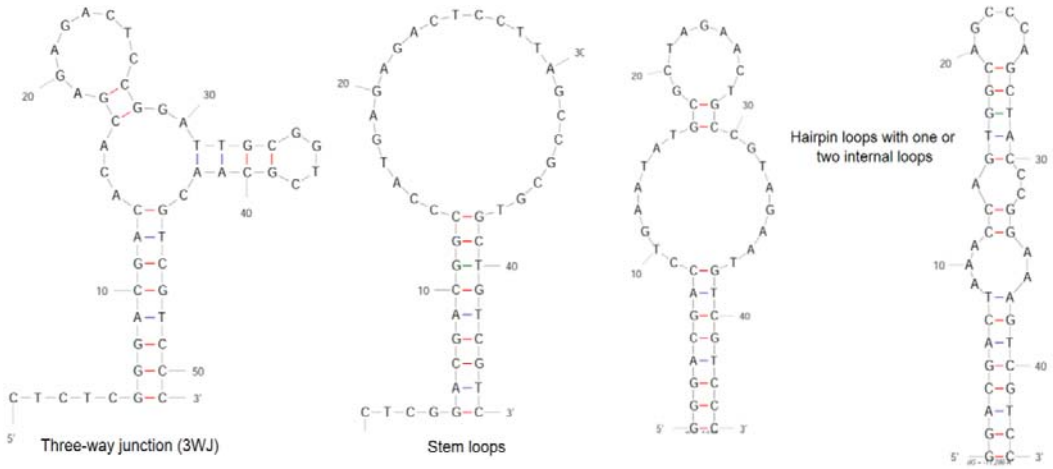

Figure 3.22. The four different forms of M-fold structures obtained from the truncated sequences in different SELEXs.

Table 3.10. The sequences of the selected 8-oxo-G sensors, and 13 or 14-mer quenchers selected for MS-SELEX. The melting temperatures (T_M) indicated in the brackets are in degree Celsius.

Sequence Name	OG sensors (5'-FAM) and quenchers (3'-Dab) The red sequence is the random N_{30} region in the sensor
OG_1	5'-FAM-GACGACAGCCAGTTGTTAGAATGGTTGAACCCGTGA (54)
14mer:	5'-AACTGGCTCTCGTC /3'Dab (58)
13mer:	5'-ACTGGCTCTCGTC /3'Dab (56)
OG_2	5'-FAM-CTCTCGGGACGACTCTATCCGAGATGCCGACTTTACGAATATCGACGTCCCG (56
14mer:	5'-AGTCGTCCCGAGAG /3'Dab (59)
13mer:	5'-GTCGTCCCGAGAG /3'Dab (56)
OG_5	5'-FAM-CTCTCGGGACGACCTCAGAGACTCCTAGCGGTAAATCTCCTGTGTCGTCCC (58)
14mer:	5'-GGTCGTCCCGAGAG /3'Dab (60)
13mer:	5'-GTCGTCCCGAGAG /3'Dab (57)
OG_6	5'-FAM-GGACGACAGGTGAGAGACTCCTAGCGGTAAATCTCCTGTC-3' (55)
14mer:	5'-CTCACCTGTCGTCC/3'Dab (58)
13mer:	5'-TCACCTGTCGTCC/3'Dab (56)
OG_9	5'-FAM-CTCTCGGGACGACGAAACAAGCCGGTTGTGGAATCATGCGATTGTCGTCCC (57)
14mer:	5'-CGTCGTCCCGAGAG /3'Dab (60)
13mer:	5'-GTCGTCCCGAGAG /3'Dab (57)
OG_12	5'-FAM-CTCTCGGGACGACACACGAGAGACTCCGGATTGCGGTCGCAACGTCGTCCC (56)
14mer:	5'-TGTGGTCCCGAGAG/3'Dab (59)
13mer:	5'-GTGGTCCCGAGAG /3'Dab (57)
OG_15	5'-FAM-CTCTCGGGACGACACGGATCGGAGATGCCGACTTTACAATATCGTCGTCCC (66)
14mer:	5'-TGTCGTCCCGAGAG/3'Dab (60)
13mer:	5'-GTCGTCCCGAGAG/3'Dab (57)
OG_MS1	5'-FAM-GCTTCGGACGACACCGGTCAGCGGTAGCCTGTCGTCCCGAGA (70)
14mer:	5'-GTGTCGTCCGAAGC/3'Dab (60)
13mer:	5'-TGTCGTCCGAAGC /3'Dab (58)

Table 3.11. The sequences of the selected 8-oxo-dG sensors, and 13 or 14-mer quenchers selected for MS-SELEX. The melting temperatures (T_M) indicated in the brackets are in degree Celsius.

Sequence Name	dOG sensors (5'-FAM) and quenchers (3'-Dab) The red sequences are randomized N_{30} regions of the sensors and numbers in brackets indicate T_M
dOG_2	5'-FAM-CTCTCGGGACGACTAATGCCTTGGTCCGAAGTTCATTTGGTAGGTCGTCC (55)
14mer:	5'-TAGTCGTCCGAGAG /3'Dab (53)
13mer:	5'- AGTCGTCCGAGAG /3'Dab (55)
dOG_7	5'-FAM-CTCGGGACGACGGGGTTCCTGCTGATATAGGTCCGTCGTAG (62)
14mer:	5'-CCCGTCGTCCCGAG /3'Dab (64)
13mer:	5'-CCGTCGTCCCGAG /3'Dab (60)
dOG_8	5'-FAM-CTCTCGGGACGACTAGGATTTTCAGCTCTCCTGCCAGGGGCCCGTCGTCC (53)
14mer:	5'-AGTCGTCCCGAGAG/3'Dab (59)
13mer:	5'-GTCGTCCCGAGAG /3'Dab (56)
dOG_10	5'-FAM-CTCGGACGACGGCCCATGAGAGACTCCTTAGCCGCGTGCTGTCGTC (65)
14mer:	5'-GGCCGTCGTCCGAG /3'Dab (64)
13mer:	5'-GCCGTCGTCCGAG/3'Dab (61)
dOG_12	5'-FAM-GGCTCGGGACGACGTCCCGATGCTGCAATCGTAAAACGGATGAGTCGTCCC (59
14mer:	5'-CGTCGTCCCGAGCC/3'Dab (64)
13mer:	5'-GTCGTCCCGAGCC/3'Dab (60)
dOG_14	5'-FAM-CTCGGGACGACGGGGTTCCTGCTGATATAGGTCCGTCGTAG (62)
14mer:	5'-CCCGTCGTCCCGAG /3'Dab (64)
13mer:	5'-CCGTCGTCCCGAG /3'Dab (60)
dOG_19	5'-FAM-TCTCGACGACAGCCCATGAGAGCCGACAACAAGGACCGCAGTCGTC (52)
14mer:	5'-GGCTGTCGTCGAGA/3'Dab (60)
13mer:	5'-GCTGTCGTCGAGA /3'Dab (57)
dOG_23	5'-FAM-GACGACAGAGCTTGATGAATCATTTAATAAGGTCTAGT (54)
14mer:	5'-CAAGCTCTGTCGCT/3'Dab (58)
13mer:	5'-AAGCTCTGTCGCT/3'Dab (57)
dOG_26	5'-FAM-TCTCGGGACGACATGTTCCGTGTTACTACTCCATGAAATCTTGTCGTCC (53)
14mer:	5'-ATGTCGTCCCGAGA /3'Dab (59)
13mer:	5'-TGTCGTCCCGAGA /3'Dab (58)

Table 3.12. The sequences of the selected (-)-(*R*)-dSp sensors, and 13 or 14-mer quenchers selected for MS-SELEX. The melting temperatures (T_M) indicated in the brackets are in degree Celsius.

Sequence Name	(R)-(-)-dSp sensors (5'-FAM) and quenchers (3'-Dab) The sequences in red are N_{30} random regions and the numbers in brackets indicate T_M.
dSpA8_8	5'-FAM-GACGACAGCGAAAGTAACCGGATGTGTTCCTAGACTGTCGTC (56)
14mer	5'- CTTTCGCTGTCGTC-3'Dab (57)
13mer	5'-TTTCGCTGTCGTC-3'Dab (55)
dSpA8_10	5'-FAM-GGACGACACCATCGGGTATTTGAACAGCCACTCCAATGTCGTCC (56)
14mer	5'-CGATGGTGTCGTCC-3'Dab (58)
13mer	5'-GATGGTGTCGTCC-3'Dab (55)
dSpA8_19	5'-FAM-GGGACGACGGCCTTTGCCCATAGCGGTAAGTACTACCGGTCGTCCC (62)
14mer	5'-AAGGCCGTCGTCCC -3'Dab (64)
13mer	5'- AGGCCGTCGTCCC -3'Dab (63)
dSpA7_13	5'-FAM-GGGACGACAGGAGAGTCGTTAGGTACTAAGACCGAAAAGTCGTCCC (59)
14mer	5'-TCTCCGGTCGTCCC -3'Dab (62)
13mer	5'-CTCCGGTCGTCCC -3'Dab (60)

Table 3.13. The sequences of the selected (+)-(*S*)-dSp sensors, and 13 or 14-mer quenchers selected for MS-SELEX. The melting temperatures (T_M) indicated in the brackets are in degree Celsius.

Sequence Name	(S)-(-)-dSp sensors (5'-FAM) and quenchers (3'-Dab) The sequences in red represent N_{30} random regions and the numbers in brackets represent T_M.
dSpB5_4	5'-FAM-GACGAGGCGGTCTGAGACACCGACACAAGCCTGGTC (47)
14mer	5'-CAGACCGCCTCGTC/3'Dab (53)
13mer	5'-AGACCGCCTCGTC/3'Dab (50)
dSpB5_9	5'-FAM GGACGACGCGAATCTCAGTTAGCTTTGAGATTTTGAAGTCGTCC (59)
14mer	5'-GATTCGCGTCGTCC/3'Dab (60C)
13mer	5'-ATTCGCGTCGTCC/3'Dab (58C)
dSpB5_12	5'-FAM GGACGACCCAGTCACGGCGTAGGCATACACCCCGAGAGTCGTCCC (58)
14mer	5'-GACTGGGTCGTCCC/3'Dab (60)
13mer	5'-ACTGGGTCGTCC/3'Dab (59)
dSpB7_7	5'-FAM GACGACGGTTAGGGACGGATTAAAAGGACCGACACGGTCGTC (51)
14mer	5'-CCCTAACCGTCGTC/3'Dab (58)
13mer	5'-CCTAACCGTCGTC/3'Dab (54)

Table 3.14. The sequences of the selected (*R*)-Sp sensors, and 13 or 14-mer quenchers selected for MS-SELEX. The melting temperatures (T_M) indicated in the brackets are in degree Celsius.

Sequence Name	(R)-Sp sensor (5'-FAM) and quenchers (3'-Dab) The red sequences represent the random N_{30} regions; values in brackets indicate T_M.
SpA8_8	5'-FAM-GGGACGTCCGAATCTAGCTATCGGGAGTCTCATCGGGTGTCGTCCC (56)
14mer	5'-GATTCGGTCGTCCC-3'Dab (58)
13mer	5'-ATTCGGTCGTCCC-3'Dab (57)
SpA8_36	5'-FAM-GGGACGACACCTGAGAGACTCCCGATAAAGTCGCGACTGTCGTCCC (61)
14mer	5'-TCAGGTGTCGTCCC-3'Dab (60)
13mer	5'-CAGGTGTCGTCCC-3'Dab (57.4)
SpA8_37	5'-FAM-GGGACGACACCTGAGAGACTCCGCAATTAGAATGGCATGTCGTCCCG (57)
14mer	5'-CAGGTGTCGTCCCG-3'Dab (61)
13mer	5'-AGGTGTCGTCCCG-3'Dab (59)
SpA8_40	5'-FAM-GACAGGTGAGAGACTCCTAGCGGTAAATCTCCTGTC (54)
14mer	5'-GTCTCTCACCTGTC-3'Dab (54)
13mer	5'-TCTCTCACCTGTC-3'Dab (52)

analyzer with the same ionic strength as in the experimental studies.

A fixed concentration of 5 nM of sensor strand showed substantial quenching of fluorescence upon hybridization. Various concentrations 0-500 nM of capture strand where selected. The sensor-capture strand fixed ratio that showed more than 60% quenching was selected to determine K_{deff2} with target to see an increase in fluorescence signal upon addition of higher concentration of target until saturation occurs. The ratio of both K_{deff1}/K_{deff2} was used to determine the K_d for the aptamer. Two dOG sensors (Figure 3.23), two OG sensors (Figure 3.24), two (-)-(*R*)-dSp sensors (Figure 3.25), one (+)-(*S*)-dSp (Figure 3.26), and two (-)-(*R*)-Sp sensors (Figure 3.27) showed a significant change in fluorescence upon hybridization with 13- or 14-mers. All these figures show the two graphs obtained each for 13 and 14-mer capture strand along with the sequences and
M-fold structures for each sensors and the calculated K_{deff1} for each 13 and 14-mers. The K_{deff1} was calculated by Equation (1) from Scheme 3.1 by determining the amount of free capture, free aptamer, and the amount of aptamer-capture dsDNA at the half maximum value according to the plots obtained.

Among the dOG sensors, the lowest K_{deff1} of 1.5 nM was obtained for 13-mer with dOG_7, both 13- and 14-mer for sensor dOG_10. Among the OG sensors, the K_{deff1} were around 2-3 nM for all combinations. All (-)-(*R*)-dSp sensors had much higher K_{deff1}, the highest one being ~68 nM for 13-mer with (-)-(*R*)-dSp8_8. Also, for the only sensor (+)(*S*)-dSp7_7, the K_{deff1} was 75 nM for both capture strands. For all (-)-(*R*)-Sp capture strands the K_{deff1} ranged from 25-50 nM.

Once the K_{deff1} was calculated, the ratio of the capture strand with higher than 60% quenching was selected to titrate various concentrations of target and determine the K_{deff2}.

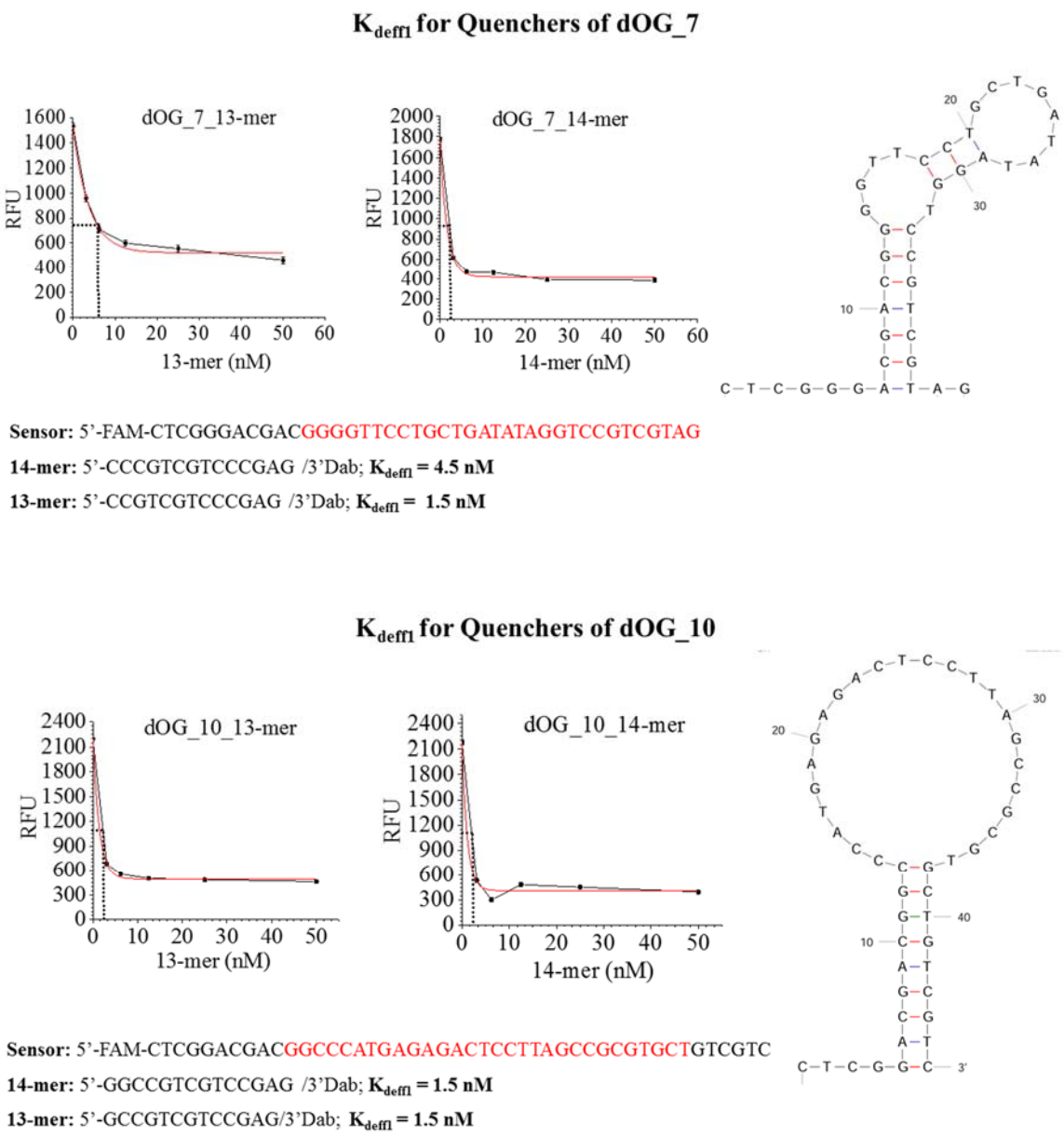

Figure 3.23. dOG sensors with respective 13 and 14-mer hybridization quenching plots.

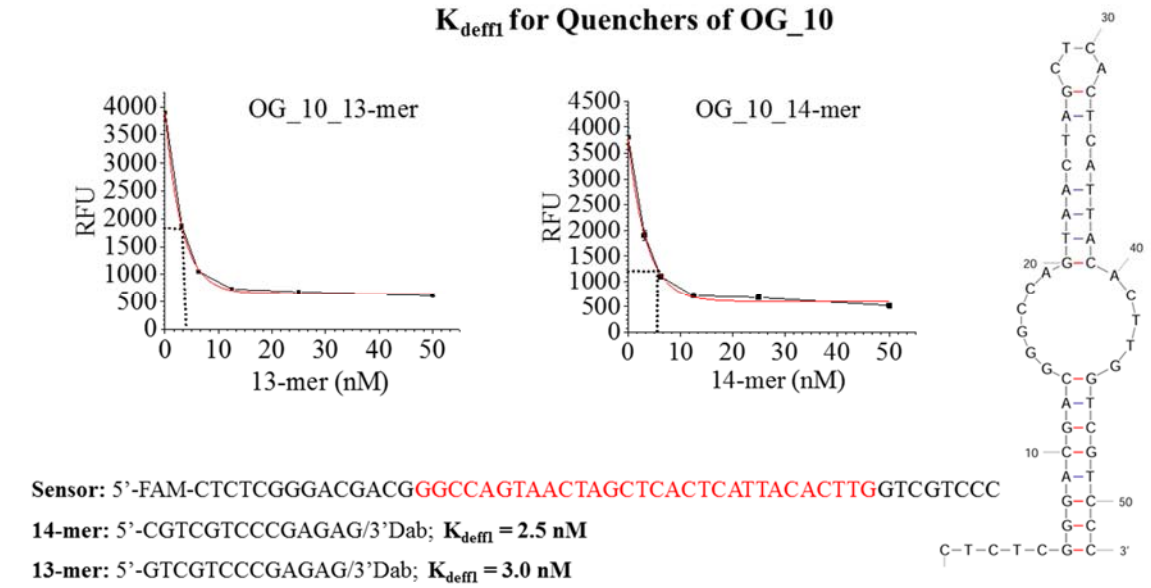

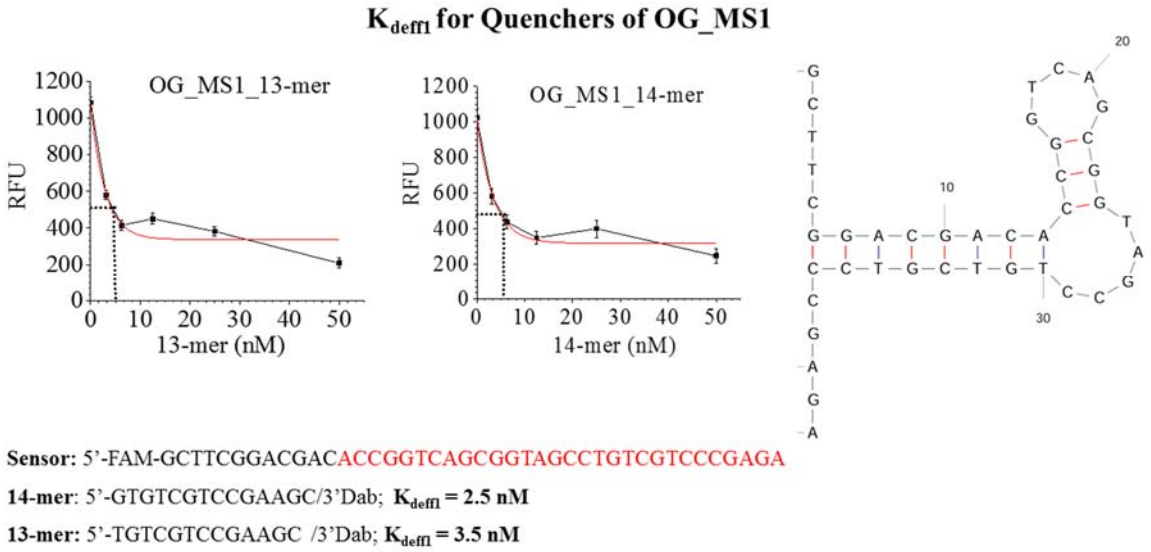

Figure 3.24. OG sensors with respective 13-and 14-mer capture strands and their hybridization fluorescence quenching plots and their K_{deff1}.

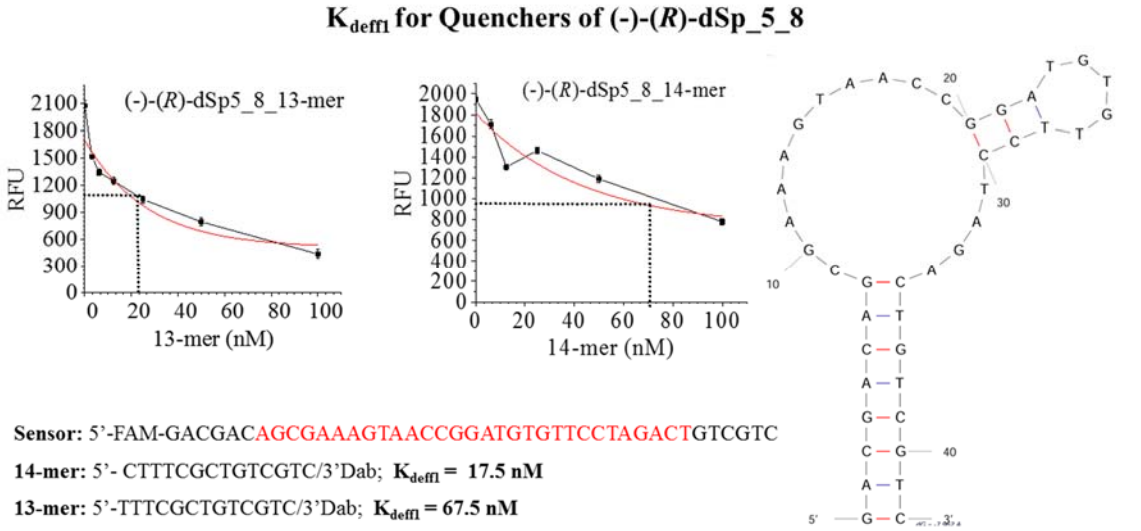

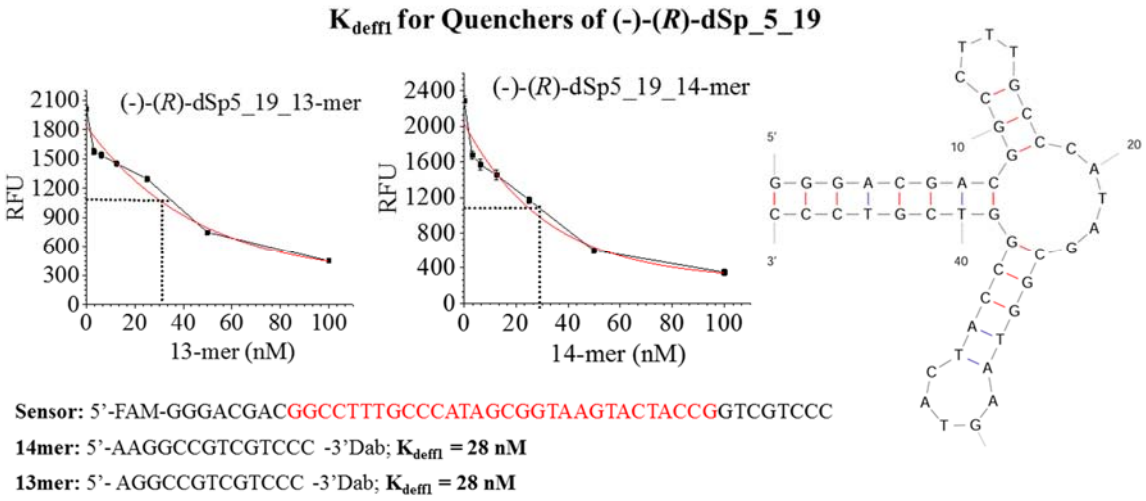

Figure 3.25. (-)-(*R*)-dSp sensors with respective 13-and 14-mer capture strands and their hybridization fluorescence quenching plots and their K_{deff1}.

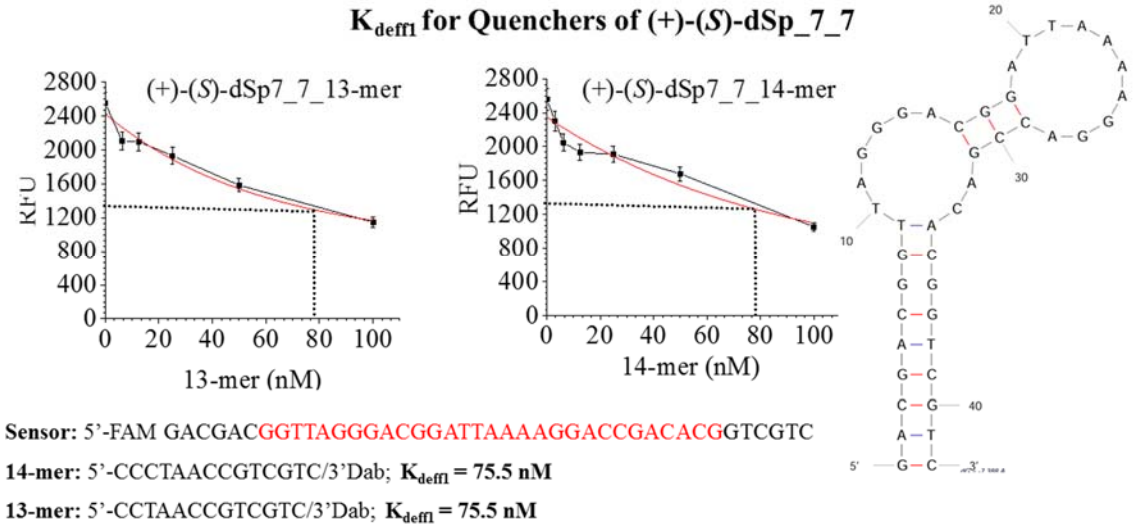

Figure 3.26. (+)-(*S*)-dSp sensors with respective 13-and 14-mer capture strands and their hybridization fluorescence quenching plots and their K_{deff1}.

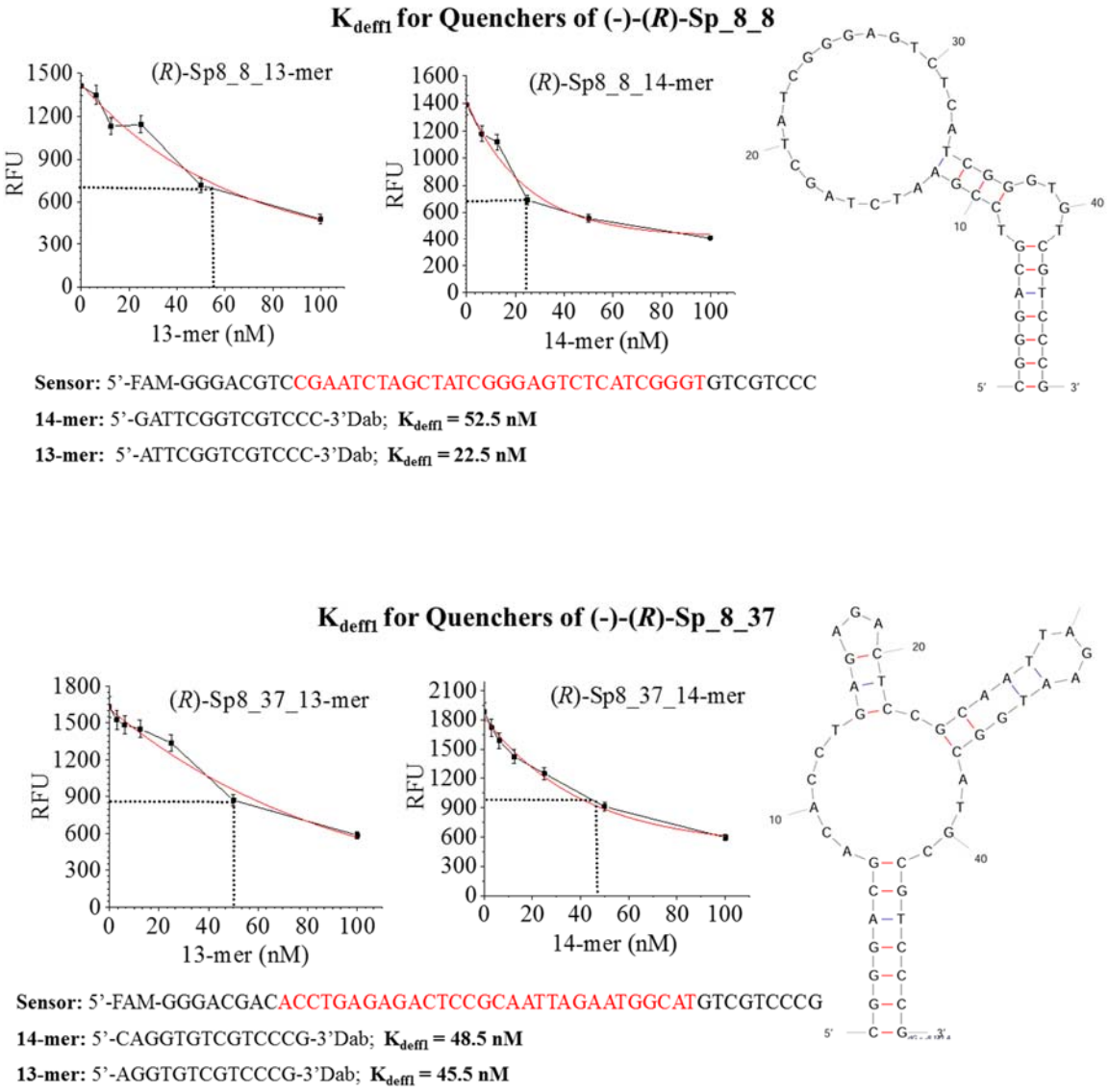

Figure 3.27. (-)-(*R*)-Sp sensors with respective 13-and 14-mer capture strands and their hybridization fluorescence quenching plots and their K_{deff1}.

The target was serial diluted from 500 μM to 2 nM and added to constant sensor and capture strand concentration. The fluorescence increases with higher concentration of target and eventually results in saturation. The K_{deff2} obtained for all targets dOG (Figure 3.28), OG (Figure 3.29), (-)-(*R*)-dSp (Figure 3.30), (+)-(*S*)-dSp (Figure 3.31), and (-)-(*R*)-Sp (Figure 3.32) are shown. The K_{deff2} was calculated with the Equation (2) in Scheme 3.1 and the concentration of free target, free competitor, aptamer-target complex, and aptamer-competitor were obtained from the graph. The $K_{d,aptamer}$ is then calculated from both the K_{deff1} and K_{deff2} obtained. Among the several sensors, the one obtained with lowest binding affinity was determined as a high affinity aptamer for the target.

Conclusion

We performed MS-SELEX on various targets that are products of guanine oxidation. The nucleosides are the products of nucleotide excision repair (NER), whereas the nucleobases are products of base excision repair (BER) pathway. We were successfully able to carry out the SELEX on all the targets separately in 8-13 rounds. The sequences were obtained had great diversity with respect to the target. None of the sequences matched between two targets and is a good indication that these sequences are not background.

The 8-oxo-G free base had both OG10 and OGMS1 DNA aptamers with K_d 5 nM. The very low K_d obtained can be explained by the high stacking interaction of the OG free base with the aptamers. The structure of both the OG and (-)-(*R*)-Sp aptamers was similar and had a hairpin structure with internal loop present. The only other free base for which the SELEX was done, (-)-(*R*)-Sp8_8 aptamer, had a K_d of 10nM. The free base DNA aptamer in general showed lower K_d than the nucleoside counterparts. (-)-(*R*)-dSp5_8, DNA aptamer for the diastereomer of dSp had K_d of 14nM, whereas for the other diastereomer *(+)*-

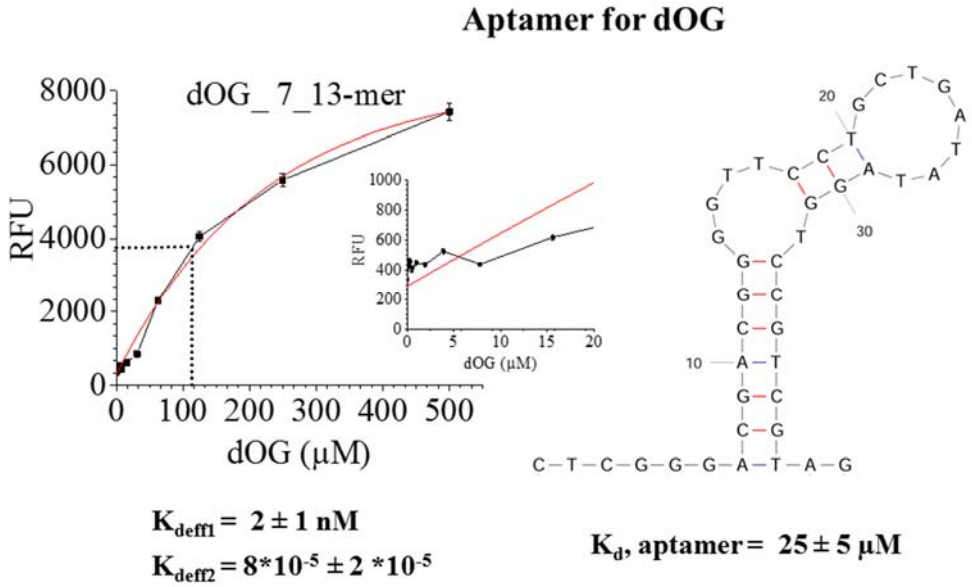

Figure 3.28. The dOG_7 sensor with increased concentration of the target and the determination of K_{deff1} with the capture strand and the $K_{d,aptamer}$.

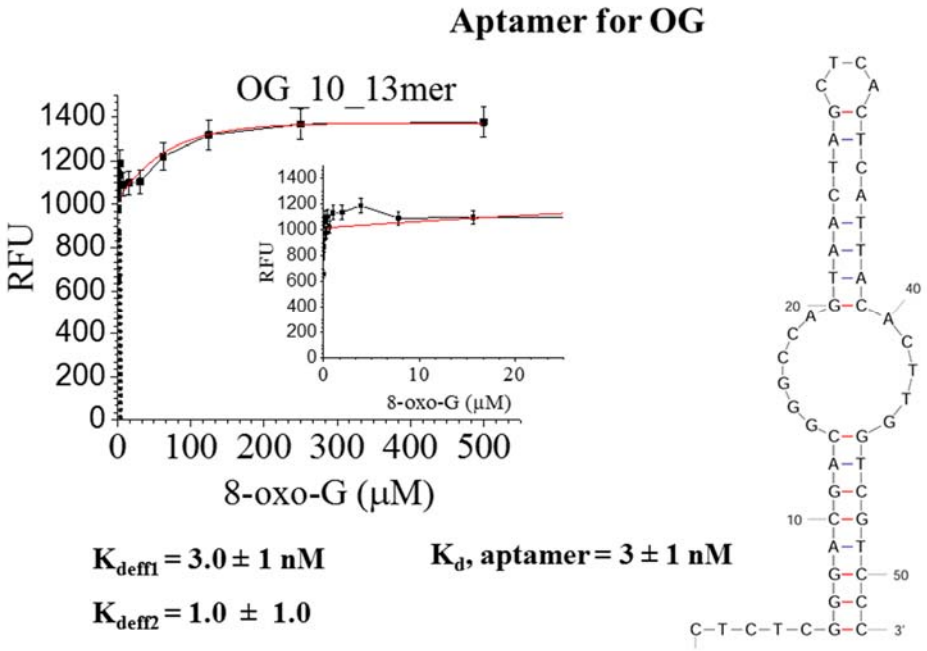

Figure 3.29. The OG_10 sensor with increased concentration of the target and the determination of K_{deff1} with the capture strand that lead to determination of $K_{d,aptamer}$.

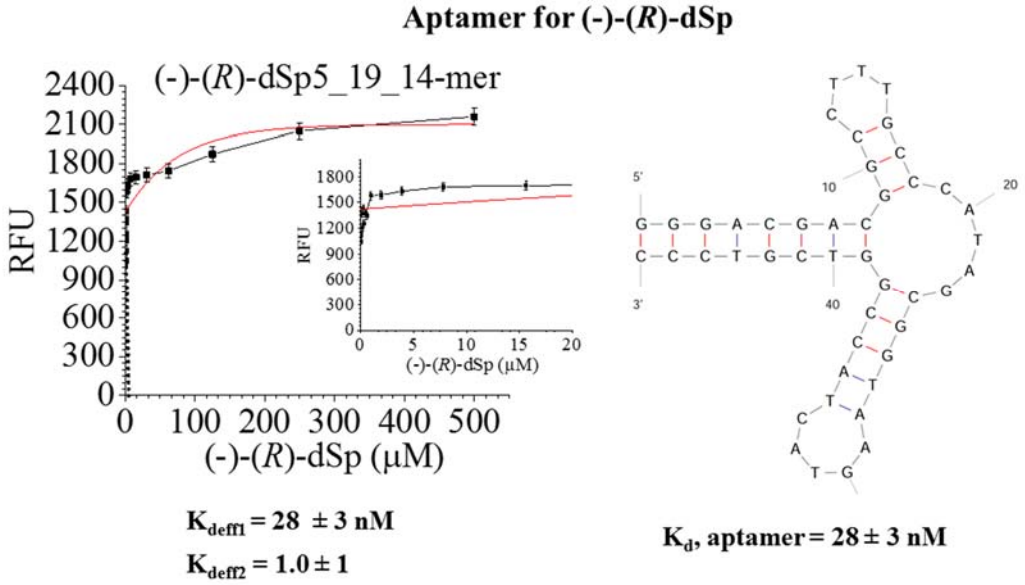

Figure 3.30. (-)-(*R*)-dSp_5_19 sensor and 14-mer capture strand with increased concentration of the target and the determination of K_{deff1} and eventually $K_{d,aptamer}$.

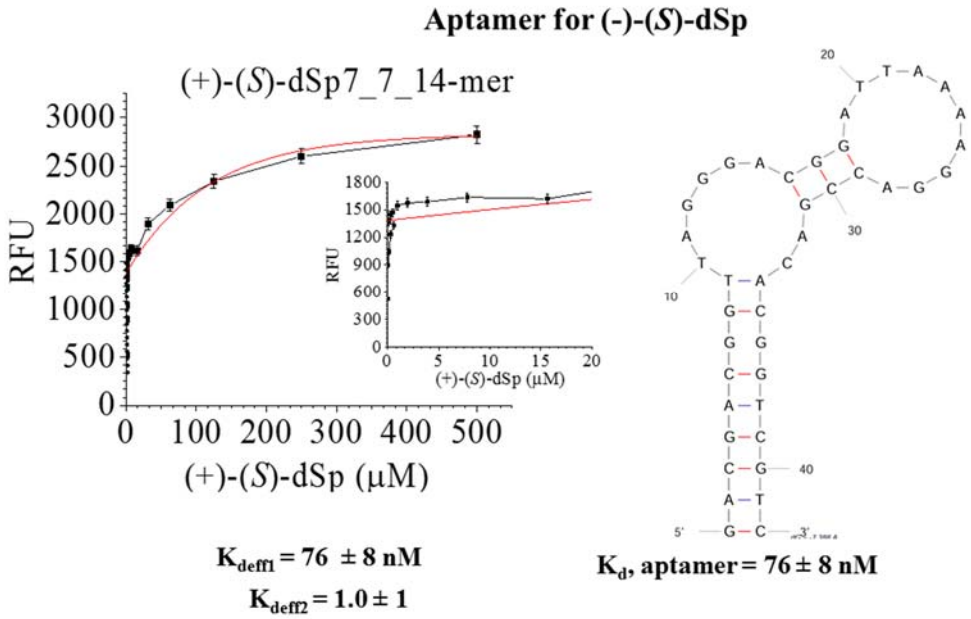

Figure 3.31. (+)-(*S*)-dSp7_7 sensor with increased concentration of the target and the determination of K_{deff1} with the capture strand that leads to determination of $K_{d,aptamer}$ eventually.

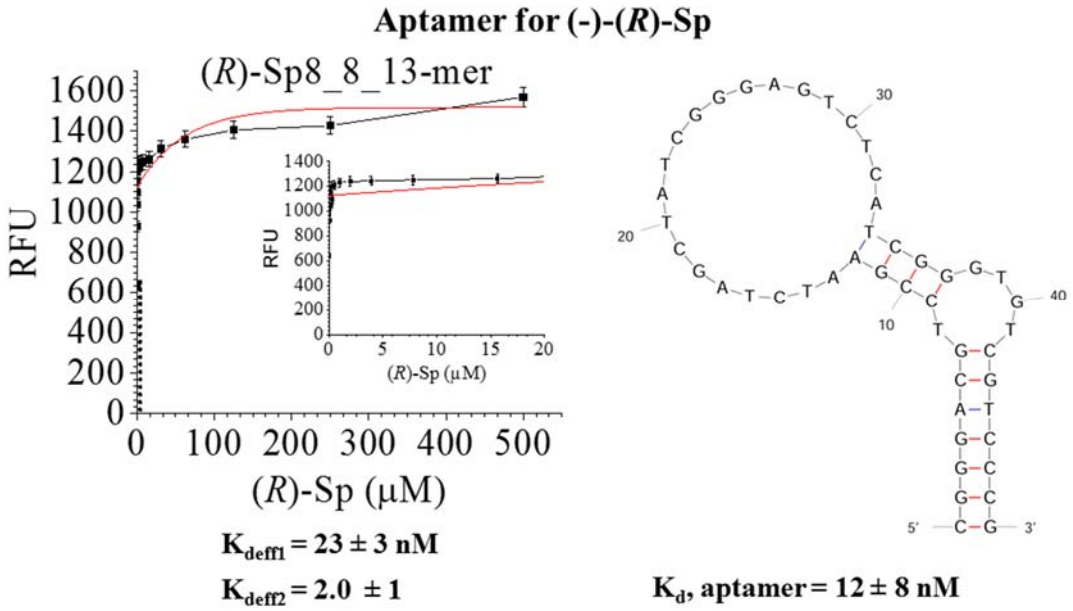

Figure 3.32. (-)-(*R*)-Sp8_8 sensor with increased concentration of the target and the determination of K_{deff1} with the capture strand that leads to determination of $K_{d,aptamer}$.

(*S*)-dSp, the K_d of the DNA aptamer (+)-(*S*)-dSp7_7 was 95 nM. These aptamers are surprisingly similar in their secondary structure to the OG, and (-)(-)-(*R*)-dSp5_8, a DNA aptamer for the diastereomer of dSp with K_d of 14nM. The (*R*)-Sp base aptamer, however, has a hairpin with internal loops. This is the only other case where the aptamers are reported for diastereomers apart from the (*R*) and (*S*)-ibuprofen (K_d = 4μM) and (*R*)-thalidomide (K_d = 1μM). We were able to obtain K_d in lower nM range for these diastereomers.

The only DNA aptamers that had K_d in micromolar range was for dOG target. The 8-oxo-dG aptamers, dOG_7 and dOG_10 had K_d as 20 μM. This was unexpectedly higher than the previously reported 8-oxo-dG RNA aptamer that had K_d of 270 nM and a DNA aptamer with K_d 100 nM. [45, 46] However, one needs to mention that there might be better aptamers among the other sequences that have not been tested in the binding studies.

The further aim with respect to this project in our lab will be explained briefly in Chapter 4. The short-term goal is to test these aptamers for their specificity and affinity in vitro and further test them in cellular samples and be able to measure the oxidative stress in a cell.

References

1. Hamaguchi, N.; Ellington, A. D. Aptamer Beacons for the Direct Detection of Proteins. *Anal. Biochem.* **2001,** 294, 126-131.

2. Stojanovic, M. N.; Kolpashchikov, D. M. Modular Aptameric Sensors. *J. Am. Chem. Soc.* **2004,** 126, 9266-9270.

3. Jhaveri, S. D.; Kirby, R.; Conrad, R.; Maglott, E. J.; Bowser, M.; Kennedy, R. T.; Glick, G.; Ellington, A. D. Designed Signaling Aptamers that Transduce Molecular Recognition to Changes in Fluorescence Intensity. *J. Am. Chem. Soc.* **2000,** 122, 2469-2473.

4. McKeague, M.; DeRosa, M. C. Challenges and Oppurtunities or Small Molecule Aptamer Development. *J. Nucl. Acids* **2012,** 2012, 1-20.

5. Stojanovic, M. N.; de Prada, P.; Landry, D. W. Fluorescent Sensors Based on Aptamer Self-Assembly. *J. Am. Chem. Soc.* **2000,** 122, 11547-11548.

6. Yamamoto, R.; Kumar, P. K. Molecular beacon aptamer fluoresces in the presence of Tat protein of HIV-1. *Genes Cells* **2000,** 5, 389-396.

7. Stolenburg, R.; Reinemann, C.; Strehlitz, B. SELEX-A (R)-Evolutionary Method to Generate High Affinity Nucleic Acid Ligands. *Biomol. Eng.* **2007,** 24, 381-403.

8. Davis, J. H.; Szostak, J. W. Isolation of High-affinity GTP Aptamers from Partially Structured RNA Libraries. *Proc. Nat. Acad. Sci.* **2002,** 99, 11616-11621.

9. Tyagi, S.; Krammer, F. R. Molecular Beacons: Probes that Fluoresce upon Hybridization. *Nat. Biotech.* **1996,** 14, 303-308.

10. Li, N.; Ho, C.-M. Aptamer-Based Optical Probes with Separated Molecular Recognition and Signal Transduction Modules. *J. Am. Chem. Soc.* **2008,** 130, 2380-2381.

11. Westhof, E.; Patel, D. J. Nucleic Acids From Self-Assembly to Induce-Fit Recognition. *Curr. Opin. Struct. Biol.* **1997,** 7.

12. Nutiu, R.; Li, Y. Structure-Switching Signaling Aptamers. *J. Am. Chem. Soc.* **2003,** 125, 4771-4778.

13. Nutiu, R.; Li, Y. Structure-Switching Signaling Aptamers: Transducing Molecular Recognition into Fluorescence Signaling. *Chem. Eur. J.* **2004,** 10, 1868-1876.

14. Jhaveri, S.; Rajendran, M.; Ellington, A. D. In Vitro Selection of Signalling Aptamers. *Nat. Biotech.* **2000,** 18, 1293-1297.

15. Burrows, C. J.; Muller, J. G. Oxidative Nucleobase Modifications Leading to Strand Scission. *Chem. Rev.* **1998,** 98, 1109-1152.

16. Luo, W.; Muller, J. G.; Rachlin, E. M.; Burrows, C. J. Characterization of Spiroiminodihydantoin as a Product of One-Electron Oxidation of 8-Oxo-7,8-dihydroguanosine. *Org. Lett.* **2000,** 2, 613-616.

17. Luo, W.; Muller, J. G.; Rachlin, E. M.; Burrows, C. J. Characterization of Hydantoin Products from One-Electron Oxidation of 8-Oxo-7,8-dihydroguanosine in a Nucleoside Model. *Chem. Res. Toxicol.* **2001,** 14, 927-938.

18. Famulok, M. Oligonucleotide Aptamers That Recognize Small Molecules. *Curr. Opinion. Struct. Biol.* **1999,** 9, 324-329.

19. Gopinath, S. Methods developed for SELEX. *Anal. Bioanal. Chem.* **2007,** 387, 171-182.

20. McKeague, M.; Bradley, C. R.; Girolamo, A. D.; Visconti, A.; Miller, J. D.; DeRosa, M. C. Screening and Initial Binding Assessment of Fumonisin B1 Aptamers. *Int. J. Mol. Sci.* **2010,** 11, 4864-4881.

21. Nutiu, R.; Li, Y. In Vitro Selection of Structure-Switching Signaling Aptamers. *Angew. Chem. Int. Ed.* **2005,** 44, 1061-1065.

22. Yang, K.-A.; Pei, R.; Stefanovic, D.; Stojanovic, M. N. Optimizing Cross-reactivity with Evolutionary Search for Sensors. *J. Am. Chem. Soc.* **2012,** 134, 1642-1647.

23. Stoltenburg, R.; Strehlitz, B.; Nikolaus, N. Capture-SELEX: Selection of DNA Aptamers for Aminoglycoside Antibiotics. *J. Anal. Methods Chem.* **2012,** 1-14.

24. Tuerk, C. Using the SELEX Combinatorial Chemistry Process to Find High Affinity Nucleic Acid Ligands to Target Molecules. In *PCR Cloning Protocols*, White, B., Ed. Humana Press: 1997; Vol. 67, pp 219-230.

25. Svobodová, M.; Pinto, A.; Nadal, P.; O' Sullivan, C. K. Comparison of different methods for generation of single-stranded DNA for SELEX processes. *Anal. Bioanal. Chem.* **2012,** 404, 835-842.

26. Marimuthu, C.; Tang, T.-H.; Tominaga, J.; Tan, S.-C.; Gopinath, S. C. B. Single-stranded DNA (ssDNA) Production in DNA Aptamer Generation. *Analyst* **2012,** 137, 1307-1315.

27. Levine, H. A.; M., N.-H. A mathematical analysis of SELEX. *Comput. Biol. Chem.* **2007,** 31, 11-35.

28. Nieuwlandt, D. In Vitro Selection of Functional Nucleic Acid Sequences. *Curr. Issues Mol. Biol.* **2000,** 2, 9-16.

29. Jenison, R. D.; Gill, S. C.; Pardi, A.; Polisky, B. High-resolution molecular discrimination by RNA,. *Science* **1994,** 263, 1425–1429.

30. Win, M. N.; Klein, J. S.; Smolke, C. D. Codeine-binding RNA aptamers and rapid determination of their binding constants using a direct coupling surface plasmon resonance assay. *Nucl. Acids Res.* **2006,** 34, 5670-5682.

31. Cruz-Aguado, J. A.; Penner, G. Determination of Ochratoxin A with a DNA Aptamer. *Journal of Agricultural and Food Chemistry* **2008,** 56, 10456-10461.

32. Hu, J.; Easley, C. "A simple and rapid approach for measurement of dissociation constants of DNA aptamers against proteins and small molecules via automated microchip electrophoresis," *Analyst* **2011,** 136, 3461–3468.

33. Deng, Q.; German, I.; Buchanan, D.; Kennedy, R. T. Retention and Separation of Adenosine and Analogues by Affinity Chromatography with an Aptamer Stationary Phase. *Anal. Chem.* **2001,** 73, 5415-5421.

34. Drabovich, A. P.; Berezovski, M.; Okhonin, V.; Krylov, S. N. Selection of Smart Aptamers by Methods of Kinetic Capillary Electrophoresis. *Anal. Chem.* **2006,** 78, 3171-3178.

35. Bao, J.; Krylova, S. M.; Reinstein, O.; Johnson, P. E.; Krylov, S. N. Label-Free Solution-Based Kinetic Study of Aptamer–Small Molecule Interactions by Kinetic Capillary Electrophoresis with UV Detection Revealing How Kinetics Control Equilibrium. *Anal. Chem.* **2011,** 83, 8387-8390.

36. Flinders, J.; DeFina, S. C.; Brackett, D. M.; Baugh, C.; Wilson, C.; Dieckmann, T. Recognition of Planar and Nonplanar Ligands in the Malachite Green–RNA Aptamer Complex. *ChemBioChem* **2004,** 5, 62-72.

37. Cruz-Aguado, J. A.; Penner, G. Fluorescence Polarization Based Displacement Assay for the Determination of Small Molecules with Aptamers. *Anal. Chem.* **2008,** 80, 8853-8855.

38. Guédin, A.; Lacroix, L.; Mergny, J.-L. Thermal Melting Studies of Ligand DNA Interactions. In *Drug-DNA Interaction Protocols*, Fox, K. R., Ed. Humana Press: 2010; Vol. 613, pp 25-35.

39. Ravanat, J. L.; Cadet, J. Reaction of singlet oxygen with 2'-deoxyguanosine and DNA. Isolation and characterization of the main oxidation products. *Chem. Res. Toxicol.* **1995,** 8, 379-388.

40. Fleming, A. M.; Orendt, A. M.; He, Y.; Zhu, J.; Dukor, R. K.; Burrows, C. J. Reconciliation of Chemical, Enzymatic, Spectroscopic and Computational Data To Assign the Absolute Configuration of the DNA Base Lesion Spiroiminodihydantoin. *J. Am. Chem. Soc.* **2013,** 135, 18191-18204.

41. Durandin, A.; Jia, L.; Crean, C.; Kolbanovskiy, A.; Ding, S.; Shafirovich, V.; Broyde, S.; Geacintov, N. E. Assignment of Absolute Configurations of the Enantiomeric Spiroiminodihydantoin Nucleobases by Experimental and Computational Optical Rotatory Dispersion Methods. *Chem. Res. Toxicol.* **2006,** 19, 908-913.

42. Eckenroth, B. E.; Fleming, A. M.; Sweasy, J. B.; Burrows, C. J.; Doublié, S. Crystal Structure of DNA Polymerase β with DNA Containing the Base Lesion Spiroiminodihydantoin in a Templating Position. *Biochemistry* **2014,** 53, 2075-2077.

43. Gedik, C. M.; Collins, A. F. Establishing the Background Level of Base Oxidation in Human Lymphocyte DNA: Results of an Interlaboratory Validation study. *FASEB J.* **2005,** 19, 82-84.

44. David, S. S.; O'Shea, V. L.; Kundu, S. "Base-excision Repair of Oxidative DNA Damage" *Nature* **2007,** 447, 941-50.

45. Rink, S. M.; Shen, J.-C.; Loeb, L. A. Creation of RNA Molecules That Recognize The Oxidative Lesion 7,8-Dihydro-8-Hydroxy-2'-Deoxyguanosine (8-oxodG) in DNA. *Proc. Nat. Acad. Sci.* **1998,** 95, 11619-11624.

46. Miyachi, Y.; Shimizu, N.; Ogino, C.; Fukuda, H.; Kondo, A. Selection of a DNA aptamer that binds 8-OHdG using GMP-agarose. *Bioorg. Med. Chem. Lett.* **2009,** 19, 3619-3622.

CHAPTER 4

FUTURE DIRECTIONS

The aim of this dissertation research is to aid in developing a new method for detection of damaged bases that is sensitive at very low concentrations. After several attempts, I have been able to develop an approach to select aptamers effectively against these damaged bases. The aptamers selected have also been truncated to design sensors and determine their binding affinity that are mostly in the low nM range. The long-term goal of this project is to detect damages in cellular samples effectively. There are several ways one can test the aptamer developed for the target before proceeding to *in vitro* studies.

Aptamers as molecular recognition elements have found a wide variety of applications as biosensors. Split aptamers that comprise two nucleic acid strands, designed by systematic truncation of aptamer stem regions, can be applied to test these aptamers. These truncated strands assemble selectively in the presence of the desired target. The assembly of these DNA strands can be translated into a ligation reaction based on the split aptamer proximity ligation technology (StAPL) developed recently by the Heemstra lab (Figure 4.1).[1] This has been applied to three-way junction aptamers for cocaine detection. They have also recently developed a general approach applied to other architectures of DNA aptamers like hairpins or stem loops (Figure 4.2).[2]

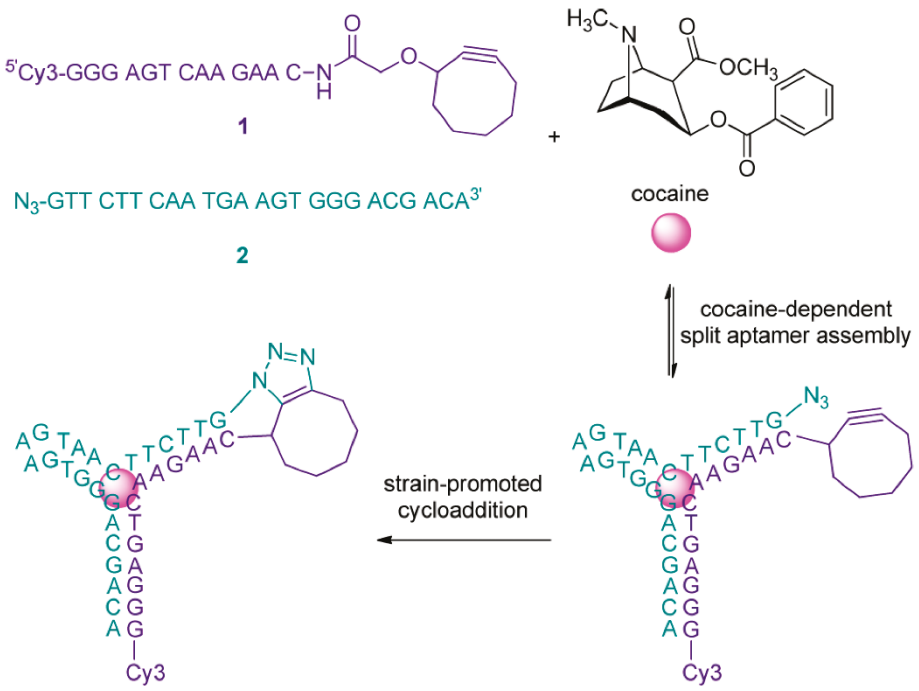

Figure 4.1. Cocaine-dependent split aptamer ligation using strain-promoted azide-alkyne cycloaddition. This diagram has been adapted from *J. Am. Chem. Soc.* **2011**, 133, 12426.

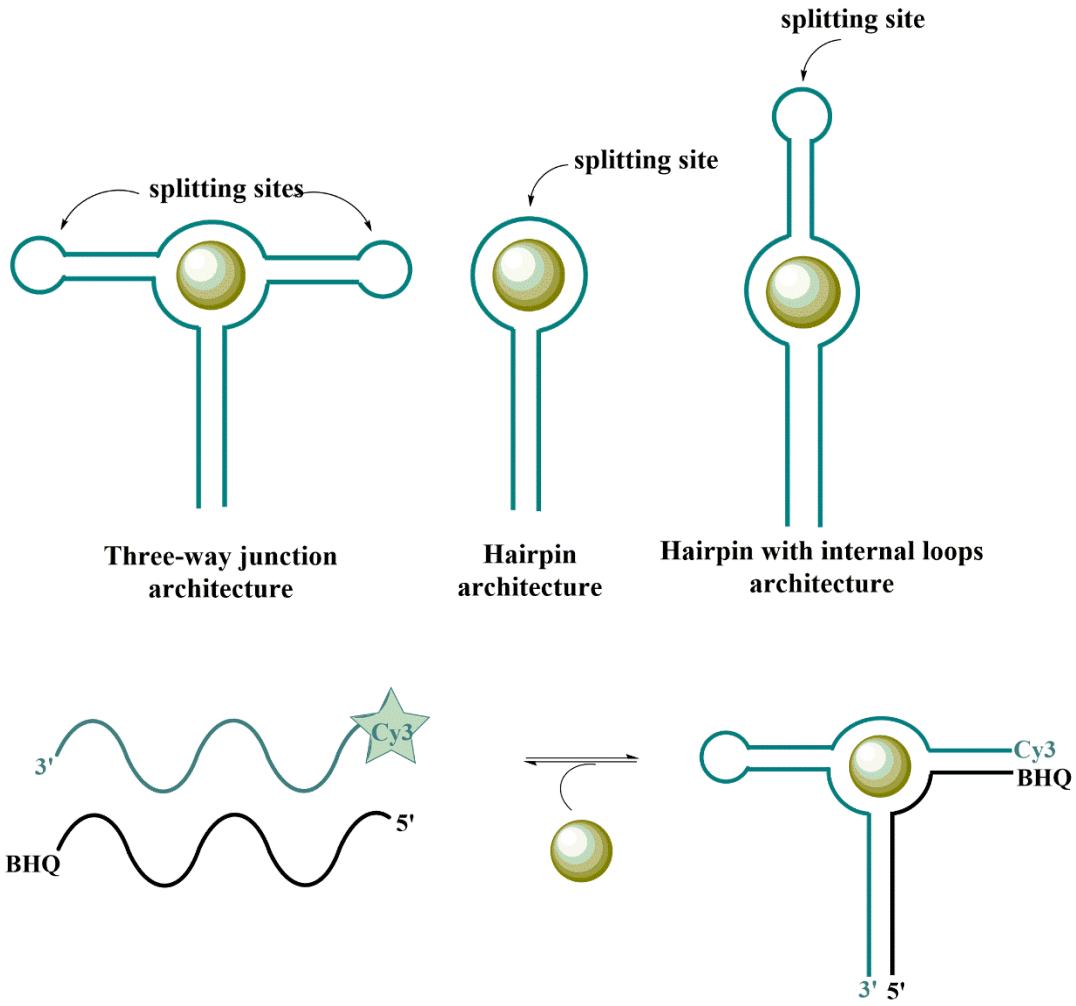

Figure 4.2. Possible sites of splitting aptamers based on their architecture (above). The fluorescence and quenching strategy used as a general approach to split aptamer dependent detection of small-molecule targets (below).

However, the three-way junctions are more "privileged structures" to study small molecule detection using this technology. Aptamers developed as sensors for some of the targets in Chapter 3 show three-way junction architecture, and this technology can be applied to the study of these aptamers. Besides, one can also test other aptamer architectures, like hairpins, obtained in the study by selectively truncating the stem regions and optimizing the buffer conditions. Diastereomeric lesions can also be studied by adding a diastereomeric excess of one target and using this technology. By using the split aptamer technology, one can confirm that the selected truncated aptamer assembles selectively in the presence of the desired diastereomeric target.

Using the split aptamer technology sheds some light on the structural aspect of aptamer binding to a small molecule where X-ray and NMR data are unavailable. However, chemical modification of the aptamers provides inadequate information about the part of aptamer regions that are in close proximity or in contact with the target. To evaluate the significance of specific base compositions on aptamer binding, exploring the sequence space of the aptamer by mutation might provide some insight into the target binding topology of the aptamer. Research has shown that mutations play a significant role in either completely disrupting the secondary structure or forming a new secondary structure or a new recognition loop in the aptamer.[3] Attempts have been made in the past to evolve aptamers with altered specificity. One of the examples for this is the arginine aptamer obtained after 30% mutagenesis of the citrulline aptamer.[4] Mutation of a few bases in the aptamer changes its secondary structure and results in small changes in target specificity. This might be a very useful approach to evolve aptamers specifically for various other DNA oxidation lesions being discovered by the Burrows group and other laboratories.

Single, double, or triple mutations can be created by using DNA microarrays to test base composition on aptamer binding and identify the possible structural motif in binding. Single mutations from G to T at position 1 (increase affinity), T to A at position 17 (much weaker affinity), or C to T at position 19 (similar affinity) at different positions have shown a significant affect in binding affinity of the original IgE aptamer (Figure 4.3).[5] The binding affinity (K_D) was determined using fluorescence anisotropy. The original aptamer had K_D of 15 nM, whereas G to T mutation had higher binding affinity K_D of 7 nM, C to T mutation had similar K_D of 19 nM as original aptamer, whereas, the binding affinity decreased drastically for T to A mutation with K_D of 450 nM. Double and triple mutation combinations at certain positions (11, 18, 19, 22, 23 and 24) have significant binding signal for IgE aptamer.[5]

In vitro studies can be performed on cell lysates that are treated with ROS to generate oxidative stress resulting in a specific type of lesions based on optimized conditions (buffer, pH, and the type of oxidant used) and treated with proteases and nucleases to detect a specific lesion using any of the abovementioned biosensor methods for the selected aptamer.

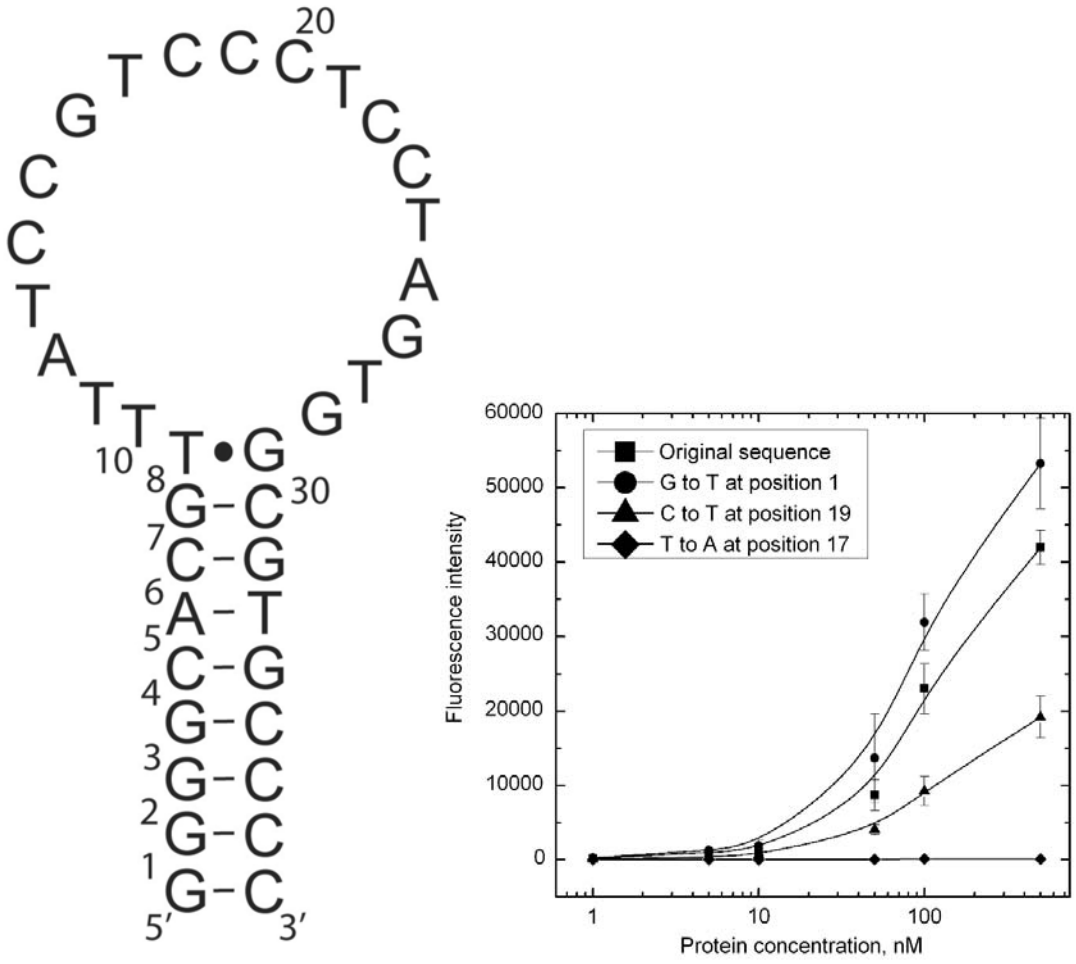

Figure 4.3. Predicted secondary structure of IgE-binding aptamer. The effect of single mutation on the binding of the aptamer to the target. This figure has been adapted from *Nucl. Acids Res.* **2007,** 35, 7626-7635.

References

1. Sharma, A. K.; Heemstra, J. M. Small Molecule-Dependent Split Aptamer Ligation. *J. Am. Chem. Soc.* **2011,** 133, 12426-12429.

2. Kent, A. D.; Spiropulos, N. G.; Heemstra, J. M. General Approach for Engineering Small-Molecule-Binding DNA Split Aptamers. *Anal. Chem.* **2013,** 85, 9916-9923.

3. Huang, Z.; Szostak, J. W. Evolution of aptamers with a new specificity and new secondary structures from an ATP aptamer. *RNA* **2003,** 9, 1456-1463.

4. Famulok, M. Molecular recognition of amino acids by RNAaptamers: An L-citrullin binding RNA motif and its evolution into an L-arginine binder. *J. Am. Chem. Soc.* **1994,** 116, 1698–1706.

5. Katilius, E.; Flores, C.; Woodbury, N. W. Exploring the sequence space of a DNA aptamer using microarrays. *Nucl. Acids Res.* **2007,** 35, 7626-7635.